Environmental Chemistry Letters (2022) 20:519–562
https://doi.org/10.1007/s10311-021-01351-3

REVIEW

Engineered magnetic oxides nanoparticles as efficient sorbents for wastewater remediation: a review

M. I. A. Abdel Maksoud[1] · Ramy Amer Fahim[1] · Ahmed G. Bedir[2] · Ahmed I. Osman[3] · Marwa Mohamed Abouelela[2,4] · Gharieb S. El-Sayyad[5,6] · M. Abd Elkodous[4,7] · Amira S. Mahmoud[8] · Maisara M. Rabee[9] · Ala'a H. Al-Muhtaseb[10] · David W. Rooney[3]

Received: 9 October 2021 / Accepted: 21 October 2021 / Published online: 19 November 2021

Abstract

The rapid urbanization and industrialization is causing worldwide water pollution, calling for advanced cleaning methods. For instance, pollutant adsorption on magnetic oxides is efficient and very practical due to the easy separation from solutions by an magnetic field. Here we review the synthesis and performance of magnetic oxides such as iron oxides, spinel ferrites, and perovskite oxides for water remediation. We present structural, optical, and magnetic properties. Magnetic oxides are also promising photocatalysts for the degradation of organic pollutants. Antimicrobial activities and adsorption of heavy metals and radionucleides are also discussed.

Keywords Magnetic oxides · Spinel ferrites · Iron oxides · Perovskite oxides · Photodegradation · Sorption

Disclaimer The views and opinions expressed in this review do not necessarily reflect those of the European Commission or the Special EU Programmes Body (SEUPB).

✉ M. I. A. Abdel Maksoud
muhamadmqsod@gmail.com

✉ Ramy Amer Fahim
dr.ramyfahim@gmail.com

✉ Ahmed I. Osman
aosmanahmed01@qub.ac.uk

[1] National Center for Radiation Research and Technology (NCRRT), Egyptian Atomic Energy Authority (EAEA), Nasr City, Cairo, Egypt

[2] Egyptian Petroleum Research Institute (EPRI), Nasr City, Cairo 11727, Egypt

[3] School of Chemistry and Chemical Engineering, Queen's University Belfast, Belfast BT9 5AG, Northern Ireland, UK

[4] Department of Electrical and Electronic Information Engineering, Toyohashi University of Technology, 1-1 Hibarigaoka, Tempaku-cho, Toyohashi, Aichi 441-8580, Japan

[5] Department of Microbiology and Immunology, Faculty of Pharmacy, Galala University, New Galala city, Suez, Egypt

[6] Drug Microbiology Lab., Drug Radiation Research Department, National Center for Radiation Research and Technology (NCRRT), Egyptian Atomic Energy Authority (EAEA), Cairo, Egypt

[7] Center for Nanotechnology (CNT), School of Engineering and Applied Sciences, Nile University, Sheikh Zayed, Giza 16453, Egypt

[8] Department of Environmental Studies, Institute of Graduate Studies and Research, Alexandria University, 163 Horreya Avenue, El-Shatby, P.O. Box 832, Alexandria, Egypt

[9] Department of Materials and Nanosciences, Faculty of Science, Ain Shams University, Cairo, Egypt

[10] Department of Petroleum and Chemical Engineering, College of Engineering, Sultan Qaboos University, Muscat, Oman

Introduction

One of the most significant challenges of the recent decades faced by the global community is providing safe, reliable, and cost-effective water. The rapid increase in the field of industrialization, the growing population, and the evolution of people's lifestyles began have commenced to an abnormal increment in production in sequence with the inappropriate disposal of hazardous industrial pollutants in water systems, such as organic dyes, radionuclides, heavy metals, pesticides, and pharmaceuticals residues. Thus, under this situation, environmental remediation has become a fundamental need to protect environmentally friendly stability and public health (Alvarez et al. 2018; Kalita and Baruah 2020; Abdel Maksoud et al. 2020a; Ajiboye et al. 2021; Karthik et al. 2021; He et al. 2021; Chinthala et al. 2021). Various proper technologies have been used for the remedy of water. Among them, the most common are membrane filtration, coagulation and flocculation, ion exchange, alternative chemical processes, and adsorption procedures (Abdel Maksoud et al. 2020a; Lu and Astruc 2020; Leonel et al. 2021). Among water remediation techniques, the adsorption technique is practical in eliminating diverse types of hazardous pollutants in water. As a consequence, it is the common broadly applied method in water remedy processes. Recently, advanced materials composites based on carbon materials, silica, zeolites, clay have become proper materials in water remediation (Osman et al. 2019; Singh et al. 2019a; Zhang et al. 2017a; Tu et al. 2019; Mahani et al. 2018; Buruga et al. 2019; Zhang et al. 2021a).

Among the various adsorbent materials, the magnetic oxides nanoparticles (iron oxides, spinel ferrites, and perovskite oxides) possess extraordinary research interest attributable to their magnetically responsive nature to the applied magnetic field. Controlling these nanoparticles' spatial distribution and particle size affords distinct merits for interface-related purposes, such as adsorption and photocatalysis (Wang and Yin 2016; Kim et al. 2018; Hodges et al. 2018).

In recent decades, the iron oxides nanoparticles have possessed exceptional features in sorption activities ascribing to their specific surface area, porosity structure, and high magnetic response, resulting in a remarkable sorption ability. In the same context, the iron oxides nanoparticles have existed in nature in diverse compositions, such as the hematite (α-Fe_2O_3) and magnetite (Fe_3O_4), whose suitable properties make them candidates in water remediation such as polymorphism that involves phase transition by temperature-induction (Abdel Maksoud et al. 2020a; Leonel et al. 2021; Huang and Chen 2009; Nizamuddin et al. 2019; Cornell and Schwertmann 2003; Hammad et al. 2021).

Due to their novel electronic and magnetic characteristics, spinel ferrite oxides have been recognized as a class of up-and-coming materials for numerous technological utilizations. They have displayed exceptional merits for purposes in high-density magnetic storage media, antimicrobial agents, anticancer, sensors, batteries, supercapacitors, and absorption of toxic heavy metals, ascribing to their unique redox performance, extraordinary chemical stability (particularly in acidic solutions), superparamagnetic or ferromagnetic nature, and large saturation magnetization (Pereira et al. 2012; Vadiyar et al. 2017; Vadiyar et al. 2016; Skliri et al. 2018; Abdel Maksoud et al. 2021a; Abdel Maksoud et al. 2020b; Ashour et al. 2018a; Abdel Maksoud et al. 2018; Abdel-Rafei et al. 2021a; Alshahrani et al. 2021). Besides, spinel ferrites possess progressing interest as suitable photocatalysts ascribing to their narrow bandgap, desirable conduction band alignment towards water splitting, excellent photo-induced stability, cost-effectiveness, and simple magnetic recovery (Abdel Maksoud et al. 2020c; Jia et al. 2019; Abdel Maksoud et al. 2021b, c).

Perovskite oxides also won exceptional attention in water remediation, ascribing to their novel structure characteristics, remarkable chemical stability, unique electronic conduction, and outstanding optical merits (Das and Kandimalla 2017; Fang et al. 2019). The substitution of cations in perovskite oxides with various valences and radii of atomic causes the distortion in the perovskite structure, showing numerous physic-chemical features such as oxygen vacancies, superior thermal stability, excellent electric conduction, and active redox sites. Consequently, perovskite oxides have been observed as a blossoming concern in diverse areas, such as in solar cells, energy conversion, and water remediation (Wang et al. 2021; Djellabi et al. 2022; Polo-Garzon and Wu 2018; Zhang et al. 2020; Liu et al. 2020a; Liu et al. b).

Here we review the most conventional synthesis techniques of iron oxides, spinel ferrites, and perovskite oxides materials. Also, the properties of these materials and their combination with other materials are addressed. Detailed investigation of the mechanistic pathways based on these materials as promising photocatalysts towards removing organic pollutants is presented. Furthermore, the antimicrobial activity of magnetic oxides towards the pathogenic microbes' species is detailed. Besides, appropriating magnetic oxides as promising adsorbents for heavy metals and radionuclides are discussed.

Synthesis

Spinel ferrites can be synthesized via many fabricating techniques that reflect on their morphology. Spinel ferrites can be produced in multiple forms and dimensions. For instance, (1) zero-dimensional nanoparticles and nanospheres, (2)

one-dimensional nanotubes, nanowires, and nanofibers, (3) two-dimensional nanosheets and nanoplates, and (3) three-dimensional nanofoams and nanoflowers. Indeed, each morphology has its distinctive characteristics that meet its structure. Nevertheless, the most common advantages are their superparamagnetic behaviour, superb physio-chemical properties such as optical and catalytic properties, chemical and thermal stability, and easy functionalization (Pham et al. 2020). A different number of synthesis ways for spinel ferrites were discussed (Andersen et al. 2018), such as sol–gel auto-combustion (Ai and Jiang 2010) thermal decomposition, (Hyeon et al. 2002) microemulsion techniques (Mathew and Juang 2007), microwave-assisted routes, (Solano et al. 2012) hydrothermal synthesis, (Schuele and Deetscreek 1961) and solvothermal synthesis (Sun et al. 2004). Perovskite oxides are promising photocatalysts and candidates for water remediation applications due to their diverse structures. This is because different metal cations can (partially or totally) be substituted in their general formula ABO_3, generating a large family with varied and controllable physico-chemical properties. Several synthesis methods are soft- and hard-, colloidal-crystal-template, hydrothermal, electrospinning, and ultrasonic methods for perovskite oxides preparation (Huang et al. 2018; Okejiri et al. 2020; Hu et al. 2020; Dai et al. 2020; Shi et al. 2017). Iron oxides are among the magnetic materials that gained extensive attention in the photocatalysis and water treatment fields. The most obvious properties are their stability, para-/ferrimagnetism, and environmental-friendly nature. They also should have a higher surface area, narrow bandgaps for higher visible light activity, and an unambiguous ability to absorb heavy metals (Abdel Maksoud et al. 2021c; Singh et al. 2019b; Bhateria and Singh 2019; Gusain et al. 2019). Although iron oxides exist naturally, they can also be synthesized and fabricated via many routes such as co-precipitation (de Mello et al. 2019), hydrothermal (Phumying et al. 2021), sol–gel (de Oliveira Guidolin et al. 2021), and solvothermal (Medinger et al. 2021).

The synthesis of homogenous spinel ferrites nanoparticles is critical because their optical, electrical, and magnetic properties are heavily impacted by their size and the method used to prepare them (Baykal et al. 2013; Khishigdemberel et al. 2020). The fabrication of spinel ferrites usually utilizes M(II) and Fe (III) salts as precursors. By controlling their quantity and composition, the structural composition of spinel ferrites can be altered (Qin et al. 2021). The process for fabricating perovskite oxides must be chosen based on the application, specific requirements for activity, and selectivity because these are based on the arrangement of the atoms on the surface (Lim et al. 2019; Ao et al. 2021; Chien et al. 2021). One of the difficulties in developing perovskite catalysts is attaining the appropriate structure while preserving a high surface area, as high temperatures for calcination were used in some cases. As a result, the selection of the preparation method is a significant consideration (Akinlolu et al. 2019).

Co-precipitation

The co-precipitation method is a low-cost, simple procedure that does not require the use of organic solvents. It is more suitable for adjusting particle size and producing a high product yield (Deepapriya et al. 2019; Hussain et al. 2021a; Alzaid et al. 2020; Aslam et al. 2021a). It uses water as a solvent and mixes Fe (II) and Fe (III) solution salts in the presence of a base to prepare iron oxides, and it can occur under mild conditions (Dong et al. 2018; Yazdani and Seddigh 2016). The factors which have influenced the phase-type and particle size are operating pH, temperature, time, and with or without a stabilizing agent. Besides, the precursors' type is an essential factor herein (Mascolo et al. 2013; Sim et al. 2019).

Reza Asadi et al. synthesized $CoFe_2O_4$ and $MnFe_2O_4$ spinel ferrite nanoparticles using $MnSO_4.4H_2O$ or $CoCl_2.6H_2O$ and $FeCl_3.6H_2O$ salts. The field emission scanning electron microscopy (FE-SEM) analysis indicated the cubic morphology of $CoFe_2O_4$ and $MnFe_2O_4$ nanoparticles with crystal size of 20–80 nm. It was noted that $MnFe_2O_4$ nanoparticles had a larger crystal size than $CoFe_2O_4$ due to their larger ionic radius of Mn^{2+}. Additionally, the specific surface areas of $CoFe_2O_4$ and $MnFe_2O_4$ were 50.4 and 84.5 m^2/g, with saturation magnetization of 37.54 and 61.39 emu/g, respectively (Asadi et al. 2020). Simi Debnath et al. fabricated $Mn_{0.5}Zn_{0.5}Fe_2O_4$ in a face-centred cubic phase with a particle size of about 28 nm, which was confirmed by X-ray diffraction analysis. The electron microscopic analysis revealed the spherical morphology and the average size of the formed ferrite nanocrystals matched with that from the X-ray diffraction analysis (Fig. 1) (Debnath and Das, 2020). R. Ghasemi et al. prepared $Cu_{1-x}Cd_xFe_2O_4$ ($0 \le x \le 1$) via co-perception utilizing Cd (II), Cu (II) and Fe (III) salts. X-ray diffraction analysis showed the formation of the spinel cubic phase (space group Fm3m) and the detection of CdO as the secondary phase. Furthermore, transmission electron microscopy revealed a high level of nanoparticle aggregation (Ghasemi et al. 2020). L P S Sagala et al. (Sagala, et al. 2021) prepared $Zn_{0.7}Ni_{0.15}Cu_{0.15}Fe_2O_4$ with particle size 14.5 nm utilizing co-precipitation process at 100 °C. The X-ray diffraction measurement illustrated that $Zn_{0.7}Ni_{0.15}Cu_{0.15}Fe_2O_4$ was formed in the cubic spinel shape with the highest peak (311). Additionally, the hematite phase was formed with low intensity. The field emission scanning electron microscopy indicated that $Zn_{0.7}Ni_{0.15}Cu_{0.15}Fe_2O_4$ morphology was spherical with agglomeration. F.A.Hezam et al. fabricated $Ni_{0.5}MgxZn_{0.5\text{-}x}Fe_2O_4$ with particle size less than 30 nm. The X-ray diffraction analysis indicated that all ferrites were a single-phase cubic spinel structure (Hezam et al. 2021). T.

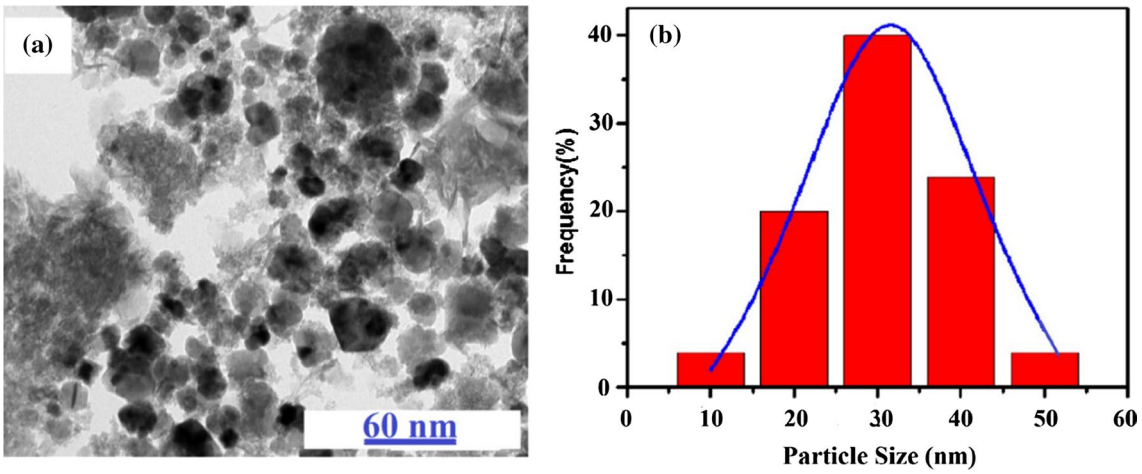

Fig. 1 **a** Transmission electron microscopy image confirms the spherical shape and **b** Size distribution of $Mn_{0.5}Zn_{0.5}$ Fe_2O_4 nanoparticles. Reprinted with permission of Elsevier from (Debnath and Das 2020). The electron microscopic analysis revealed the spherical morphology and the average size of the formed ferrite nanocrystals matched with that from the X-ray diffraction analysis

Ajeesha et al. synthesized $Mg_{1-x}Ni_xFe_2O_4$ (x = 0.0, 0.6, 1.0) nanoparticles with crystal size of 20–30 nm. X-ray diffraction and transmission electron microscopy measurements were showed the cubic spinel structure corresponding to the space group Fd3m. The photocatalytic activity for methylene blue degradation was enhanced by increasing the quantity of Ni substitution owing to its small bandgap (Ajeesha et al. 2021a).

Peiwei Han et al. adjusted the quantity of polyethylene glycol through the preparation of $CaZrO_3$ via the co-precipitation process. X-ray diffraction analysis indicated that the $CaZrO_3$ structure prepared with different polyethylene glycol added amounts was orthorhombic. The results showed that oxygen vacancies were generated in $CaZrO_3$ treated with polyethylene glycol, which had a higher activity for catalytic ozonation of organic contaminants than $CaZrO_3$ that had not been modified (Han et al. 2021). Choe Earn Choong et al. fabricated $CeFeO_3$-doped g-C_3N_4 composite using co-precipitation followed by calcination at 550˚C for four hrs. The X-ray diffraction analysis indicated that $CeFeO_3$ was formed in orthorhombic structure with *Pbnm* space group. $CeFeO_3$-doped g-C_3N_4 composite with 1% $CeFeO_3$ displayed high photocatalytic activity for organic pollutant removal and nitrogen photo-fixation (Choong et al. 2021). V. I. Popkov et al. observed that the particle size and surface area of $GdFeO_3$ depended on the solution temperature during the co-precipitation process (Popkov and Albadi, 2021). Tien A. Nguyen et al. prepared $HoFeO_3$ nanoparticles by co-precipitation procedure using NH_3 5% as a precipitating agent and annealed at 850 °C for one hr. The analysis manifested that the co-precipitation conditions influenced the structure of the $HoFeO_3$ nanoparticles and their optical and magnetic properties (Nguyen et al. 2021).

Zn-Mn-doped Fe_3O_4 with particle size about 10–15 nm was fabricated using $FeSO_4.7H_2O$ and $FeCl_3$ as precursors. X-ray diffraction measurement indicated that all synthesized samples with varied ratios of Zn and Mn generated spinel structure with truncated octahedral shape; the magnetometry analysis revealed that the Mn and/or Zn doping in the magnetite structure enhanced the saturation magnetization with the excellent value for Zn-Mn equal doped magnetite (de Mello et al. 2019). Fe_3O_4/ZnO/Ag composite was prepared via sono-coprecipitation process utilizing silver nitrate, zinc acetate, and ethylene glycol as reagents and NH_4OH as a precipitating agent. Fe_3O_4/ZnO/Ag with grain size 17 nm showed high efficiency for Titan Yellow degradation (Fadillah et al. 2021). Innocent Nkurikiyimfura et al. synthesized Fe_3O_4 through co-precipitation at room temperature, a pH of 10, and a stirring rate of 200 rpm. The X-ray diffraction analysis displayed the formation of the pure FCC spinel structure of Fe_3O_4. The transmission electron microscopy images showed the spherical shape of Fe_3O_4 with an average crystal size of 11 nm.

Additionally, the preparation temperature (5–300 K) highly affected the magnetic properties and demonstrated the super magnetic properties at 300 K (Nkurikiyimfura et al. 2020). Sometimes passivation is necessary because iron oxide nanoparticles are less stable in acidic solutions and can lose their magnetic properties due to agglomeration. For instance, Vitalii Serdiuk et al. fabricated Fe_3O_4 nanoparticles with the shell of the peroxide-containing polymer via co-precipitation technique using peroxide-containing copolymer with Fe (III) and Fe (II) salts solutions. The results showed that the starting concentration of peroxide-containing copolymer significantly

impacted the magnetic characteristics of Fe_3O_4 nanoparticles (Serdiuk et al. 2021). Several magnetite composites as adsorbents were synthesized. For example, Sahil Lakhanpal et al. prepared Fe_3O_4 covered sand adsorbent via the co-precipitation technique using $FeCl_3.6H_2O$, $FeCl_2$, NH_4OH, and sand a substrate. The Fe_3O_4 coated sand particles displayed were formed in particle size of about 30–210 nm, and manifested high photocatalytic activity for heavy metal removal (Lakhanpal et al. 2021). Sri JuariSantosa et al. prepared Fe_3O_4/Zn/Al layered double hydroxide utilizing sodium hydroxide as a precipitating agent. Transmission electron microscopy analysis displayed that pure Fe_3O_4 has a larger particle size than Fe_3O_4-Zn/Al LDH composite. The morphology of pure Fe_3O_4 was hexagonal, but the morphology of the Fe_3O_4-Zn/Al layered double hydroxide was irregular diffuse, with Fe_3O_4 nanoparticles distributed as darker spots inside Zn/Al layered double hydroxide as brighter forms. Fe_3O_4-Zn/Al layered double hydroxide composite was also magnetically active due to the good dispersion of Fe_3O_4 and showed high activity for humic acid removal (Santosa et al. 2021). Eliane V. Rosa et al. fabricated g-C_3N_4/Fe_3O_4 composite through homogenous precipitation of Fe^{2+} and Fe^{3+} salts using urea decomposition. This magnetic nanocomposite displayed the highest surface area, efficient light absorption, and the best photocatalytic activity compared with pure g-C_3N_4 and magnetic nanocomposite formed by traditional co-precipitation with NH_4OH (Rosa et al. 2021). Zn-doped α-Fe_2O_3 was prepared by co-precipitation process, with altering zinc precursors molar ratio. The formed nanoparticles were found to be rhombohedral, with spherical shape and their size was about 44 nm which dropped to roughly 22 nm after Zn doping.

Furthermore, increasing Zn doping quantity reduced the bandgap and magnetic characteristics (Lassoued 2021). Jing Deng et al. prepared S-α-Fe_2O_3 using co-precipitation, hydrothermal and followed by calcination and investigated it to activate persulfate for degradation of carbamazepine under Ultra-Violet illumination. X-ray diffraction analysis confirmed the formation of hematite (JCPDS 33–0664) with high purity, illustrating that prepared samples' high purity and crystalline structure were well-preserved during the S doping procedure. Additionally, transmission electron microscopy analysis indicated that S-α-Fe_2O_3 displayed the shape of a short-rod with a diameter of 100 nm and length from 200 to 600 nm with some aggregation. At the same time, high-resolution transmission electron microscopy manifested the mesoporous structure S-α-Fe_2O_3 (Deng et al. 2021). Additionally, many hematite composites were prepared using the co-precipitation technique and demonstrated high photocatalytic activity (Rehman et al. 2020; Belaidi et al. 2021; Mansour et al. 2020).

Hydrothermal

The hydrothermal approach is based on using a sealed, high-pressure reactor or autoclave holding aqueous solutions, in which a chemical reaction occurs at high pressure and temperature (Xie et al. 2021a). A hydrothermal method is inexpensive for producing ultrafine materials that can alter particle size and shape at varying temperatures and pressures while maintaining a fast reaction rate (Rouhani et al. 2019).

Many studies indicated that the utilization of hydrothermal process to prepare spinel ferrites is better than other techniques. For example, Xuesong Zhu et al. illustrated that the magnetization of $ZnFe_2O_4$ fabricated using the hydrothermal method was better than that synthesized using the ceramic technique. This was due to the different Fe ion occupancy caused by the loss of Zn ions during the hydrothermal method (Zhu et al. 2021). Farzana Majid et al. reported that $NiFe_2O_4$ produced using the hydrothermal technique had different structural, electrical, and magnetic properties than $NiFe_2O_4$ synthesized using the sol–gel route (Majid et al. 2021). T.A. Nhlapo et al. (Nhlapo et al. 2021) fabricated $Mn_{0.1}Mg_{0.2}$(Co, Ni, Zn)$_{0.7}Fe_2O_4$ with the grain size of 11–17 nm using the hydrothermal procedure. X-ray diffraction analysis showed the formation of $Mn_{0.1}Mg_{0.2}$(Co, Ni, Zn)$_{0.7}Fe_2O_4$ in cubic spinel lattice with high purity. Transmission electron microscopy images revealed the spherical shape of the prepared samples with the size distribution 10.6–14.4 nm, which was consistent with X-ray diffraction analysis (Nhlapo et al. 2018). A.G. Ramu et al.(Ramu et al. 2021) used a hydrothermal technique to synthesize $CuFe_2O_4$, $NiFe_2O_4$, and $CoFe_2O_4$ nanoparticles and tested them for hazardous nitro compound degradation. X-ray diffraction analysis confirmed the formation of metal ferrites with high purity and crystallinity. Field emission scanning electron microscopy images revealed that $CuFe_2O_4$, $NiFe_2O_4$, and $CoFe_2O_4$ nanoparticles formed in pencil-like tetragonal crystals with a large surface area. Due to the fast-kinetic rate constant, $CuFe_2O_4$ displayed the best catalytic reduction of nitro compounds.

The hydrothermal technique is advantageous in manufacturing perovskite oxides because of the flexibility to manipulate grain size and shape by adjusting reactants concentration, reaction pH, Temperature, and time (Biasotto et al. 2011). Jiana Jing and co-workers (Jing et al. 2021) fabricated $LaCo_{0.5}Fe_{0.5}O_3$ photocatalysts via hydrothermal process, and it demonstrated high efficiency for bisphenol A removal. The X-ray diffraction analysis confirmed the formation of $LaFeO_3$ in orthorhombic structure, while $LaCo_{0.5}Fe_{0.5}O_3$ revealed the rhombohedral structure. Additionally, all samples formed in high crystallinity and

purity. Scanning electron microscopy images showed the formation of $LaCo_{0.5}Fe_{0.5}O_3$ in hierarchical micron-spheres with nano-rods.

In addition, the transmission electron microscopy image confirmed the same morphology. The high-resolution transmission electron microscopy image displayed that the lattice space of $LaCo_{0.5}Fe_{0.5}O_3$ was 0.275 Å, in agreement with the (110) lattice plane of the rhombohedral structure perovskite. Egor M.Kostyukhin et al. synthesized orthorhombic $LaFeO_3$ using a hydrothermal procedure with microwave illumination during the preparation, which resulted in a high yield of $LaFeO_3$ nanocrystals with small particle sizes at a lower temperature (220 °C) and in a shorter period (3 h) than the usual heating process (Kostyukhin et al. 2021) as well as, a hydrothermal process has been adopted for the synthesis of doped perovskite oxides. R.Abirami et al. prepared pure $PbTiO_3$ and (Ag–Fe) co-doped $PbTiO_3$ using the hydrothermal method and calcined the prepared samples at 600 °C. X-ray diffraction analysis confirmed the tetragonal form of $PbTiO_3$ and proved no tremendous change in the (Ag–Fe) co-doped $PbTiO_3$ pattern compared to pure $PbTiO_3$. Thus, the Ag and Fe doping did not influence the phase and structure of $PbTiO_3$. The (Ag–Fe) co-doped $PbTiO_3$ nanoparticles demonstrated the highest photocatalytic activity due to efficient charge separation with high stability and reusability (Abirami et al. 2021). Canh VanNguyen et al. fabricated Ir-doped $SrTiO_3$ nano-cubes via the hydrothermal procedure. Different Ir quantities were doped into $SrTiO_3$ at pH = 13 and 210 °C without utilizing any surfactant. Scanning electron microscopy analysis of pure $SrTiO_3$and Ir-doped $SrTiO_3$ revealed cubic-like structure. Ir-doped $SrTiO_3$ demonstrated the highest efficiency for hydrogen production compared to neat $SrTiO_3$ (Van Nguyen et al. 2021). Chenxiaoning Meng et al. (Meng et al. 2021) prepared reduced graphene oxide-$KTaO_3$ nanocomposites by a hydrothermal process. Scanning electron microscopy and transmission electron microscopy revealed that pure $KTaO_3$ had formed a cubic structure with a 500 nm diameter. The graphene oxide had a wrinkled feature owing to its thin and large sheet shape.

Meanwhile, reduced graphene oxide -$KTaO_3$ showed that the $KTaO_3$ morphology was reserved, and the crystals were wrapped by layered graphene oxide. Due to improved charge separation and transfer, the nanocomposite displayed strong photocatalytic activity and stability. These studies illustrate that the hydrothermal process is ideal for synthesizing pristine perovskite oxides and composites, including perovskite oxides. However, the effectiveness of the hydrothermal process is based on different changes in reaction conditions, such as the solvents utilized in the dissolving of precursor reactants and the temperature.

Additionally, the hydrothermal technique was widely applied to fabricate magnetite and hematite. For example, Santi Phumying et al. (Phumying et al. 2021) fabricated Fe_3O_4 nanoparticles via a hydrothermal process by utilizing an egg white solution as a surfactant to reduce impurities in the generated products. Additionally, they studied the effect of reaction temperature on the morphology and particle size of prepared samples. The X-ray diffraction pattern revealed that all products had a cubic spinel ferrite structure, and the crystallinity improved by raising the reaction temperature. Transmission electron microscopy analysis manifested that the reaction temperature considerably influenced the particle size and morphology of Fe_3O_4 nanoparticles. The Fe_3O_4 nanoparticles formed at 433 K displayed higher agglomeration with ~5–30 nm particle size. Samples formed at 453, 473, and 493 K demonstrated low accumulation with a particle size of ~10–35 nm, ~10–40 nm, and ~10–50 nm, respectively. Maruthupandy et al. (Maruthupandy et al. 2021) prepared Fe_3O_4 nanoparticles, bacterial cellulose/Fe_3O_4, and graphene/bacterial cellulose/Fe_3O_4 composites. The X-ray diffraction analysis confirmed the formation of sphere-like Fe_3O_4 with high purity, which agrees with scanning electron microscopy analysis. The graphene/bacterial cellulose/Fe_3O_4 composite demonstrated high photocatalytic activity for organic dye removal. Zirconium-lanthanum @ Fe_3O_4 composite was prepared using the hydrothermal process and showed high photocatalytic activity for water treatment (Altaf et al. 2021). Pantharee Kongsat et al. (Kongsat et al. 2021) prepared α-Fe_2O_3 nanoparticles utilizing a surfactant-assisted hydrothermal technique. They investigated the use of three surfactant types with different concentrations to adjust the shape, phase, and particle size of α-Fe_2O_3. The results revealed that all prepared iron oxides with and without surfactants were formed in spherical α-Fe_2O_3 with a diameter range of 15–205 nm based on the surfactant sort and concentration. As well many hematite composites were fabricated using a hydrothermal route, such as activated carbon/α-Fe_2O_3 (Ermanda et al. 2021), Co-doped α- α-Fe_2O_3 (Cai et al. 2021), α-Fe_2O_3/g-C_3N_4 (Lee and Park 2020), and chitosan-coated-α-Fe_2O_3 (Badry et al. 2021).

Sol–gel

The sol–gel method is prominent owing to its low cost, low sintering temperature, and ability to adjust particle size with homogeneous components (Hakeem et al. 2021; Meng et al. 2014). So-gel technique initiates hydrolysis and poly-condensation to produce a gel form (Masudi et al. 2020).

The sol–gel auto-combustion process is cost-effective to prepare spinel ferrites at a lower temperature (about 110 °C) with no thermal treatment (Verma et al. 2020). For example, $Ni_{1-x}Cd_xFe_2O_4$ (Verma et al. 2021), $NiCr_XFe_{2-X}O_4$ (Borikar et al. 2021), $Ni_{0.4}Zn_{0.6}Fe_{1.9-x}Al_{0.1}Gd_xO_4$ ($x = 0$ and $x = 0.1$) (Ahmed et al. 2021). Lichao Yu et al. studied the impact of complexing agents on morphological, structural,

and magnetic properties of $Mg_{0.1}$-$Co_{0.9}Fe_2O_4$ (Yu and Sun 2021). The results revealed that the complexing agent was involved in the reaction and impacted the size and magnetization of the prepared samples. L. S. Kaykan et al. studied the impact of preparation techniques (sol–gel auto-combustion and solid-phase methods) on the structure and electrical characteristics of $Li_{0.5}Al_xFe_{2.5-x}O_4$ samples which prepared using the sol–gel auto combustion method displayed a higher degree of element distribution homogeneity, high crystallinity, tiny crystallite size, and good stoichiometry than those synthesized using the solid-phase method (Kaykan et al. 2021).

Swapnil A.Jadhav and his colleagues (Jadhav et al. 2021) prepared $Zn_xNi_{1-x}Fe_2O_4$ ($0.0 \leq x \leq 1$) utilizing urea as fuel. The X-ray diffraction pattern indicated the generation of cubic structure with the Fd-3 m space group. The Field emission scanning electron microscopy images manifested that all samples are formed in Spherical nanocrystalline particles with high agglomeration, ascribed to the magnetically active dipole interface (Rahimi et al. 2013). Besides, the accumulation decreased by increasing the quantity of Ni–Zn. The $Ni_{0.5}Zn_{0.5}Fe_2O_4$ nanoparticles manifested the highest photocatalytic degradation of rhodamine B owing to their smaller crystalline size (Jadhav et al. 2021). Milena P. Dojcinovic et al. (Dojcinovic et al. 2021) synthesized $Co_xMg_{1-x}Fe_2O_4$ utilizing citric acid as fuel and tested them for photocatalytic removal of Methylene Blue. The analysis manifested a cubic spinel structure where the Co^{2+} and Mg^{2+} quantity affected the cation distribution and inversion degree. The spinel ferrites photocatalyst with the lowest cobalt ($Co_{0.1}Mg_{0.9}$-Fe_2O_4) displayed excellent photocatalytic activity under visible light.

The most extensively used approach for perovskite oxide manufacture is the sol–gel technique, which produces high crystalline materials with very small grain sizes and narrow distributions, increasing surface area (Feng et al. 2017; Mishra and Prasad 2014). Cristian Daz et al. studied the effect of the $La_{0.9}K_{0.1}Co_{0.9}Ni_{0.1}O_3$ synthesis technique on the catalytic activity for soot oxidation. Three different preparation methods (self-combustion, microwave-assisted, and sol–gel) were studied, each with an additional synthesis time and energy supply. The results revealed that the preparation technique affected the textural and physicochemical characteristics of the material and the availability of the active site (for example, oxygen vacancies) and reducible sites. The Catalytic soot oxidation of the $La_{0.9}K_{0.1}Co_{0.9}Ni_{0.1}O_3$ depending on the preparation method was in the following order: sol–gel > microwave-assisted > self-combustion (Díaz et al. 2021). Liangbo Xie et al. prepared rhombohedral $LaCo_xCu_{1-x}O_{3-\delta}$ structure via sol–gel process. They reported the vital role of Cu incorporation into $LaCoO_3$, which formed oxygen vacancies and boosted the redox efficiency towards ciprofloxacin (Xie et al. 2021b). Bhuyan et al. prepared Gd_2FeCrO_6 double perovskite nanoparticles using a citrate-based sol–gel process. Gd_2FeCrO_6 was developed in a monoclinic structure with a particle size of about 70 nm, demonstrating high thermal stability (Bhuyan et al. 2021a). A.S.Basaleh et al. 2021 synthesized La-doped $NaTaO_3$ nanoparticles via sol–gel approach using a P-123 template. They added a small quantity of CdO nanocrystals (1.0–4.0 wt %) to the La-doped $NaTaO_3$ via the impregnation process to boost the photocatalytic activity under visible light. 3% CdO/La-doped $NaTaO_3$ displayed complete ciprofloxacin photodegradation after 90 min (Basaleh et al. 2021a). They also reported that 3% Bi_2O_3/La-doped $NaTaO_3$ demonstrated complete photodegradation of ciprofloxacin within 120 min (Basaleh et al. 2021b). Deniz Çoban Özkan prepared $LaMnO_3$ using sol–gel process and annealed it at two different temperatures (500 °C and 850 °C). The analysis showed that crystallinity, grain size, and magnetic properties altered the annealing temperature (Özkan et al. 2021).

Magnetite nanoparticles with a crystal size of 7.92 were prepared by the sol–gel citrate–nitrate process and demonstrated high efficiency for methylene blue removal (de Oliveira Guidolin et al. 2021). Md Rakibuddin et al. (Rakibuddin and Kim 2020) Fe_3O_4 quantum dot/silica composite was fabricated using a sol–gel process under various conditions. The X-ray diffraction pattern confirmed the formation of Fe_3O_4 with a crystal size of ~ 5 nm and mesoporous silica in Fe_3O_4 quantum dot/silica composite. The measurements revealed that the synthesis conditions affected the purity, spherical morphology, and physical and chemical properties of the composite. Superparamagnetic α-Fe_2O_3 nanocrystals with a particle size of 30–40 nm were prepared using a sol–gel process. The results confirmed that the α-Fe_2O_3 was formed in spherical morphology and demonstrated high efficiency for dye removal (Gaidhane et al. 2021). Asmae Bouziani et al. synthesized α-Fe_2O_3/TiO_2 composite using the sol–gel process. The analysis indicated that the annealing temperature (300 to 600 °C) significantly influenced the morphology and photocatalytic efficiency of the α-Fe_2O_3/TiO_2 composite, which increased by increasing the annealing temperature (Bouziani et al. 2020).

Solvothermal

The solvothermal process is a promising preparation technique for reasonable control of morphology and particle size distribution (Tatarchuk et al. 2016). It involves heating a mixture of reactants and solvent in an autoclave near or above the solvent boiling point to undergo the chemical reaction (Demazeau 2008). The heating time and temperature is based on the required nanoparticles type (Kefeni et al. 2017a).

Manijeh Shaterian et al. (Shaterian et al. 2021) fabricated zinc ferrite sub-microparticles utilizing poly

diallyldimethylammonium chloride-assisted solvothermal procedure. The X-ray diffraction pattern confirmed the formation of $ZnFe_2O_4$ in spinel structure with a crystallite size of 11–41 nm. The prepared samples exhibited a spherical-like shape with particles sizes about 95–345 nm that were altered based on reaction conditions. Liling Hu et al. fabricated $CoFe_2O_4$ and octahedral $CoFe_2O_4$-reduced graphene oxide by using a solvothermal process. The X-ray diffraction pattern indicated the formation of $CoFe_2O_4$ cubic spinel structure with high purity and crystallinity. The morphology of $CoFe_2O_4$ nanoparticles changed from a sheet (or granular) to octahedral after the incorporation of reduced graphene oxide. Additionally, various spinel ferrites were prepared via solvothermal processes, such as $CuFe_2O_4$ (Kurian et al. 2021), $Co_xFe_{3-x}O_4$ (Vasil'ev et al. 2021), and $ZnFe_2O_4$(Habibi et al. 2021).

Jianjun Sun et al. (Sun et al. 2021) prepared pure $KTaO_3$ and Cu^{2+}-doped $KTaO_3$ cubic nanoparticles via a solvothermal approach. The analysis indicated that the modification of $KTaO_3$ with Cu^{2+} did not obviously affect the microstructure and phase type of $KTaO_3$ but significantly altered the electrochemical and optical properties. The size of $KTaO_3$ was about 200 nm, while the dimensions of Cu^{2+}-doped $KTaO_3$ were about 180–300 nm. This result revealed that the Cu^{2+} incorporation increased the particle size distribution. According to Yu and his team, the Cu^{2+}-doped $KTaO_3$ displayed more significant photocatalytic degradation of methylene blue than pure $KTaO_3$ (Yu et al. 2018). Aadil Ahmad Bhat et al. used solvothermal to fabricate $MnSnO_3$ and Fe-doped $MnSnO_3$ nanoparticles in a rhombohedral form at room temperature. The particle size of Fe-doped $MnSnO_3$ was reduced as the Fe concentration in the host material was increased (Bhat et al. 2021). Anderson Thesing et al. fabricated $SrTiO_3$ using poly vinylpyrrolidone, which adsorbed on (110) facet, so promoting the growth of (100) facet. As a result of this interaction, a hierarchical flower-like $SrTiO_3$ nanostructure was formed (Thesing et al. 2020). Additionally, Harsha Bantawal et al. synthesized V-doped $CaTiO_3$ via solvothermal process with avoiding high-temperature annealing. The measurements confirmed the successful doping of V^{4+} into the $CaTiO_3$ lattice with a noticeable reduction in the bandgap and thereby demonstrated higher photocatalytic activity than neat $CaTiO_3$ (Bantawal et al. 2021).

Several magnetite nanoparticles such as Fe_3O_4 nanocrystals (Medinger et al. 2021), Fe_3O_4 nanoparticles (Sani et al. 2021; Namikuchi et al. 2021; Gandon et al. 2021), Fe_3O_4/graphene (Farghali et al. 2021), and Fe_3O_4@Au@mTiO_2 composites (Rahman et al. 2021) were prepared by the solvothermal technique. Many hematite composites have also been created, for example, α-Fe_2O_3 nanoplates and nanocubes (Guo et al. 2021a), α-Fe_2O_3 thin films (Platnich et al. 2021), Fe_2O_3 photoanode (Zhang et al. 2021b), Cu-doped α-Fe_2O_3 nanoplates (Guo et al. 2021b), and Au@TiO_2/α-Fe_2O_3 (Mezni et al. 2021).

Structural and magneto-optical properties

Structural analysis

Spinel ferrites are metal oxides of homogenous materials with a spinel structure (AB_2O_4) as a general chemical formula. A- and B-sites represent metallic cations located at two crystallographic sites, tetrahedral; and octahedral, respectively, with ferric ion (Fe^{+3}) as a prime component in their structure. The metallic cations of the two mentioned sites are tetra-/octahedrally connected to the oxygen, respectively (Kefeni and Mamba, 2020; Kirankumar and Sumathi, 2020a). Also, the spinel ferrites with the general structure MFe_2O_4 or $MO.Fe_2O_3$ have a crystallographic building similar to the mineral spinel $MgAl_2O_4$, which occurs naturally (Bragg, 1915). Spinel ferrites are classified into three possible structures as follows:

(A) Normal

The divalent metal ions filled the A-sites. While the iron (III) ions are located at B-sites and $(M)^A\ [Fe_2]^B\ O_4$ represents the cation distribution. If A-site has lower valency than B-sites, the O(II) ions will be polarized towards B-sites. For instance, cadmium and zinc ferrites ($CdFe_2O_4$ and $ZnFe_2O_4$), divalent metallic ions Cd^{2+} or Zn^{2+}, and Fe^{3+} are at A-sites B-sites, respectively (Jadhav et al. 2020).

(B) Inverse

In the inverse type, the A-site contains a single ferric ion (III); meanwhile, B-site comprises the residual ferric ions (III) besides the metallic ions M^{2+}. This cations distribution can be formulated as $(Fe)^A\ [M\ Fe]^BO_4$. For instance, Ni and Co ferrites with the lowest lattice energy are inverse structures (Verwey and Heilmann, 1947).

(C) Random

Both divalent metal (M^{2+}) ions and trivalent Fe (III) ions are scattered at A- and B-sites. The distribution of cations can be represented by $(M_{1-x}Fe_x)^A\ [M_xFe_{2-x}]^BO_4$ as copper ferrites (Hu et al. 2000). To simplify that, M (II) is positioned at the tetrahedral and at the octahedral for normal and inverse spinel ferrites, respectively. At the same time, Fe (III) sited at the octahedral position for the normal type and distributed equally at both (octa- and tetrahedral) sites for the inverse spinel ferrite. The M (II)

and Fe (III) ions are scattered randomly at the octa- and tetrahedral sites regarding the mixed type. For instance, $ZnFe_2O_4$ and $NiFe_2O_4$ are examples of normal and inverse, respectively, while $MnFe_2O_4$ is an example for mixed-types spinel ferrites.

The type, position, and amount of metal cations in the crystallographic structure of ferrites mastered their physicochemical properties (Kefeni and Mamba 2020; Kusigerski et al. 2019; Tatarchuk et al. 2017). They are widely used in multiple applications from biomedical to industrial, besides their application in cancer diagnosis, therapy, and drug delivery (Valente et al. 2017; Kefeni et al. 2020), gas sensors (Šutka and Gross 2016), water splitting, and membrane modifications (Ng et al. 2015; Domínguez-Arvizu et al. 2019). Later they are used intensively as a catalyst and in pollutant degradation via photodegradation and adsorption (Kefeni and Mamba, 2020; Kefeni et al. 2017b; Fayyaz et al. 2021; Reddy and Yun 2016).

Due to their compositional flexibility, outstanding electronic, excellent magneto-optical, exceptional thermal properties, and resistance to photo-corrosion, perovskite oxides are considered promising photocatalysts for different photocatalytic applications. These superb properties are likely to increase their necessary photocatalytic activity and high stability (Wang et al. 2015a). Perovskites are in numerous forms, for instance, oxides, nitrides, and sulfides that depend on their ability to hold several anionic and cationic sites (Aftab et al. 2021).

The general formula of single perovskite oxides is represented as (ABO_3), wherever A and B are the metal cations. Both A and B cations can be designated from alkali metal cations, earth-, or transition metal cations. Thus, many structures of perovskite oxides can be designed by altering these cations. More than 265 structures out of 2346 (theoretically estimated structures) were successfully prepared (Yin et al. 2019). Several single perovskite oxides, like $KTaO_3$, $SrTiO_3$, $NaTaO_3$, $NaNbO_3$, and $KNbO_3$, were studied morphologies their surface properties studied which strongly influence the photocatalytic activities (Grabowska 2016; Nguyen et al. 2020).

There are different polymorphs and oxidations states for iron oxides such as (FeO, Fe_2O_3, α-, β-, γ-, ε-Fe_2O_3, and Fe_3O_4). Iron oxides can show diverse stoichiometries due to the Fe different oxidation states, which permits the formation of different single-crystalline phases such as wüstite, hematite, magnetite, and maghemite) with different physicochemical properties (Abed et al. 2019). However, out of these, hematite and magnetite with the formulae (α-Fe_2O_3 and Fe_3O_4, respectively) are the most substantial, readily accessible, and low-priced oxides (Can et al. 2012). The natural hematite nanoparticles' H-nanoparticles' and magnetite 'M- nanoparticles' have occurred in rhombohedral and cubic structures, respectively (Noh et al. 2014).

Hematite and magnetite nanoparticles have electromagnetic properties related to their structure, where Magnetite nanoparticles are more magnetic than hematite nanoparticles, which are considered canted antiferromagnetic (Ramana et al. 2014). Moreover, magnetite is exceptional in its features due to the tri- and divalent (Fe^{3+}, Fe^{2+}) ion forms. Consequently, it assumed an inverse -cubic- spinel structure, where Fe^{2+} ions occupy half of the octahedral positions, whereas Fe^{3+} joined the lateral tetrahedral and octahedral positions. Magnetite nanoparticles exist as both p-and n-types with a minor bandgap of 0.1 eV, while Hematite nanoparticles are predominantly n-type with a bandgap > 2.0 eV (Khan and Qurashi 2018; Rioult et al. 2016).

Magnetic Properties

Magnetic properties can be analysed from the hysteresis curves of the tested material. Remanence (or remnant) magnetization (Mr) indicates the substance magnetization in the nonappearance of an applied field. Its value can be calculated when the hysteresis curve crosses the y axis. Mr is the spontaneous magnetization quantity in the material at the temperature of the experiment. The saturation magnetization (Ms) is the highest magnetization value obtained when the substance is subjected to a strong magnetic field. The coercivity parameter clarifies the required field for the magnetization direction inversion. This is the field where the hysteresis curve can cross the x-axis. Coercivity (Hc) is associated with the difficulty in stirring the magnetic domain walls inside a crystal. Hence, any property that might delay or smooth this movement will directly impact the material's coercivity. Numerous criteria manage this property, for instance, crystallite size, defects in the crystal structure, and magnetic anisotropies (e.g., stress, shape, and magnetocrystalline) also outline the final intensity of the coercive field.

Magnetism is the most remarkable feature of spinel ferrites, directly resulting from the different metallic ions' spin alignment. Ions located in the tetrahedral sub-lattice can line up their spins (e.g., parallel or antiparallel) to octahedral ions through the exchange interactions facilitated by the oxygen anions. Generally, ferrites are categorized into soft and hard based on their magnetic properties as follows (Jadhav et al. 2020; Almessiere et al. 2021).

(A) Soft ferrites

This type of ferrites is expansively used in telecommunication, military devices, and space research. They are ferromagnetic materials that show momentary magnetism, cubic crystal structures. Moreover, they are represented as $MO{\cdot}Fe_2O_3$ where M is Fe, Ni, Mn, zinc, or transition metal ion. Ferromagnetism begins when a magnetic field

is applied. The most obvious, they can be magnetized and demagnetized easily. Therefore, they can transfer or store magnetic energy in an alternating or changing wave form. For instance, Mn-Zn ferrites are soft magnets that reach 10 MHz.(Ranganathan and Ray 2002; Sugimoto 1999).

(B) Hard ferrites

They are exploited in magneto-optic media, microwave, telecommunication, recording media, and electronic devices. (Pullar 2012; Ullah et al. 2013) in the absence of a magnetic field; Hard ferrites show ferromagnetism behaviour. After magnetization, they deliver high coercivity (Hc) in addition to remanence (Mr). They consist of iron and strontium or barium oxides; they well manner magnetic flux by a high magnetic permeability at magnetically saturated state.

Generally, the spinel ferrites have magnetic interaction mainly intermediated via oxygen atoms and happen between the spins of metallic cations situated at tetra- and octahedral interstitial spits. A super exchange mechanism rules them, and they are of three types, namely J_{AA} (A-O-A), J_{BB} (B-O-B), and J_{AB} (A-O-B). The distance between the oxygen and the metallic ions controlled and determined the magnitude of these interactions. The A-O-B super-exchange interaction is the strongest one. A-O-A interactions are almost ten folds weaker, and B-O-B is the lowest. In the inverse spinel, the influence of Fe cations at B-sites cancels that of Fe cations at A-sites. Thus, the net moment is only due to the divalent cations at the B-sites. While in normal spinel, the magnetic moment of Fe ions at the B-sites are in an antiferromagnetic orientation.

For spinel ferrites, the magnetization can be calculated by the difference between the contributions of two average sub-lattice magnetic moments, the resultant saturation magnetization (M_s at T = 0) could be written as follows:

$$M_s = \frac{N.d}{M_M}\left[\sum_B n_{B,B} - \sum_A n_{B,A}\right]\mu_B = \frac{N.d}{M_M}\mu_{eff} \quad (1)$$

where, $n_{B,i}$ is the value of Böhr magnetons, μ_B Related to the i site of the unit cell. M_M and d are the molar mass and density of ferrite. While N is Avogadro's number (Silva et al. 2019).

Sherstyuk and his team studied the consequence of Co on the magnetic features and SPIN states in nickel-zinc spinel ferrite. Co^{2+} ions partly replace the Ni^{2+} ions $Zn_{0.3}Ni_{0.7-x}Co_xFe_2O_4$ ($0 \le x \le 0.7$). The difference in ionic radii Co^{2+}/Ni^{2+} can explain the linear increase in the lattice parameters as cobalt increases. They found that Co content increased from x = 0.0 to 0.7 with Curie temperature decreasing from 419 to 326 °C, respectively. Ms, Mr, and Hc values increased. This is because of the more significant moment of cobalt ions compared to nickel ions (Sherstyuk et al. 2021).

Almessiere and co-workers successfully prepared $Mn_{0.5}Zn_{0.5}Dy_xFe_{2-x}O_4$($x \le 0.3$) via ultrasonic irradiation. They found that as Dy^{3+} concentration increases, the saturation magnetization increases. Moreover, the magnetic moment increases with increase the Dy^{3+} 0.952 to 1.173 μ_B at room temperature and increases 2.31–2.54 μ_B at 10 K. Thus, the distance between the magnetic ions reduces, which causes the strengthening of A-B interaction (Almessiere et al. 2020). Tanbir et al. studied the synthesis of $Mn_{0.5}Zn_{0.5}Fe_{2-x}Gd_xO_4$ via chemical co-precipitation procedure and discussed the magnetic behaviour at different temperatures. They found that the saturation magnetization; Ms, decreases as the concentration of Gd^{3+} increases while but coercivity (Hc) increases at 5 K. This may attribute to that La^{3+} magnetic moment of Gd^{3+} (7.94 μ_B) is > the Fe^{3+} (5.92 μ_B), and the Gd^{3+} fill the B-site besides the spin pinning and canting (Tanbir et al. 2020). Feng and his team reported $Mn_{0.6}Zn_{0.4}La_xFe_{2-x}O_4$ synthesis by hydrothermal method and stated that increasing the concentration of La^{3+} decreases the saturation magnetization due to La^{3+} having 0 magnetic moment. Additionally, as the concentration of La^{3+} increases, the anisotropy, magnetic moment, and saturation magnetization decreases (Ding et al. 2020). Jian-ming Gao et al. (Gao et al. 2021) reported that the dopping of zinc into spinel ferrites would significantly enhance the magnetic properties. In numbers, as the substituted Zn content elevated from 0 to 0.50, the Ms will jump from ~ 40 to ~ 59 emu. g^{-1}, and then slightly decrease to ~ 53 emu. g^{-1}. On the contrary, the Hc value declines from ~ 105 Oe to ~ 45 Oe.

Using the hydrothermal method, K.P. Remya et al. (Remya et al. 2020) studied the magnetic parameters for $BiFeO_3$ nanosized synthesized. Magnetic properties discussed at room temperature with the maximum applied magnetic field = 20 kOe. Figure 2 shows the M-H loops of 4 forms of $BiFeO_3$. The bulk $BiFeO_3$ is antiferromagnetic with fragile ferromagnetism behaviour. The values of Ms ranged from 0.27 to 0.67 emu/g for the synthesized forms of $BiFeO_3$. The higher Ms was for the micro-flower form and may be related to the high anisotropy than the other forms (nanoparticles, nanoflakes, and nano-rods).

Ismat Bibi and his colleagues (Bibi et al. 2021) synthesized $La_{1-x}Gd_xCr_{1-y}Ni_yO_3$ nanoparticles via the microemulsion method. The Ms values were more remarkable in Gd^{3+}, and Ni^{3+}-doped $LaCrO_3$ than that of the undoped nanoparticles display the ferromagnetic properties of prepared structures, which steadily elevated by increasing the dopant concentration. The Hysteresis loops curves and the effect of dopant concentration on Ms, Mr, and Hc, respectively, were studied (Bibi et al. 2021).

Jiawei Bai et al. (Bai et al. 2017) studied thin-film perovskite $SrMnO_3$ that formed by molecular beam epitaxy.

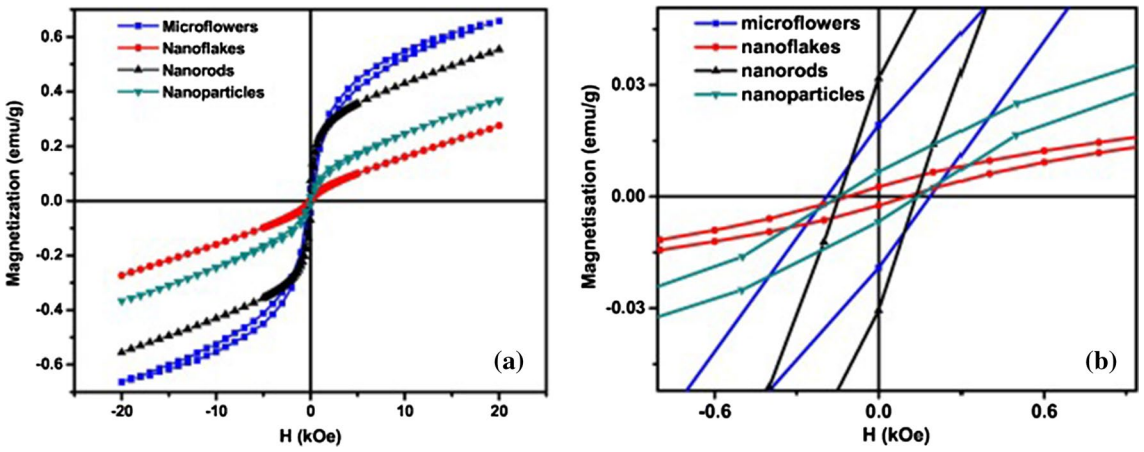

Fig. 2 **a** Magnetic hysteresis loop of morphologically tailored $BiFeO_3$ at room temperature **b** enlarged hysteresis loop of it. Reprinted with permission of Elsevier from (Remya et al. 2020). The bulk $BiFeO_3$ is antiferromagnetic with fragile ferromagnetism behaviour. The values of Ms ranged from 0.27 to 0.67 emu/g for the synthesized forms of $BiFeO_3$. The saturation magnetisation value was 0.36, 0.27, 0.55 and 0.67 emu/g for nanoparticles, nanoflakes, nanorods and microflowers, respectively. The higher saturation magnetization for microflowers could be due to the shape anisotropy arising from the particular arrangement of nanostructured cubes forming the flower-like structure

The Ms ≈ 0.57 μB/Mn, at 3 K and the magnetization (1 kOe FC) rises swiftly below the (temperature ≈ 48–50 K). After oxygen purge, Mn valence changes from + 3 to + 4 and decreases the macroscopic ferromagnetism. The Mn^{3+}-Mn^{4+} double exchange coupling, oxygen vacancies, and strain may be the reason for the observed ferromagnetism in the $SrMnO_3$ thin film.

Hematite is considered a paramagnetic material at (temperature > 956 K, its curie temperature; T_C) and weak ferromagnetic that can undergo a phase transition at Morin temperature (T_M = 260 K) to antiferromagnetic. Generally, the magnetic property of hematite depends on the particle size, the extent of cations substitution, and the crystallinity (Cornell and Schwertmann, 2003; Zysler et al. 2001; Raming et al. 2002). Magnetite is ferromagnetic with a Tc = 580 K. However, Magnetic Particles that are ≤ 6 nm are considered superparamagnetic at room temperature. However, the magnetic behaviour depends on the synthesis method. The magnetic behaviour of magnetic nanosized depends strictly on the crystal charges. Also, the crystal morphology changes the coercivity in the order: Spheres < Cubes < Octahedra as the magnetic axes increase. Thus, Magnetic nanoparticles have Hc = 2.4: 20 KA/m produced by controllable synthesis (Cornell and Schwertmann 2003; Teja and Koh 2009; Meisen and Kathrein 2000).

R.N. Araujo et al. (Araujo et al. 2021) reported a photocatalyst from α-Fe_2O_3 fibres, synthesized via solution blow spinning technique. According to the M-H data, the hematite fibres are soft ferromagnetic material. At 1.5 T field, the magnetization, Remnant magnetization, and the coercivity were M ~ 0.78 emu/g, Mr = 0.22 emu/g, and Hc = 856 Oe, respectively. This magnetization value was relatively high compared to the bulk α-Fe_2O_3, which is (≈ 0.3 emu/g) at 1.5 T and still less than that of hematite nanoparticles (≈ 0 0.83 and 1.11 emu/g) with crystalline sizes (of 35.6 nm and 23.9 nm), respectively. The hysteretic performance is due to the feeble ferromagnetism probable at a temperature (> Morin's transition = 280 K). The small crystallite size permits a more considerable amount of uncompensated Iron magnetic moments on the crystallite exterior (Araujo et al. 2021).

Lassoued and co-workers (Lassoued 2021) have synthesized Zinc-doped α-Fe_2O_3 nanoparticles via the co-precipitation method. M_s was found to decrease as the zinc concentration increased. Zn-doped α-Fe_2O_3 exposed the improved photocatalytic properties within photodegradation of methyl orange. The magnetic data determine that the 6% Zn-doped α-Fe_2O_3 nanoparticles show a minor hysteresis loop that decreases as the synthesised nanoparticles' Zn to Fe ratio increases from 0 to 6%.

Optical properties

The spinel ferrites prevail good photocatalytic performance from their (1) narrow optical bandgap (< 2.2 eV) for efficiently harvesting light of the visible solar spectrum. Usually, they have a band structure between 0.8 and 2.0 V, making them act as good semiconductors. Also, their multiple oxidation states are stabilized by the spinel structure with individual transition metals of known catalytic properties. Besides the lower cost and the availability of their constituent transition metals, they became talented candidates for water purification and large-scale photocatalytic applications. Moreover, the soft band energies classically impart

black or dark reddish-brown colours (Taffa et al. 2016; Casbeer et al. 2012; Kirankumar and Sumathi, 2020b).

Substitution of some elements in the spinel lattices can greatly promote and affect their properties. For instance, Ajeesha and coworkers (Ajeesha et al. 2021b) studied the optical properties of $Mg_{1-x}Ni_xFe_2O_4$ nanoparticles prepared via chemical co-precipitation. From the optical data analysis, the synthesized system confirms an absorption activity in the visible radiation making the system desirable in photocatalytic applications, especially their degradation to the methylene blue (the optical band gaps obtained for the synthesized 3 nanomaterials were 2.13 eV, 2.25 eV, and 2.02 eV). By increasing the substituted nickel, their narrow band gap leading to increasing the photocatalytic activity to be 86% degradation was observed for $Mg_{1-x}Ni_xFe_2O_4$ catalysts after 3 h of degradation. Khalid Hussain et al. (Hussain et al. 2021b) synthesized nanosized $Cu_{0.5}Cd_{0.25}Co_{0.25}Fe_{2-x}O_4$ doped with Ce^{3+} and studied its optical properties. The indirect energy band gaps (E_g) decreased from 3.48 to 2.50 eV at 303 K with Ce^{3+}. This reduction in (E_g) is due to the increment in the hooping of electrons between di and trivalent iron ions. Another study, published by Heidari et al. (Heidari and Masoudpanah, 2021), focused on the optical properties and photocatalytic performance of Mg-Ca ferrites. They found that the Ca^{2+} can decrease the band gap energy from 1.97 to 1.87 eV, favouring photocatalytic activity. Although the $MgFe_2O_4$ presented the highest photodegradation efficiency (~63%) under visible illumination, the photodegradation rate of Methylene Blue dye decreased and then increased with the addition of Ca dopants. Asma and her team (Aslam et al. 2021b) proposed the synthesis of lanthanum-doped $Zn_{0.5}.Co_{0.5}.La_x.Fe_{2-x}.O_4$ by co-precipitation method and evaluate their optical properties. The resulted ultraviolet–vis pattern of La^{3+}-doped Zn-Co ferrite samples is shown in Fig. 3.

The optical behaviour of the polycrystalline perovskites is better than that of the single counterpart due to their enhanced optical properties in many optical-dependent applications such as photocatalysis, photovoltaics, scintillation, and displays, and others (Chen et al. 2016a; Yang et al. 2018). The majority of double perovskite oxides are like single perovskite in their ability to absorb light only in the Ultraviolet region with a high electron–hole recombination rate resulting in low photocatalytic efficiency. Fortunately, in double perovskite oxides, the facility to flexibly change the ions of the A or B sites makes it relaxed to modify the optical properties to fascinate the photocatalytic properties. Moreover, the little interaction between the double perovskites facilitates the introduction of hetero-cations, increasing the light absorption range and advancing photocatalytic activity (Chen et al. 2016a; Ma et al. 2021). M. Bhuyan and his colleagues focused on the optical properties of Gd_2FeCrO_6 nanoparticles as a double perovskite. The tested material was synthesized via sol–gel and Ultraviolet–Visible, and PL spectroscopy ensured the semiconducting nature of fabricated material and unveiled an optical band gap of 2.0 eV. Thus, the thermally stable as-synthesized Gd_2FeCrO_6 semiconductors were utilized in photocatalytic and solar energy applications due to their ability to absorb the visible spectrum of solar light (Bhuyan et al. 2021b). Alsabah et al. (Alsabah et al. 2019) studied

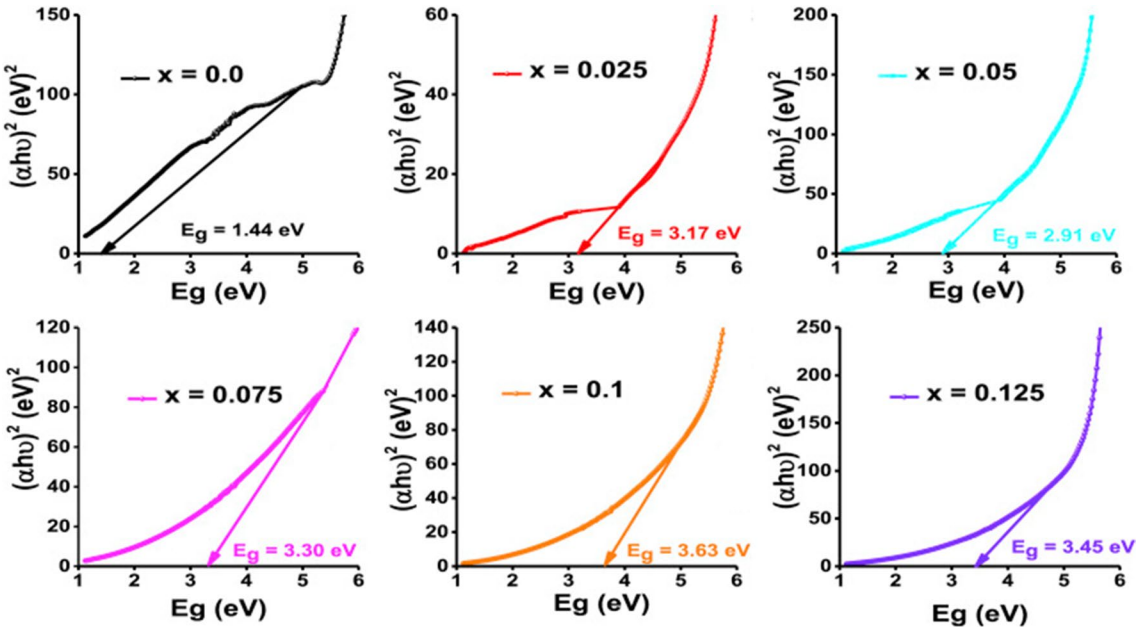

Fig. 3 Tauc plot for La^{3+} doped Zn-Co ferrites. Reprinted with permission of Elsevier from (Aslam et al. 2021b). The optical bandgap of lanthanum-doped $Zn_{0.5}.Co_{0.5}.La_x.Fe_{2-x}.O_4$ varied between 1.44 eV at x = 0.0 to 3.63 eV at x = 0.3

the optical properties of A_2YVO_6 (A = Mg, Sr) double perovskite oxides. The optical absorption performance of an insulator was evaluated based on the bandgap energy. The bandgap energy of Mg_2YVO_6 was 2.9 eV, while the value in the case of Sr_2YVO_6 was 2.48 eV. Another perovskite oxide, the two-dimensional Ruddlesden−Popper perovskites with $A_{n-1}A'_2B_nO_{3n+1}$ as a formula composed of $nABO_3$ layers between two A′O rock salt layers. They have attention due to their unique optical and electronic properties, making them a talent for photocatalytic water splitting and water remediation. Doping in the A- and O- sites can suppress the band gap. Non-metal "N" doping in the X-site of RP perovskites enhanced the photocatalytic performance under visible light illumination. (Xiao et al. 2020).

Nasab et al. (Nasab et al. 2021) succeeded in preparing praseodymium titanate nanoparticles loaded on core–shell silica-coated magnetite. The optical band gap energies (OBGE) of Fe_3O_4, Fe_3O_4@SiO_2, and Fe_3O_4@SiO_2@$Pr_2Ti_2O_7$ were ≈ 3.1, 3.05, and 2.96 eV, respectively. These values are smaller than TiO_2 nanoparticles, which equal ≈ 3.2 eV indicate that the praseodymium titanate nanoparticles reduced the band gap of titanium dioxide. The photodegradation of Methylene orange in the presence of Fe_3O_4@SiO_2@$Pr_2Ti_2O_7$ nanoparticles was detected. Photoluminescence spectroscopy results supported these data. After around 45 min, ≈ 98% of methylene orange was removed in the presence of the optimal core–shell nanosized catalyst. Juan et al. (García et al. 2021) studied a photoactive semiconductor nanomaterial (magnetite nanoparticles embedded in a bismuth ferrate matrix using a microwave-assisted hydrothermal approach. The as-fabricated bismuth ferrate samples display a 2nd absorption wavelength 535 nm equivalent to an energy value of ~ 2.3 eV that matched the stated E_g for bismuth ferrate bulk systems. The optical description of the magnetic nanoparticles permits us to detect an absorption pattern like that of the semiconductor a bismuth ferrate with (a bandgap energy ≈ 1.6 eV), encouraging the possibility of substitutes for heterogeneous catalysis.

Emre and his team (Alp et al. 2021) studied the plasmonic photocatalytic activity of hematite nanostructures decorated with Au nanoparticles synthesized via the hydrothermal method. The plasmonic Au nanostructures are known to offer efficient solar energy conversion of semiconductors. Mostly, the plasmonic Au nanosized displayed a broad absorption wavelength from ultraviolet to near-infrared spectroscopy that could vary according to their shape, size, surrounding medium, and high light-harvesting efficiency upon the localized surface plasmon resonance-effect. (Abouelela et al. 2021) Popov et al. (Popov et al. 2021) reported the effect of Cr doping on the α-Fe_2O_3 nano-rods. Ultraviolet and near-infrared spectroscopy of $(Fe_{1-x}Cr_x)_2O_3$ revealed that doped Cr narrows the optical band gap for the hematite and thus expands the absorption of hematite, which increases the photocatalytic and photoelectrochemical performance in visible light (Popov et al. 2021).

Photodegradation performance

Nanoferrites are widely employed in information storage systems, magnetic fluid technology, microwave devices, and other applications because of their superior electromagnetic properties, high permeability, and capacity to absorb electromagnetic waves (Ahmed et al. 2021b).

Ajeesha, T. et al. have produced spinel $Mg_{1-x}Ni_xFe_2O_4$ (x = 0.0, 0.6, 1.0) nanoparticles through the chemical co-precipitation method, and their structural, magnetic, optical, and photocatalytic properties were investigated (Ajeesha et al. 2021b). The results obtained showed a cubic spinel structure with an average crystallite size around 20–30 nm. The loops collected results revealed ferrimagnetism and magnetically soft ferrites because of its magneto-crystalline anisotropic effect. The spinel ferrites' semiconducting characteristics were discovered through optical research, which also proved the absorption activity in the visible region, indicating that the synthesized materials are acceptable for photocatalytic applications, which were tested to degrade methylene blue. Fenton-like degradation of methylene blue was used to investigate the catalytic activity of nanoparticles of pure and substituted spinel ferrites. Recyclability studies were used to assess the photocatalysts' stability. Even after five cycles, no substantial degradation of nano photocatalysts was observed. The photocatalytic results showed that under visible light illumination, nickel substituted spinel ferrite had better catalytic activity than pure spinel ferrites, which could be owing to the small particle size of a nickel, the narrow bandgap energy, and increased (e/h +) separation at the catalyst surface (Almessiere et al. 2019; Slimani et al. 2019).

The photo-spinel nano ferrites are seemed to be promising photocatalysts to degrade dyes from wastewater. So (George et al. 2021) synthesized copper substituted magnesium ferrite Cu–$MgFe_2O_4$ spinel nanoparticles using the co-precipitation method. The lack of electron exchange between Fe^{2+} and Fe^{3+} ions caused the dielectric constant of the produced nanomaterials to decrease with increasing frequency. Nanoparticles have a smaller crystalline size and a larger surface area, making them magnetic heterogeneous photocatalysts that aid in transferring photo-induced load carriers. Furthermore, motivate the degradation of methylene blue dye.

Another technique used to produce spinel ferrite nanoparticles is microwave irradiation, which causes a rapid increase in the heat of the precursor due to intermolecular friction.

Products were generated in a matter of minutes with higher yields (Manikandan et al. 2015).

(Geetha et al. 2021) have used aloe vera plant extract as a biofuel to produce cerium substituted spinel $MgFe_2O_4$ ferrite nanoparticles using microwave combustion. The results obtained confirmed the formation of spinel structure cubic. The photocatalytic behaviour of malachite green dye was examined under visible light irradiation, with an efficiency of 98.94% achieved in 90 min. The synthesized catalyst has superior structural and photocatalytic stability, as well as a greater degradation efficiency. The catalyst could be used in the treatment of industrial effluent.

Also, (Mohan et al. 2021) investigated the spherical zinc ferrite (Zn/Fe_2O_4) nanoparticles with a bandgap of 2.00 eV as evenly sized (65 0.5 nm) nanoparticles in the visible light region and used for photocatalytic degradation of carbamazepine. Zn doping reduced the bandgap (from 2.00 to 1.98 eV) and increased visible light absorption. Zinc doping also resulted in successful photogenerated carrier separation and subsequent charge migration to the $ZnFe_2O_4$ nanoparticle's surface. Because of the material's benefits, a high removal efficiency (100%) of carbamazepine was attained through photocatalytic degradation. Carbamazepine degradation has pseudo-first-order kinetics, with a rate constant of 0.0367 min 1. The in-vitro and in-vivo toxicity of nanoparticles were investigated to promote environmental consequences.

(Ahmed et al. 2021b) used rare-earth to replace nickel-zinc ferrite by utilizing a sol–gel auto-combustion synthetic process with metal nitrates, citric acid ethylene–glycol, and ammonia as precursors. They also looked into the magnetic, and magnetocaloric properties of spinel ferrite substituted gadolinium and their photocatalytic efficacy. When Gd^{3+} replaced a portion of Fe^{3+}, the Curie temperature rose. At the Curie temperature, the most significant change in magnetic entropy of the samples occurred. They also proved that the gadolinium substitution ferrite nanoparticles are nanoporous in nature. As a result, the photocatalytic degradation performance of nanoparticles demonstrates their efficiency as photocatalysts capable of degrading various organic dyes when irradiated with multiple wavelengths of light and has provided advice for the construction of more efficient photocatalysts.

Zinc ferrites semiconductors have a small bandgap (1.9 eV). They are preferred for researchers due to their advantages: easy controlling, magnetic property, inexpensive preparation, better reproducibility, and others. Zinc ferrite semiconductor is doped with other magnetic ferrites to get favourable photocatalytic activity. So, it is doped with cobalt. As a result, their bandgap becomes narrower, and the absorption is shifted to the visible range (Fan et al. 2012). Cobalt spinel nano-ferrites have enhanced photocatalytic efficiency. Chahar et al. [10] used cobalt–zinc ferrite to degrade methylene blue with irradiation of visible light observed that the efficiency of removal for the dye of methylene blue was increased with increasing the concentration of cobalt. The removal efficiency of methylene blue dye had a maximum value (77%) for $X = 0.5$ and a minimum value (65%) at $X = 0.0$, where the composite equation was $Co_xZn_{1-x}\ Fe_2O_4$. So, cobalt–zinc ferrites have intense catalytic degradation activity for the treatment of water and removing organic pollutants. This mechanism is safe for the environment.

Cobalt ferrites have a great interest due to their advantages, such as enhanced electrical parameters and absorption applications within the microwave range. Graphene is used for making nanocomposites due to its large surface area. Graphene-based nanocomposites are very useful for water treatment. Metals such as Mg can be used to make composites with graphene due to their stable properties, enhancing their biological properties. Zirconium as a dopant in the magnesium–cobalt spinel nano-ferrite $Mg_{0.2}Co_{0.8}Fe_2O_4$ used by (Shabbir et al. 2019). As a result, the electrical resistivity was decreased. The spinel ferrites were dispersed on graphene sheets. The electrons were excited to conduction band under ultraviolet/visible light; the charge transfer was increased, preventing the recombination of electrons and holes. The photo-degradation activity was investigated using methylene blue dye irradiating with UV visible light. The time of degradation of methylene blue by graphene composite was less than that without graphene. The degradation activity of zirconium doped in the magnesium-cobalt spinel nano-ferrite and zirconium doped in the magnesium-cobalt spinel nano-ferrite activated with reduced graphene oxide were investigated using alizarin yellow R dye irradiating. The performance of photo-degradation by zirconium doped in the magnesium-cobalt spinel nano-ferrite activated with reduced graphene oxide was 92.49% in 70 min, while the performance of photo-degradation by zirconium doped in the magnesium-cobalt spinel nano-ferrite was 52.45% in 120 min. The higher performance of graphene composites was due to large surface areas and low magnetization (Ahmed et al. 2021c).

Rhodamine B is a water-soluble organic compound that is used in industries. It harms the environment and significant resistivity to be degraded. Zinc spinel ferrite doped with carbonate-rich lanthanum and dispersed in reduced graphene oxide nanocomposites in the photo-degradation of Rhodamine B dye using ultraviolet light activated by peroxydisulfate (Fig. 4) (Jun et al. 2020). Sulfate radicals such as peroxydisulfate have a high oxidative character under oxidation–reduction (redox) reaction (2.5–3.1 V). So that, magnetic nanohybrid materials were activated with persulfates to get higher degradation efficiency. Due to the large surface area of graphene oxide, reduced graphene oxide has a great interest for photocatalytic degradation to prevent

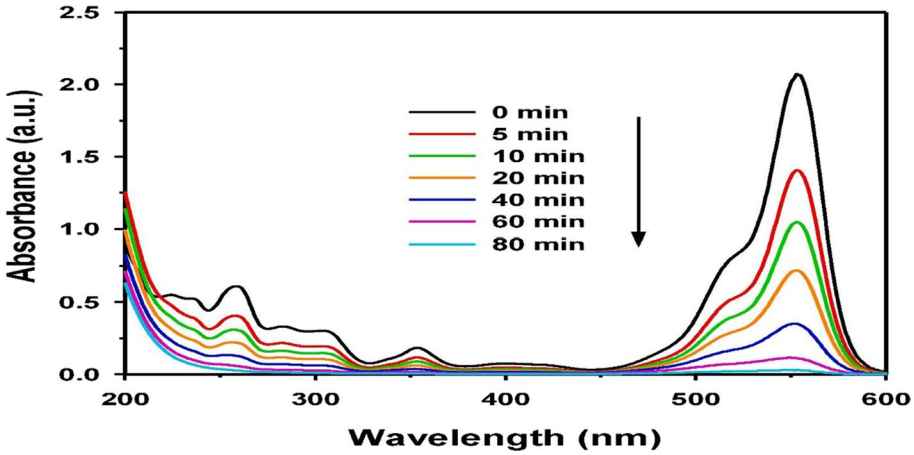

Fig. 4 Spectra of Rhodamine B degradation at different time intervals. Reprinted with permission of Elsevier from (Jun et al. 2020). The degradation performance of carbonate-rich lanthanum-substituted zinc spinel ferrites had twice the performance of zinc spinel ferrites dispersed in reduced graphene oxide

electron–hole recombination. Zinc ferrites have a very narrow bandgap, which is favourable for photocatalytic degradation. Carbonate-free materials have low photocatalytic degradation efficiency. So that, Carbonate-rich species such as lanthanum overcome electron–hole recombination and enhance the photocatalytic degradation activity. The degradation performance of carbonate-rich lanthanum-substituted zinc spinel ferrites had twice the performance of zinc spinel ferrites dispersed in reduced graphene oxide. As a result, carbonate-rich lanthanum zinc spinel ferrites dispersed in reduced graphene oxide nanocomposites had the best performance in degrading rhodamine B using ultraviolet light activated by peroxydisulfate.

Aluminium-substituted zinc spinel ferrites have great interest in the degradation of harmful dyes due to their magnetic and photocatalytic properties. The magnetic behaviour of zinc spinel ferrites is significantly affected by the substitution of nanoparticles; the substitution of aluminium nanoparticles reduces the magnetic saturation. The synthesis of zinc ferrites within the nanoscale makes their behaviour extremely maximum. The methylene blue dye is exposed to degradation via aluminium-substituted zinc spinel ferrites by (Gul et al. 2020). It was observed that the performance of photo-degradation of the dye by aluminium-substituted zinc spinel ferrites was 55% in 120 min. Aluminium- zinc ferrites are favourable in water treatment due to their safe properties for the environment. Due to their magnetic properties, they can be easily removed from water by a magnet.

Magnesium ferrites are semiconductors of N-type crystals. They are soft-magnetic materials with low coercivity and can easily change their magnetization under the external magnetic field. Cobalt ferrites are hard-magnetic materials that have high coercivity that can maintain their magnetic behaviour. It was observed that introducing the cobalt into magnesium ferrites reduces the bandgap. The bandgap of magnesium ferrite is 2.09 eV. By increasing the cobalt substitution, the bandgap decreases to 1.42 eV, the coercivity and magnetization were increased. The magnetization also was raised with the substitution of cobalt. As a result, the hysteresis loops become broadened.

Cobalt substituted magnesium ferrites were used to explore their performance for the degradation of methylene blue dye under visible light (Dojcinovic et al. 2021). The performance of photo-degradation by cobalt substituted magnesium ferrites was 79% in 4 h.

Cobalt ferrites are hard-magnetic materials that have high coercivity. Nickel has less magnetic moment than cobalt. The magnetic behaviour is significantly affected by the concentration of nickel. By the substitution of nickel into cobalt ferrites, the coercivity decreases. Subsequently, the hysteresis loop is strongly influenced. The photocatalytic activity also increases by the substituting of nickel into cobalt ferrites.

Nickel substituted cobalt ferrites were used to explore their performance for the degradation of methylene blue dye under visible light (Lassoued and Li 2020). The version of photo-degradation was 79% in 150 min. Conge red is an azo dye that harms health, the environment and can cause cancers. It is a water-soluble dye that is difficult to be removed from the water and causes pollution.

The effect of doped and un-doped nickel substituted cobalt ferrites on the degradation of congo red dye explored by (Abbas et al. 2021). Nickel substituted cobalt ferrites were doped with bismuth to enhance the photocatalytic behaviour. Bismuth has a large surface area and promotes electron–hole pairs formation, which is great for photocatalytic degradation. The degradation performance of doped nickel–cobalt ferrites was 96%, while undoped nickel–cobalt ferrites' performance was 78%.

Titanium oxide substituted copper-magnesium ferrite was used to degrade rhodamine B dye with visible light irradiation (Tran et al. 2021). Copper-magnesium ferrite has bandgap of 1.65 eV. Titanium oxide has a high bandgap energy (3.25 eV). Doping copper-magnesium ferrite with Titanium oxide shifted the bandgap (1.65 eV to 2.86 eV), and the charge separation was strongly increased. As a result, it is

recommended for photocatalytic activity and can easily be removed from water using a magnetic bar. The degradation activity was investigated using rhodamine B dye irradiating with visible light. The performance of photo-degradation by copper-magnesium ferrite was 21.5%, while the performance of photo-degradation by titanium oxide substituted copper-magnesium ferrite was 100% in 3 h. Subsequently, it has a great interest in water treatment.

Mixed Zn–Ni spinel ferrites using the solvothermal reflux process synthesized by (Manohar et al. 2021). In a photoreactor, they investigated the photocatalytic activity of the samples by degrading organic methylene blue dye under visible light. The data reveal that when the Ni^{2+} concentration in the sample increases, so does the degradation efficiency. Photocatalytic activity reaches 96.21 per cent at $x = 0.5$ Ni^{2+} concentration.

Also, (Febrialita et al. 2021) used Simbang Darah (Iresine herbstii) leaf extract to manufacture $ZnFe_2O_4$ spinel ferrite nanoparticles hydrothermally. The biochemical components in Simbang Darah leaf extract work as a capping agent and a stabilizer. After two hours of solar light irradiation, $ZnFe_2O_4$ nanoparticles were effective in direct red 81 dye photo-degradation (99.66 per cent). $ZnFe_2O_4$ calcination transforms ferrite behaviour from paramagnetic to superparamagnetic. Because it can be separated from the liquid using an external magnetic field, magnetic characteristics proved the usefulness of zinc ferrite as a photocatalyst. As a result, these materials can be applied to subsequent photocatalytic processes.

Also, (Jadhav et al. 2021) produced Ni–Zn spinel ferrite using urea as a fuel in the sol–gel auto combustion process. They evaluated the produced samples for the elimination of Rhodamine B from the industrial wastewater. The photocatalytic activity of the produced nanoparticles was tested under daylight, and the percentage of maximal degradation reached 98 per cent at 180 min. This solar response is seen due to the reduced bandgap energy of the produced nanoparticles, ranging from 1.91 to 2.75 eV.

Besides, (Makofane et al. 2021) investigated the Photocatalytic degradation of methylene blue and sulfisoxazole from water using the green produced Zinc ferrite nanoparticles ($ZnFe_2O_4$) by the hydrothermal process employing the plant extract. The best conditions for the 99.8 per cent elimination of methylene blue was achieved at pH12, in 45 min and at the optimal value of 25 mg of the catalyst. The as-prepared $ZnFe_2O_4$ nanoparticles demonstrated to be readily separated and reused and kept effective even after five reuses, indicating that the material is highly stable. Upon examining the photocatalytic efficiency of the sulfonamide antibiotic, sulfisoxazole in water revealed degradation of 67%. The optical energy bandgap of the produced nanoparticles was determined to be 2.32 eV. From the optical absorption investigation, the nanoparticles of $ZnFe_2O_4$ were determined to be in the ultraviolet range with green emission. Magnetic research demonstrated that an external magnetic field might separate the $ZnFe_2O_4$ photocatalyst. The prepared sample displayed superparamagnetic properties under the action of an external magnetic field. This study has proven that these materials can be employed in targeting textile and pharmaceutically polluted water. This work has confirmed that it is possible to manufacture an ecologically friendly photocatalyst used in textiles and pharmaceutical products for waste-water treatment.

(Magdalane et al. 2021) tested microwave synthesized porous $CoFe_2O_4$ and TiO_2-doped $CoFe_2O_4$ nanostructures using L-threonine as a fuel for the photocatalytic degradation of congo red dye on visible light irradiation. The measured bandgap of the corresponding $CoFe_2O_4$ and TiO_2-doped $CoFe_2O_4$ nanostructures are 3.01 and 2.88 eV. The overall percentage of decomposition of congo red dye was 85% and 97% with only catalyst and catalyst/H_2O_2 at pH value 3.0. The decolourization of dye solution was observed nearly at 120 min in the acid medium. Nevertheless, in the case of only catalyst, the dye was decomposed after 250 min.

(Meena et al. 2021) examined the catalytic performance of Ce-doped $MnFe_2O_4$ ferrites under daylight. The optical bandgap was estimated and was found about 2.3–2.8 eV. An outstanding photocatalytic performance of cerium-doped $MnFe_2O_4$ ferrites (3 mol%) towards methylene blue and alizarin red dye degradation was reported to be 1.5 and 1.67 times higher than the host matrix under sunlight irradiation linked to the decreased bandgap, Ce dopant, and effective separation of charge carriers. the Ce-doped $MnFe_2O_4$ degraded methylene blue and alizarin red dye with 98 and 89% under Solar irradiation.

Tony and his group (Dhiwahar et al. 2021) examined the improved photocatalytic decomposition of rhodamine B with visible light employing Ni-doped copper ferrite spinel nanostructures. The Kubelka–Munk model was applied to evaluate the bandgap energy of $Cu_{1-x}Ni_xFe_2O_4$ and observed to fluctuate from 2.30 to 2.06 eV. The photo-degradation efficiency when rhodamine B dye was exposed by visible light was 99.6 per cent.

Perovskite-type oxides have been intensively explored for various applications due to their flexible structure (Fodil and Omari 2017; Fodil and Omari 2016; Souza and Muccillo 2010; Hu et al. 2005; Teraoka et al. 2006). Recently, (Jamil et al. 2018) used The Pechini methods to prepare $BaFe_{1-x}CuxO_3$ nanopowders ($x = 0.01$,0.05, and 0.10), then investigated them as photocatalysts for the degradation of atrazine. Toxicity testing revealed that all the manufactured components and the treated water are suitable for use in water treatment. The best reaction conditions were the pH 11, 120-min irradiation time, and 0.75 g/L catalyst loadings. Pseudo-order kinetics were observed in the reaction. The ring breakage formed short

organic chains mineralized to carbon dioxide and water with ammonia release; the copper-doped phases had higher activity. When Fe^{4+} is partially substituted with Cu^{2+}, the oxygen vacancy increases, resulting in an improved activity, this finding is consistent with prior research that has shown the importance of surface defects in preventing electron/hole recombination. However, barium oxides are unstable in the presence of CO_2, resulting in the catalyst's complete breakdown into barium carbonate and amorphous iron oxide species. This is most likely the cause of the catalyst's deactivation over time. Copper-doped samples have better catalytic characteristics, which opens up new possibilities for oxygen-deficient perovskite as a photocatalyst.

One of the most efficient methods for the degradation of wastewater is semiconductor photocatalysis. Photocatalytic activity of metal oxides such as TiO_2, ZnO, and ZnS (Etacheri et al. 2012; Etacheri et al. 2013) is well recognized. Because of its excellent chemical stability, low cost, and high catalytic performance, TiO_2 has been widely employed as a photocatalyst. A complex polymeric method was used to synthesize cubic and tetragonal phase $BaTiO_3$ nanoparticles and use methylene blue dye to investigate the photocatalytic activities of cubic and tetragonal $BaTiO_3$(Kappadan et al. 2016). The results showed that the photocatalytic activity of tetragonal $BaTiO_3$ was greater than that of cubic $BaTiO_3$. The photoluminescence results also supported the increased photocatalytic activity of tetragonal $BaTiO_3$. However, altering the quantity of $BaTiO_3$ resulted in a substantial shift in the photocatalytic property.

Calcium titanate ($CaTiO_3$) is the first known orthorhombic perovskite mineral made of readily available and low-cost components. The crystal structure is stable ensures that it can endure continuous and long-term photochemical reactions in the presence of water. However, the wide bandgap of about 3.6 eV restricts its photocatalytic response only within UV light irradiation (Jang et al. 2011; Huo et al. 2014; Kwak and Kang 2015). Therefore (Pei et al. 2019) overcome this disadvantage by creating nano-sized calcium titanate $CaTiO_3$ powder with a hierarchical structure and an expanded adsorption profile in the visible light area using a hydrothermal reaction polyvinyl alcohol as a structure-directing agent. They proved that the bandgap narrowing and improved separation efficiency of photogenerated charge carriers were related to oxygen vacancies created with the hierarchical web structure, which improved photocatalytic activity in response to visible light. This work gives excellent information on the design and production of other perovskite materials and visible light active semiconductor photocatalysts for improving solar-driven photocatalytic performance, as the yellow $CaTiO_3$ had a much higher visible-light-driven photocatalytic hydrogen production performance than white $CaTiO_3$.

$SrTiO_3$ has been demonstrated to be one of the few efficient catalysts capable of splitting pure water into H_2 and O_2 (Wang et al. 2015b). However, Due to its excessively high bandgap, it can only respond to UV light. (about 3.1 eV) (Luo and Maggard 2006; Townsend et al. 2012).

Chen and his group (Chen et al. 2016b) produced a polymerizable complex method of photocatalysts of Cr/Ta co-doped $SrTiO_3$ (STO: Cr/Ta). Moreover, the data revealed that the photocatalyst has a high photocatalytic activity for water splitting under visible light and was responsible for good photocatalytic performance. The photocatalysis activity (1 per cent Cr/Ta) for H_2 evolution obtained using a polymerizable complex technique is ten times higher than the sample prepared by a solid-state reaction. This requires a high reaction temperature and a long reaction time, resulting in a low surface area. Compared with the polymerizable complex method, low photocatalytic activity enhances the high crystalline quality and relatively large specific surface area photocatalytic activity.

Also, (Liu et al. 2021), by using a thermal treatment process, synthesized surface reconstructed $SrTiO_3$ nanocrystals in the presence of $NaBH_4$ and $SrTiO_3$ nanocrystals. The photoelectrochemical characteristics of the material were investigated using a traditional three-electrode setup.

The introduction of surface oxygen vacancies or Ti sites (such as in $SrTiO_3$ nanocrystals) is credited with surface reconstruction during the hydrogenation procedure process. Due to surface oxygen vacancies or Ti sites (such as Ti^{3+} and Ti^{2+}), the light absorption and charge-transfer capabilities of $SrTiO_3$ nanocrystals are both increased. Photocatalytic water splitting benefits from the presence of titanium dioxide (Ti^{2+}). Also, it was found that the sample of $SrTiO_3$ at 350 °C still maintains a stable photocatalytic activity after three recycles, demonstrating that $SrTiO_3$ has good stability.

On the other hand, (Kumar et al. 2021) presented an in-situ hydrothermal approach for fabricating a new solar active heterojunction Fe_3O_4@$SrTiO_3$/$Bi_4O_5I_2$. The anti-inflammatory medicine diclofenac was used as a target pollutant, and the heterojunction was used to degrade and mineralize it under the influence of simulated sun irradiation. According to current findings, the optimized junction removed 98.4 per cent diclofenac in 90 min and had 87.2% mineralization, and the degradation rate was about six times that of bare $SrTiO_3$. However, the operational parameters for removing diclofenac have been set. The catalysts showed high optical activity, high photocurrent response, and charge transfer capacity. According to the results obtained, both OH and O_2 radicals are active species in diclofenac degradation. The removal efficiency is high, and the catalyst may break down diclofenac in waste-water conditions.

Perovskite oxides have promising efficiencies for photocatalytic activity due to their advantages. Double perovskites have high adsorption activity for light, good stability, and

electric properties. The synthesis of perovskite in nanoscale has a great interest due to its high surface area and crystallinity. Recently (Cui et al. 2020) used $SrFe_{0.5}Ta_{0.5}O_3$ to degrade nitric oxide (NO) with visible light irradiation. The bandgap of $SrFe_{0.5}Ta_{0.5}O_3$ is 2.06 eV (visible light range) due to the presence of Fe^{3+}. It was observed that $SrFe_{0.5}Ta_{0.5}O_3$ nanoparticles have a high density of photocurrent and prevent electron–hole recombination. Under visible light irradiation, the performance for the removal of nitric oxide by $SrFe_{0.5}Ta_{0.5}O_3$ was 35.1% in 80 min.

Recently, (Sahni et al. 2021) used bismuth ferrites doped by Yb/Co to explore their performance for the degradation of methylene blue dye under visible light. Bismuth ferrites $BiFeO_3$ are multiferroic materials that are recommended for the degradation of harmful dyes in water treatment. Bismuth ferrites have a bandgap of 2.2 eV (visible range). To improve their magnetic and photocatalytic properties, they were doped with rare-earth metals such as ytterbium (Yb) due to their unique properties. They were also doped with cobalt element to improve their magnetic behaviour. By substituting ytterbium (Yb^{3+}) and cobalt (Co^{2+}), the bandgap decreased to 1.88 eV, preventing electron–hole recombination and increasing their transferring. It was observed that there was an increase in magnetization and coercivity. Under visible light irradiation, the performance for removing methylene blue by pure bismuth ferrites was 76% in 100 min. At the same time, the performance for removing methylene blue by bismuth ferrites doped by Yb/Co was 99%.

Chen and his group (Chen et al. 2017) explored the efficiency of bismuth ferrites activated by oxygen vacancy surface on the degradation of methyl orange. Oxygen vacancy is recommended for photocatalytic activity. As the oxygen vacancy surface activated the bismuth ferrites, the bandgap became narrower. Subsequently, the surface of oxygen vacancy became an active surface for photo-induced electrons and prevented electron–hole recombination. So, the bismuth ferrites reinforced by oxygen vacancy surface have favourable efficiencies for degradation of methyl orange.

Yu and his group (Yu et al. 2016) investigated the performance of $NaNbO_3$ of different morphologies on photocatalytic applications. It was observed that $NaNbO_3$ nanoparticles of pyramid morphology have higher efficiencies of photo-degradation than that of cubic systems. Dichlorophene and rhodamine B were used to investigate their different Photocatalytic efficiencies with irradiation of Xenon arc lamp. When $NaNbO_3$ was exposed to the Xenon arc lamp, the electron–hole pairs were formed, and a group of reactive chemicals was generated from O_2, such as O^{2-}, OH and H_2O_2. This group of reactive chemicals act as active centres for photo-induced electrons and prevented electron–hole recombination. Different morphologies generated from the variations on crystal growth have other effects on photocatalytic applications. So, the $NaNbO_3$ triangular nanoparticles with facets have higher photo-degradation efficiencies than that of cubic system with facets of 100.

(Bradha et al. 2015) explored the effect of substitution on the photocatalytic activity of $LaTiO_{3.5-\delta}$ perovskites. The general form of perovskite is ABO_3. The role of the B site is that promote electron transfer which gives high efficiency of photocatalytic activity. The part of the A site is to stabilize the valence electrons of the B-site. The substitution in the A site improves photocatalytic activity and decreases the bandgap. Lanthanum (A-site) increased the photo-degradation significantly. The substitution in A site was investigated using bivalent alkaline earth elements such as Ba, Ca and Sr. The bandgap was shifted to a lower value by substituting alkaline earth elements such as Ba, Ca, and Sr. The photo-degradation activity was investigated using Congo red dye. $La_{0.8}Ba_{0.2}TiO_{3.5-\delta}$ have the higher performance to degrade the Congo red dye in a short time. Under visible light irradiation, the performance for the removal of Congo red dye by $La_{0.8}Ba_{0.2}TiO_{3.5-\delta}$ was 75.33% in 10 min and after 60 min; the performance of that was 81%. The performance for the removal of Congo red dye by $La_{0.8}Ca_{0.2}TiO_{3.5-\delta}$ and $La_{0.8}Sr_{0.2}TiO_{3.5-\delta}$ was 70.92% in 60 min. %. While the performance for removing Congo red dye by $LaTiO_{3.5-\delta}$ was 50.8% after 60 min.

Zhou and his group (Zhou et al. 2019) investigated the photocatalytic activity of lanthanum nickelate $LaNiO_3$ activated with graphitic carbon nitride sheets. Graphitic sheets of carbon nitride (g-C_3N_4) have a small bandgap of 2.7 eV but have small photocatalytic activity due to enhanced electron–hole pair recombination. Hybridization of graphitic sheets of carbon nitride with $LaNiO_3$ formed a Z-scheme system leading to enhanced photocatalytic activity with a favourable bandgap. Formation of Z-scheme system increased transferring of charges, have high reduction–oxidation activity and prevented election-hole recombination. Lanthanum nickelate $LaNiO_3$ activated with graphitic sheets of carbon nitride had favourable photo-degradation activity. It was observed that the performance of the Z-scheme system for the degradation of tetracycline was 96% in 5 h under irradiation of visible light. O^{2-} formed, which promotes oxidization of tetracycline and degrades tetracycline strongly.

The photo-degradation activity of $SrTiO_3$ injected by silver nanoparticles was investigated by (Wu and He 2018). Titanium dioxide has strong, stable oxidative properties with no harmful effect on water treatment, but it has a high bandgap and can be excited only by ultraviolet light. The intensity of light in the ultraviolet region is very low, reducing their photo-degradation activity. So the performance of degradation of dyes using $SrTiO_3$ is low. Modifying $SrTiO_3$ surface by silver nanoparticles decreased the bandgap and improved their photocatalytic performance due to the surface plasmon resonance of silver nanoparticles. Reactive oxygen species were generated on the surface of degradation and played

an essential role in decreasing electron–hole recombination and increasing the degradation rate. The photo-degradation activity of $SrTiO_3$ injected by silver nanoparticles was confirmed under rhodamine B and methylene blue degradation with irradiation of visible light. The performance of degradation of rhodamine B was 93.5% in 1 h. At the same time, the performance of degradation of rhodamine B was 94.7%.

The increased visible light photocatalytic performance of curcumin-sensitized perovskite $Bi_{0.5}Na_{0.5}TiO_3$ for rhodamine 6G decomposition was evaluated by (Kushwaha and Vaish 2016). The photocatalytic breakdown of Rhodamine 6G depends on both the oxygen species and photo-induced holes. In the presence of $^{\cdot}OH$ scavengers and $O_2^{\cdot}$ scavengers, decomposition of rhodamine 6G was 46 per cent and 31 per cent, respectively. These data demonstrate that the deterioration process is highly dependent on photogenerated holes. The produced holes play a crucial function in forming active oxygen species and breaking down organic species.

The improved catalytic performance of $LaFeO_3$/Bentonite nanoparticles to remove methylene blue was investigated by (Janaki et al. 2018). Decomposing methylene blue assessed the photocatalytic activity of all the produced samples under visible irradiation. The synthesized $LaFeO_3$/Bentonite displayed extraordinary and excellent photocatalytic activity with the overall elimination rate of methylene blue up to 95 per cent for 60 min.

Perovskite $Sr_{1-x}Ba_xSnO_3$ for photocatalysts applications produced by (Alammar et al. 2017). The bandgap drops with increasing Ba^{2+} concentration from 3.85 eV to 3.19 eV. Furthermore, the photocatalytic capabilities were tested by the hydroxylation of terephthalic acid. The maximum photocatalyst effect was detected for $Sr_{0.8}Ba_{0.2}SnO_3$, which can be attributed to the synergistic impacts of the alteration of crystal structure and surface, the considerably large surface area linked with the small particle sizes and appropriate bandgap size and also band edge position.

Heterogeneous photocatalysis in aqueous media using titanium dioxide slurries and UV radiation has been a very effective method for removing organic pollutants (Gupta and Tripathi 2011). So, (Jorgetto et al. 2018) prepared a photocatalyst from a magnetically extractable combination of magnetite, silica, and titania (Anatase phase) and used it to degrade organic compounds in water. Grafting results in a low density of TiO_2 crystallites on the silica surface up to a TiO_2 content of 48.3 wt per cent, resulting in poor photoactivity. The material was shown to be chemically stable at both acidic and neutral pH levels, as well as being biodegradable. A poor adsorbent for 4-chlorophenol, implying that the breakdown pathway is linked to reactive oxygen species generation and transitory covalent bonds. The degradation of 4-chlorophenol followed zero-order kinetics at pH 3.0 and 7.2, confirming that (desorbed) reactive oxygen species are involved in 4-chlorophenol degradation. Although the hybrid material's performance (on a g-1 basis) falls short of Anatase or P25 TiO_2, the ease with which the catalyst may be separated from the purified liquid using a magnetic field favours the composite.

Iron oxide nanomaterials exist in many forms in nature. Magnetite (Fe_3O_4) and hematite (α-Fe_2O_3) are the most common forms used as nano-adsorbents (Chan et al. 2004). So (El-Gendy and Nassar 2021) emphasizes the win–win one-pot valorization process of different waste biomass that is composed of many biological macromolecules (e.g., polysaccharides, polyphenols, carbohydrates, lipids, enzymes, proteins, etc.), and other biomolecules (e.g., alkaloids, terpenoids, tannins, phenolics, carotenoids, amino acids, sugars, vitamins, etc.) into biofunctionalized magnetite (Fe_3O_4) nanoparticles which will be used in the future in the generation of biofuels from lipids and lignocellulosic wastes, biosensor manufacturing, and bio-upgrading of petroleum fractions, among other things (Osman et al. 2021). It examines the circular economy and the obstacles and potential for scaling up green synthesis with zero waste. Nonetheless, more research is needed to determine the exact rule of biological macro- and micromolecules in the synthesis of biofunctionalized magnetite (Fe_3O_4) nanoparticles, as well as the mechanisms involved in their microbicidal and photo-degradation capabilities. More research is needed to ensure the eco-safety of their green production in the environment and their toxicity or biosafety to humans and other non-target creatures.

On the other hand, (Mahasti et al. 2020) used a fluidized-bed homogeneous crystallization technique to extract iron from waste-water as magnetite (Fe_3O_4) pellets. Magnetite's catalytic effectiveness in the heterogeneous degradation of reactive black five azo dye was tested. Key fluidized-bed homogeneous crystallization parameters are effluent pH, cross-section loading (L, kg/m2.h), and cross-section loading (L, kg/m^2.h), intake supersaturation and initial iron concentration ([Fe(II)], mg/L). Total iron removal and crystallization ratio from a fluidized-bed reactor were 99 and 77 per cent, respectively, when the pH was 8.5–9.5 and the [Fe(II)] was 100–500 mg/L. To confirm the magnetic characteristic, the magnetization and coercivity of the recovered Fe_3O_4 pellets were examined. The Fe_3O_4 pellets were used to stimulate a Fenton-like degradation of the RB5 azo dye under ultraviolet-irradiation, pH = 2.75–3.0, starting peroxide concentration of 10 mM, and catalyst loading of 2 g/L. Decolourization and mineralization efficiencies were at 98–99 and 60–68 per cent, correspondingly. The A fluidized-bed homogeneous crystallization process allowed for the recovery of high-purity metal oxides while producing a small amount of sludge. Magnetic pellets made from dissolved iron in wastewater were shown to be promising materials for use as a photochemical reactant in the breakdown of organic pollutants.

Also, (Fazli et al. 2021) produced the cubic cobalt and zinc-doped and co-doped magnetite nanocatalysts with various methods. Under ultraviolet–visible irradiation, the produced photocatalysts were employed to activate hydrogen peroxide and persulfate. The addition of $Fe_{2.5}Co_{0.3}Zn_{0.2}O_4$ to the ultraviolet/$Fe_{2.5}Co_{0.3}Zn_{0.2}O_4$/persulfate procedure increased hydrogen peroxide and persulfate activation, and the ultraviolet/$Fe_{2.5}Co_{0.3}Zn_{0.2}O_4$/persulfate process displayed better Sulfalene breakdown in water as a veterinary pharmaceutical contaminant. Following that, the effect of various physicochemical factors was investigated, and the radicals produced during the process were identified using chemical scavengers. In real wastewater, the ultraviolet/$Fe_{2.5}Co_{0.3}Zn_{0.2}O_4$/ persulfate treatment resulted in approximately 67 per cent degradation.

Furthermore, 85% of total organic carbon was removed within 15 h of the procedure mentioned above. The phototoxicity of the untreated and treated animals was eventually equalized. After 120 min of the ultraviolet/$Fe_{2.5}Co_{0.3}Zn_{0.2}O_4$/ persulfate procedure, the phototoxicity of the untreated and treated solutions was investigated using Lemna minor aquatic species.

The microwave solvothermal approach reported by Zanchettin, G. et al. (2021) to manufacture Fe_3O_4 nanoparticles was efficient, yielding magnetite nanoparticles in a short reaction time with only two reactants and one iron precursor. Magnetic nanoparticles with low shape and size variation, high yield, and crystallinity were created. Compared to traditional approaches, the microwave reactor provided temperature and pressure control, homogeneous heating, and a faster reaction time. The use of magnetite nanoparticles in a photo-Fenton process under visible light resulted in 100% methyl orange dye degradation in 5 min. In the instance of tetracycline, a remarkable reaction time of 90 min was achieved. Using an external magnetic field, the procedure also allowed for the quick recovery of the catalyst.

Liu and his group (Liu et al. 2019) investigated the application of hematite in the removal of chromium dyes from water. The chromium species such as trivalent chromium (Cr (III)) and hexavalent chromium (Cr (VI)) have high toxic effects on humans and the environment. The chromium species are sensitive to reduction–oxidation reactions. So, hematite can promote the oxidation of trivalent chromium and the reduction of hexavalent chromium. Hematite induced the formation of electrons and holes under the irradiation of light. Photo-induced holes by hematite promoted the oxidation of chromium (Cr (III) trivalent to hexavalent Cr (VI)). Photo-induced electrons by hematite were not sufficient for the reduction of hexavalent chromium. So, a very small amount of hexavalent chromium was reduced to trivalent chromium. Under visible light irradiation, the performance for removing hexavalent chromium by hematite was 17% at pH 5 with complete degradation of trivalent chromium.

Recently, (Guo et al. 2021b) discussed the performance of copper substituted-hematite nanoparticles activated by peroxymonosulfate on removing tetracycline. The substitution of metal ions enhances the photocatalytic activity of hematite. Cu^{2+} substitution enhanced the degradation activity of hematite by promoting redox cycling transformation of Fe (II) and Fe (III). Cu^{2+} substitution generated oxygen free radicals that increase the photocatalytic activity. Under visible light irradiation, the performance for removing tetracycline by copper substituted-hematite nanoparticles was 74.70% after 30 min. Activation by peroxymonosulfate generated sulfate radicals (SO^{4-}) that increase the electron transport process. So, sulfate radicals had high activity for degradation of harmful dyes. Under visible light irradiation, the performance for removing tetracycline by copper substituted-hematite nanoparticles activated by peroxymonosulfate was 97.80%.

Also, (Zhang et al. 2017b) investigated the photocatalytic activity of hematite whose surface was modified by sulphur doping. Hematite can be used in heterogeneous Fenton reactions to degrade harmful dye promoted by H_2O_2 due to its photo-degradation activity and low cost. Fenton reaction generated free radicals such as hydroxyl radical (OH^-) and sulfated radical (SO_4^-), which have high oxidation activity. These free radicals promoted the degradation of dyes by absorption of H_2O_2. They also act as trapping centres for the electrons transferred to H_2O_2. It was observed that sulphur has high photocatalytic activity. As a result, hematite modified by amorphous sulphur had a higher rhodamine B dye degradation rate than pure hematite.

Also, Rojas and his group (Rojas-Mantilla et al. 2021) investigated the application of hematite supported by nontronite NAu-2 to remove sulfathiazole. Sulfathiazole is a sulfonamide antibiotic drug used in animal treatment. The existence of sulfathiazole in water causes defects in the reproductive hormones. Hematite can be used in heterogenized Fenton reaction to degrade harmful dye in the presence of H_2O_2 that induces the formation of hydroxyl radical (HO^-). It was observed that heterogenized Fenton reactions with hematite do not require specific pH and do not form the sludge. Nontronite NAu-2 supported hematite to enhance its photocatalytic activity in Fenton reactions. Nontronite is a mineral clay that has a high mesoporous surface area with maximum absorption at UV–visible range. In heterogeneous Fenton reactions, the surface of active sites was formed on the nontronite and induced electrons transport to H_2O_2 that decomposed into hydroxyl radical (HO^-). Nontronite had a high bandgap of 3.42 eV. As a result, it was modified by heat treating at 600 °C, and its bandgap was shifted to 1.98 eV leading to enhanced photocatalytic activity. Under sunlight irradiation, the performance for removing sulfathiazole by hematite supported by Nontronite NAu-2 was 86% in 20 min.

Further, (Zhai et al. 2021) described the photocatalytic activity of hematite doped on bismuth oxychloride nanosheets with a two-dimensional structure for degradation of tetracycline. The photocatalytic Fenton processes are used for the degradation of tetracycline in the presence of H_2O_2. Hematite is a ferric (Fe^{3+}) oxide that effectively absorbs visible light due to a low bandgap of 2.2 eV. The reduction of ferric ions (Fe^{3+}) to ferrous ions (Fe^{2+}) should be inhibited by generating hydroxyl radical (OH^-) to maintain the photocatalytic performance of hematite. Two-dimensional heterojunctions increase the surface area of hematite. The bismuth oxychloride heterojunction nanosheets have a great interest due to their oxidation activity and photocatalytic performance. Hematite doped on bismuth oxychloride nanosheets had a favourable large surface area that promotes the separation of photo-induced electron–hole pairs and increases the charge transport. The bismuth oxychloride caused oxygen vacancy defects on the lattice structure that act as trapping centres for the generation of electrons and prevent the recombination of the electron–hole pair. As a result, hematite and bismuth oxychloride nanosheet composites had better performance for removing tetracycline. The performance of removal of tetracycline with hematite doped on bismuth oxychloride nanosheets was 92% after 25 min with exposure to xenon lamps.

The photocatalytic activity of magnetite nanoparticles with different shapes in removing azo dyes investigated by (Radoń et al. 2019). Azo dyes are synthetic compounds widely used in the food, cosmetic, leather and textile industries. They can damage human and animal cells and cause cancers. Heterogenized photocatalytic Fenton reactions are used for the degradation of Azo dyes in the presence of H_2O_2. Fenton reactions generate highly oxidizing hydroxyl radicals leading to enhanced photocatalytic activity. Magnetite can act as a catalyst in Fenton reactions. The magnetite with rod nanoparticles had higher photocatalytic activity than that with spherical nanoparticles. The magnetite with cubic nanoparticles had high induction heating ability and magnetic field hyperthermia applications due to its large surface area and magnetic anisotropy. The photocatalytic activity of magnetite with cubic as a catalyst for heterogenized photocatalytic Fenton reactions was investigated in the removal of rhodamine B, methylene blue and Sudan I. The performances of removal of rhodamine B and methylene blue were 99.5% and 97%, respectively. While the performance of removal of Sudan, I had some defects such as the high value of pH and continuous irradiation of ultraviolet–visible light.

Also, (Gonçalves et al. 2019) investigated the application of magnetite substituted on layered double hydroxide to degrade harmful dyes. Layered double hydroxides are two-dimensional materials with a lamellar structure. Layered double hydroxides are recommended for photocatalytic activity due to their high surface area and large pore radius. After treatment, the layered double hydroxides cannot be easily separated from degraded dyes, hindering their recycling or reuse due to high energy consumption. Magnetite had favourable magnetic properties and facilitated the recycling of layered double hydroxides after degradation. The introduction of double hydroxide layers on the surface of the magnetite nanoparticles enhanced the degradation of dyes due to increased surface area, ease of recycling of composite, and decreasing bandgap (1.85 eV). The composite of double hydroxide layers with magnetite can be easily separated from treated water solutions using a magnet. The performance of this composite in photocatalytic Fenton reaction promoted by H_2O_2 was investigated on the degradation of reactive black 5 and methylene blue dyes. It was observed that a large number of active sites were formed and generated hydroxyl radicals. Under visible light irradiation, the performance for the removal of reactive black five and methylene blue dyes was above 92% after 40 min.

Gonçalves group (Gonçalves et al. 2020) described the photocatalytic activity of magnetite coated by humic acid in water remediation applications. Magnetite coated by humic acid can be used as a catalyst for heterogenized photocatalytic Fenton reactions to achieve maximum reactivity. Heterogenized photocatalytic Fenton reactions were promoted by active sites and H_2O_2 that generate highly oxidizing reactive oxygen species and increase the removal of harmful dyes. Magnetite consists of ferrous (Fe^{2+}) and ferric (Fe^{3+}) oxides. Ferrous (Fe^{2+}) ions promoted the activation of H_2O_2 in heterogenized photocatalytic Fenton reactions, but ferric (Fe^{3+}) oxides prevented the activation of H_2O_2. Ferrous (Fe^{2+}) oxides can be easily oxidized to ferric (Fe^{3+}) oxides preventing the photocatalytic activity of H_2O_2. Humic acid was used to coat the surface of magnetite to stabilize the ferrous (Fe^{2+}) oxides and enhance the photocatalytic activity of magnetite. Magnetite coated by humic acid was recommended due to its low cost and easy recycling and reuse. Under visible light irradiation, the performance of the photocatalytic activity of magnetite coated by humic acid as a catalyst for heterogenized photocatalytic Fenton reactions was investigated in the removal of Ibuprofen bisphenol A, 5-tolylbenzotriazole, and carbamazepine. The performance of removal of Bisphenol A, 5-tolylbenzotriazole, and carbamazepine was 80% in 60 min. In contrast, the performance of removal of Ibuprofen was 35%.

The photocatalytic activity of magnetite bio nanocomposite on the degradation of 4-nitrophenol was investigated by (Dinari and Dadkhah 2020). The 4-nitrophenols are used as precursors to produce drugs, but their accumulation in the environment causes very toxic effects. Ingestion and inhalation of 4-nitrophenol damage the respiratory system and cause cancers. Magnetite bio nanocomposite can convert 4-nitrophenols

to environmentally friendly products. Silver nanoparticles have high catalytic activity for the degradation of nitrophenols. Layered double hydroxides have high surface areas and high degradation activity. So, the introduction of magnetite and silver nanoparticles on layered double hydroxides had a great potential to degrade 4-nitrophenol. Starch polymers were used as a substrate for magnetite stabilization due to hydroxyl groups on their chains that act as capping agents. As a result, magnetite, silver, layered double hydroxide, and starch nanocomposite were biodegradable composites with high photocatalytic activity. The composite was separated from the treated aqueous solution with a permanent magnet and washed using distilled water. It can be reused many times with performance above 90%.

Emídio and his group (Emídio et al. 2020) investigated the performance of copper-substituted magnetite on the removal of anticancer drugs. Cytostatic agents are used very largely as chemotherapeutic drugs to kill cancer cells. Some of these cytostatic agents have cytotoxic effects on aquatic animals. So, it becomes a dangerous problem for the aquatic environment. Magnetite has an effective role in removing cytostatic agents using the heterogenized photocatalytic Fenton process promoted by H_2O_2. The magnetite is stable, low cost and has ferrous (Fe^{2+}) responsible for photocatalytic performance. So, it is recommended in the heterogenized photocatalytic Fenton process. Copper was inserted on magnetite nanoparticles due to its unique characteristics. Copper has a wide pH range, suitable reduction–oxidation properties, and generates hydroxyl radicals that enhance the degradation rate. So, copper-substituted magnetite had significant degradation performance. The performance of the photocatalytic activity of copper-substituted magnetite as a catalyst for heterogenized photocatalytic Fenton reactions was investigated in the removal of 5-fluorouracil and cyclophosphamide. The performance of removal of 5-fluorouracil was 99%. At the same time, the performance of the removal of cyclophosphamide is 97%.

Recently, (Chen et al. 2021) prepared nanocomposites of carbon dots-hematite quantum dots-loaded hydroxypropyl cellulose-chitosan and searched its photocatalytic activity for degrading 4-chlorophenol as a contaminant under sunlight irradiation. The synthesized nanocomposite demonstrated an excellent photocatalytic performance for degrading 4-chlorophenol with about 98.64% during 70 min of sunlight irradiation.

Also, (Li et al. 2020) investigated if the hematite-sulfite-photo system could be used to break down other organic contaminants, such as pesticides, dyes; four typical contaminants, atrazine, bisphenol A, rhodamine B, and methylene blue, were selected in the degradation experiments. The solution changed to colourless after 20 min to degrade rhodamine B and methylene blue dyes. For atrazine, bisphenol A, both contaminants are gradually diminished over time. After 50 min, practically all atrazine (98.67%) is destroyed. Bisphenol A is degraded by about 67.15%. These results imply that the existing hematite/sulfite/photo can be employed to break down many resistant organic contaminants.

Also, (Doan et al. 2020) developed Cu/Fe_3O_4@carboxylate-rich carbon composite and examined its photo-Fenton catalytic activity. The synthesized composite was utilized as a photo-Fenton-like catalyst for the elimination of methylene blue. The photocatalytic degradation efficiency achieved 97.5 per cent under visible irradiation for 40 min. The produced composite shows an excellent removal efficiency and stability after five cycles.

Antimicrobial activity

Research of the microbial flora in over 250 homes has been reported in recent studies (Keijser et al. 2008). The appearance of possible microbial pathogens and the potential of infection at different places, especially in the kitchen, bathroom and shower, is defined, and the associations for hygiene applications in the house are presented in various scientific papers (Bloomfield et al. 2016). Microbial contamination may happen at any process level, from fabricating in the food industry or pharmaceutical processing to patient treatment in the hospital situation (Querido et al. 2019). Disinfection is a simple microbial treatment by general disinfectant agents like H_2O_2, ethanol, and chlorine or filtration, which is considered inadequate (Wagner et al. 2002). Cryptosporidiosis is the common enteric infection to be recognized throughout waterborne disorders (Chique et al. 2020). The enteric bacteria may be subject to risks through primary faecal contamination issues that are poorly controlled (McKee and Cruz, 2021). Removing microbial contaminants is an example of the standard essential levels in Good Manufacturing and Healthy Practices (GMHP) to support food and health safety (Kendall et al. 2016). Various original materials and chemicals exhibit antimicrobial action towards the principal foodborne and health-associated pathogens, showing high potential for purpose in food and pharmaceutical manufacturing (Dandie et al. 2020). They were usually disinfected by chemical disinfectants, which had been generally applied for disinfection purposes (DeLeo et al. 2020). Some problems like unusual rapid evaporation, remaining taste or degeneration by a display to severe processing states have been summarized (Nilius et al. 2007). Nanotechnology and nanoscience seem to elevate the antimicrobial activity and present managed microbial diseases through the present high and encouraged physicochemical properties (Abd Elkodous et al. 2019). Between the synthesized nanomaterials-based disinfectant agents are magnetic nanomaterials such as iron oxides; (magnetite & hematite), spinel ferrites, and perovskite oxides which possesses great

antimicrobial potential (Asab et al. 2020a; Jamzad and Bidkorpeh 2020; Maksoud et al. 2021; Manjunatha et al. 2019), thus will summarize in the following points.

The application of the synthesized nanoparticles is increasing quickly over technology and biomedicine, posturing attention to their value on the environment and personal health (Khalil et al. 2020). Magnetite and hematite have been synthesized by nearly all the identified wet chemical processes, such as electro-deposition and co-precipitation (Hu et al. 2021). Magnetite is a colloidal iron oxide (Fe_3O_4) substance that displays superparamagnetic characteristics at room temperatures. This substance has been applied in magnetic nanotechnology study, nano-toxicology and biomedicine as antimicrobial agents (Maria Holban et al. 2014). Hematite (α-Fe_2O_3) nanoparticles have drawn researchers' consideration for holding the common steady iron oxides in the air (room conditions).

Moreover, α-Fe_2O_3 are additionally identified for their broad uses in different disciplines (Eggleston 2008). Magnetite and hematite have displayed great potential for their purposes as catalytic elements, wastewater processing adsorbents, gas sensors, suitable coatings, ion exchangers, magnetic data storage media, magnetic disc materials, inks for xerography, antimicrobial and anticancer agents, and used in magnetic resonance imaging (LI et al. 2005; Marcinowski et al. 2020; Kim et al. 2011; Singh et al. 2015; Xu et al. 2012). Still, the mechanism following antimicrobial activity is a topic of fundamental research today. Investigations have been performed to confirm the antimicrobial potential of iron oxides, as shown in Table 1. Chatterjee et al. (Chatterjee et al. 2011) demonstrated that magnetite and hematite possess antimicrobial action towards *E. coli*, and the performance improves with an increase in the iron oxides concentration.

Regarding the performance of potentials in connection at the interface, magnetite and hematite with a positive surface charge will possess a more suitable surface for microbial appendage with more effective communications than non-modified iron oxides (Chatterjee et al. 2011). The more effective communications will happen in approximately improved reactive oxygen species production like H_2O_2 (Maksoud et al. 2020a). Therefore, to confirm the condition, the exterior surface of the non-modified iron oxides was transformed by a sheet with positively charged polymers like chitosan (Attia et al. 2021). The schematic illustration in **Fig. 5** presents the possible antibacterial behaviour for magnetite and hematite nanoparticles. It is necessary to understand that magnetite and hematite nanoparticles create their potential action through penetrating at the bacterial cell's outer surface, causing membrane damage and exchanged transport activity (Farag et al. 2019). Next, the appearance of Fe^{3+} (for hematite), and both Fe^{3+}, and Fe^{2+} (for magnetite) in the bacterial cytoplasm at pH = 3.5 and scattering all the intracellular structures such as genetic materials, a plasmid, and other vital organelles. Finally, genetic and cellular toxicity alters the signal transduction pathways because of the oxidative pressure created by reactive oxygen species production (Sardana et al. 2018).

Magnetite & hematite nanoparticles may assist as a carrier to efficiently release Fe^{3+} and Fe^{2+} ions to the cytoplasm and layer, where proton motive power would lower the pH to be more invisible than 3.5 and promote the discharge of Fe^{3+} and Fe^{2+} ions.

Spinel ferrite NPs are in the flashlight of modern nanotechnology because of their extensive purpose (Maksoud et al. 2020b). The spinel ferrite nanoparticles owns unique magnetic characteristics that are frequently conducted by other valuable features, such as catalytic and antimicrobial activities (Maksoud et al. 2019; Maksoud et al. 2020c). The ferrite nanoparticles have mainly been-usage in many fields such as biomedical (Hoque et al. 2016), energy area (Martinez-Julian et al. 2014), gas sensors (Wu et al. 2019), drug distribution (Aisida et al. 2019), antimicrobial potential (Madhukara Naik et al. 2019), photocatalytic activity (Maksoud et al. 2020c; El-Sayyad et al. 2020), and wastewater treatment (El-Sayyad et al. 2020; Hassan et al. 2020). Ferrites nanoparticles have unique interesting and physical properties have started to consider possible biomedical treatments (Maksoud et al. 2018), including improved drug solubility and durability and reduced harmful effects (Maksoud et al. 2018). It has been applied for fascinating orientation in drug distribution (Nigam and Pawar, 2020), imaging agents and treatment of brain cancer (Hyder and Manjura Hoque, 2017), as a drug-delivery transport in biomedical procedures (Wang et al. 2018), for the superior antimicrobial performance (Ashour et al. 2018b; Mmelesi et al. 2020). Shape, and nano-size, and purity of spinel ferrites, high catalytic performance, and encouraging magnetic feature, in addition to high elasticity increasing the removal of pathogenic microbes and the easy connection to the microbial cell which intern elevated their antimicrobial potential (Maksoud et al. 2021b). The surface area, pore-volume, and pore size also presented a critical function in raising and encouraging ferrites nanoparticles on all pathogenic bacteria and fungi. The elevated surface area provided a higher connection with a more significant quantity of pathogenic microbial cells, improving the ferrites nanoparticles' antimicrobial activity (Maksoud et al. 2021a). Investigations have been performed to confirm the antimicrobial potential of spinel ferrites as shown in Table 1. There are several plausible mechanisms for the antimicrobial potential of ferrites. It has been proposed that the ferrites nanoparticles adheres to the microbial membranes by improving the lag step of the microbial growth phase, increasing the generation point of the pathogenic microbes, and enhancing bacterial cell division (Maksoud et al. 2019).

Table 1 Characteristics and antimicrobial performance of various similar nanocomposite magnetic-based nanocomposites

Magnetic-based materials features					Antimicrobial activity		
Type	Hybrid material	Synthetic method	Concentration	Microbial strains	Inhibition (%)	Effect-Mode of action-target	Reference
Iron oxides-based nanocomposite (Magnetite & Hematite)	Silica-coated Fe_3O_4	Micro-emulsion method	10 mg/ml	*E. coli*, , *S. aureus,* and *C. albicans*	18 mm, 14 mm, and 10 mm (ZOI), respectively	Gram-positive bacteria are more defiant to magnetite than Gram-negative which are associated with their cell wall formation, cell biology, catabolism, anabolism, or level of communication	Asab et al. 2020b
	Chitosan-coated Fe_3O_4	Co-precipitation method	10.0 µg/ml	*E. coli, B. subtilis,* and *C. albicans*	18 mm, 17 mm, and 14.2 mm (ZOI), respectively	Reactive oxygen species generation ($^{\cdot}O_2^-$ and $^{\cdot}OH$) from the coated Fe_3O_4 NPs, and the produced reactive oxygen species producing severe injury result when mixed with the organic macromolecules in the microbial cells like liposome, DNA, Carbohydrate, and lipids	El-Khawaga et al. 2020
	Hematite (α-Fe_2O_3)	Green synthesis by the aqueous extract of *Laurus nobilis* L. leaves	4 mg/ml	*Listeria monocytogenes, Aspergillus flavus,* and *Penicillium spinulosum*	12 mm, 13 mm, and 14 mm (ZOI), respectively	The mechanism by which the synthesized hematite NPs displays antimicrobial potential may be because of the oxidative pressure manner produced through ROS, which can destroy living macromolecules	Jamzad and Kamari Bidkorpeh (2020)

Table 1 (continued)

Magnetic-based materials features					Antimicrobial activity		
Type	Hybrid material	Synthetic method	Concentration	Microbial strains	Inhibition (%)	Effect-Mode of action-target	Reference
	Iron oxide	Green synthesis by avocado fruit rind aqueous extract	20.0 µg/ml	*E. coli, Streptococcus sp., Staphylococcus sp., Salmonella sp., Bacillus sp., Pseudomonas sp. and Proteus sp.*	13 mm, 12 mm, 15 mm, 11 mm, 9 mm, 12 mm and 14 mm (ZOI), respectively	The antibacterial efficiency of iron oxide NPs differed because of one or many causes such as reactive oxygen species production, oxidative pressure created by the communication of nanoscale iron among intracellular oxygen, obtaining restraint on the bacterial cell membrane, magnetic area of iron oxide, the effect of ions liberated by nanoparticles with the thiol groups (–SH) present in the bacterial cell cover proteins responding to cell damage, the electromagnetic attraction between the nanoparticles and the bacteria, and oxidative tension induced by the liberated reactive oxygen species	Kamaraj et al. (2019)
	Eugenol-functionalized magnetite	Co-precipitation method	5 mg/ml	*P. aeruginosa*	0.312 mg/ml (minimum inhibitory concentration)	The positive synergy with various hydrophobic and hydrophilic antimicrobials effective against Gram-negative bacteria is confirmed to reduce the minimum inhibitory concentration of the conjugation by a factor up to 1000, presumably by improving the permeability of the bacterial layer	Mohammed et al. (2021)

Table 1 (continued)

Magnetic-based materials features					Antimicrobial activity		
Type	Hybrid material	Synthetic method	Concentration	Microbial strains	Inhibition (%)	Effect-Mode of action-target	Reference
Spinel ferrite-based nanocomposite	Zinc ferrite	Co-precipitation method	100 µg/ml	*E. coli,* and *S. aureus*	11 mm, and 13 mm (ZOI), respectively	$ZnFe_2O_4$ exhibited antimicrobial potential by various reaction mechanisms, like bacterial protein leakage effect, bacterial cell membrane destruction, and reactive oxygen species production	Haghniaz et al. (2021)
	Cobaltferrite	Sol–gel auto-combustion method	100 µg/ml	*B. subtilis, S. aureus, E. coli,* and *P. aeruginosa*	9 mm, 9 mm, 15 mm, and 13 mm (ZOI), respectively	$CoFe_2O_4$ exist possible to eliminate both Gram-positive and Gram-negative bacteria because they possess a negative charge on the cells, which support electrostatic cooperation with Co Fe_2O_4 or liberated ions within them	Sharma et al. (2019)
	Mg substituted Mn-Zn ferrites	Sol–gel method	10 µg/ml	*P. aeruginosa, S. aureus,* and *C. tropicalis*	90.5%, 65.78%, and 88.88%, respectively	$Mn_{0.5}Zn_{0.25}Mg_{0.25}Fe_2O_4$ were determined to maintain high antimicrobial functions connected to their extraordinary UV-absorption power. The $OH^{\cdot}$ free radicals can also be performed through illuminating $Mn_{0.5}Zn_{0.25}Mg_{0.25}Fe_2O_4$ by UV light because of the electron transfer inside the bacterial cells and the synthesized ferrites, the $OH^{\cdot}$ Free radical can destroy pathogenic bacteria, creating a lack in the quantity of bacterial cell coenzyme	Abdel Maksoud et al. (2020c)

Table 1 (continued)

Magnetic-based materials features					Antimicrobial activity		
Type	Hybrid material	Synthetic method	Concentration	Microbial strains	Inhibition (%)	Effect-Mode of action-target	Reference
	Metal-substituted cobalt ferrites	Sol–gel method	5000 µg/ml	*B. subtilis, S. aureus, E. coli, P. aeruginosa,* and *C. albicans*	15 mm, 16 mm, 14 mm, 15 mm, and 15 mm, respectively	Hydrogen peroxide generated within the surface of zinc cobalt ferrite NPs directly penetrate the microbial cell wall and display cell destruction	Ashour et al. 2018b
	Metals-substituted spinel cobalt ferrite	Citrate sol–gel method	20 µg/ml	*Staphylococcus lentus, Staphylococcus sciuri, Staphylococcus vitulinus, Staphylococcus aureus, Aerococcus viridians,* and *Enterococcus columbae*	11 mm, 11 mm, 11 mm, 15 mm, 12 mm, and 13 mm respectively	*S. aureus* cells showed morphological modifications in the presence of $Zn_{0.75}Co_{0.25}Fe_2O_4$, and an apparent height in the hardness of the *S. aureus* surface and bacterial malformation suggested that it was damaged and regulated by the synthesized zinc cobalt ferrite	Maksoud et al. (2019)
	Mg^{2+}-substituted Mn–Zn ferrites NPs	Facile sol–gel method	20 µg/ml	*S. aureus, Enterococcus feacalis, Enterococcus faecium Yersinia enterocolitica, E. coli, P. aeruginosa, Salmonella typhi, Klebsiella pneumoniae, C. tropicalis* and *C. albicans*	25 mm, 14.1 mm, 20.4 mm, 12.2 mm, 18.8 mm, 11.6 mm, 12.3 mm, 10.6 mm, 13.5 mm, and 21.3 mm respectively	There were notably proposed mechanisms like reactive oxygen species generation (O_2^- and $^{\cdot}OH$) connected with the crystallite capacity and greater surface area of $Mn_{0.5}Mg_{0.5}Fe_2O_4$	Abdel Maksoud et al. (2020b)

Table 1 (continued)

Magnetic-based materials features					Antimicrobial activity		
Type	Hybrid material	Synthetic method	Concentration	Microbial strains	Inhibition (%)	Effect-Mode of action-target	Reference
	Polyaniline/Ag/MoS_2/$LiCo_{0.5}Fe_2O_4$ nanocomposite	Gamma irradiation-assisted ultra-sonication method	20 µg/ml	*B. subtilis, S. aureus, E. coli, P. aeruginosa, C. tropicalis,* and *C. albicans*	66.45%, 80.88%, 85.25%, 61.58%, 72.87% and 95.44%, respectively	Polyaniline /Ag/MoS_2/$LiCo_{0.5}Fe_2O_4$ nanocomposite owns a novel photo-degradation activity utilizing the UV-light, and it may be formed OH free radicals. The electron medium leaves into the microbial cells and makes free OH radicals that are beginning to damage the established microbial cells via the release of the bacterial coenzymes	Abdel Maksoud et al. (2021d)
	Metals-substituted cobalt ferrite	Citrate sol–gel method	1000 µg/ml	*Staphylococcus epidermidis, S. aureus, Enterococcus faecalis, Acinetobacter baumannii, Enterobacter cloacae, E. coli, B. subtilis, Klebsiella pneumoniae, P. aeruginosa,* and *C. albicans*	25 mm, 26 mm, 27 mm, 23 mm, 19 mm, 27 mm, 26 mm, 28 mm, 27 mm, and 18 mm respectively	Zinc ions in the synthesized zinc-substituted cobalt ferrite connect to the tested bacteria's layers, compared to human cells, raising the lag step of the bacterial growth phase and increasing the return time of the bacteria so, to create a cell unit, more times had spent. In addition to superoxide and hydrogen peroxide generated from zinc cobalt ferrite outside	Abdel Maksoud et al. (2018)

Table 1 (continued)

Magnetic-based materials features					Antimicrobial activity		
Type	Hybrid material	Synthetic method	Concentration	Microbial strains	Inhibition (%)	Effect-Mode of action-target	Reference
	Ce^{3+}-substituted zinc ferrite	Facile sol–gel method	10 µg/ml	*S. aureus, Proteus vulgaris, Proteus mirabilis, P. aeruginosa, E. coli, K. pneumoniae, S. typhi, C. albicans,* and *C. tropicalis*	13.2 mm, 9 mm, 9.5 mm, 9.5 mm, 8.5 mm, 8 mm, 9 mm, 13.5 mm, and 8.9 mm respectively	The metal NPs change the ionic structure (Ce^{3+}) in the bacterial cell at pH = 3, and conflict with the intracellular constructions like plasmids, genetic material, and another essential organelle. Genetic and cellular toxicity happens because of the oxidative pressure caused by the reactive oxygen species generation	Abdel-Rafei et al. (2021b)
	Ag-decorated zinc ferrite nanoparticles	Gamma irradiation-coupled sol–gel method	50 µg/ml	*S. aureus, Staphylococcus sciuri, Staphylococcus lentus, Staphylococcus vitulinus,* and *Enterococcus columbae*	21.4 mm, 13 mm, 15 mm, 24.7 mm, and 23.6 mm respectively	$Ag_{0.75}$@ZFO NPs begin potency by penetrating the bacterial exterior surface, creating membrane destruction and changed transport movement. Then, the distribution of Ag^{+} ions in the bacteria at pH = 3 and distributing all intracellular buildings such as a plasmid, genetic substance, and different active organelles	Maksoud et al. (2021)

Table 1 (continued)

Magnetic-based materials features					Antimicrobial activity		
Type	Hybrid material	Synthetic method	Concentration	Microbial strains	Inhibition (%)	Effect-Mode of action-target	Reference
Perovskite oxide-based nanocomposite	Doped $LaCoO_3$ perovskite with Fe	Citrate precursor sol–gel method	400 µg/ml	*P. aeruginosa*, and *S. aureus*	50 µg/ml, and 50 µg/ml, respectively (minimum inhibitory concentration)	The presumable mechanism could be more favourable adsorption of the because of the cationic charge, which improved communication with Gram -ve cell outside because of the appearance of great lipopolysaccharide including negative charge (carboxylic group) and more limited width of peptidoglycan film	Singh et al. (2017)
	$ZnTiO_3$ perovskite	Sol–gel method	0.4 mg/l	*B. subtilis,* and *Acinetobacter baumannii*	47 mm, and 46 mm (ZOI), respectively	There were notably proposed mechanisms like ROS generation (O_2^- and $^{\cdot}OH$) connected with the crystallite capacity and greater surface area of $ZnTiO_3$ perovskite	Rheima et al. (2021)
	Perovskite lanthanum aluminate	L ow-temperature solution combustion method	200 µg/ml	*B. subtilis,* *S. aureus,* *E. coli,* and *P. aeruginosa*	87 µg/ml, 95 µg/ml, 70 µg/ml, and 63 µg/ml, respectively (minimum inhibitory concentration)	The impact of the antibacterial bacterial strains produced by perovskite lanthanum aluminate may be because of the communication within the positive charge of the synthesized perovskite nanoparticle and the negative charge regarding bacterial cell wall	Manjunatha et al. (2019)

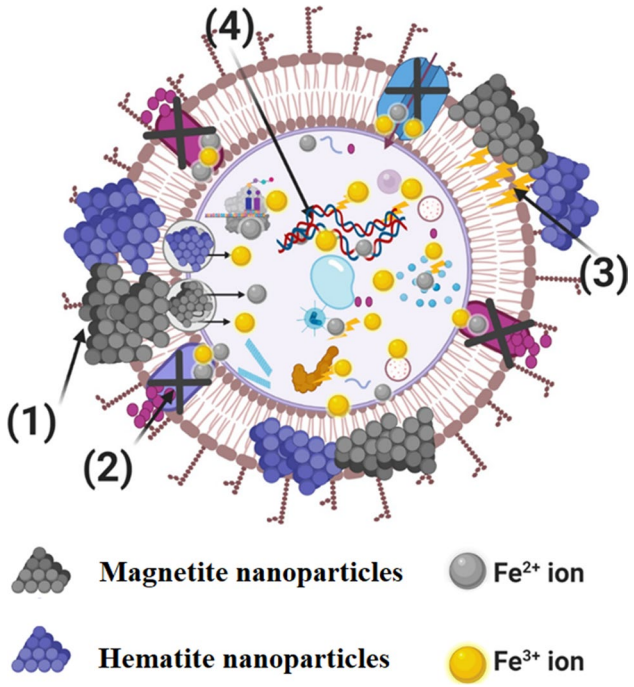

Fig. 5 Four main steps of antibacterial action of iron oxides (magnetite & hematite), where: (1) Magnetite and hematite nanoparticles on the bacterial cell outside and finishes in membrane destruction, followed by endocytosis and endosome formation, and changed transport potential. (2) Magnetite & hematite nanoparticles hinder the ions transportation from and over the bacterial cell. (3) Magnetite & hematite nanoparticles generate and enhance the reactive oxygen species, pointing to weakening bacterial cell walls. (4) Magnetite & hematite nanoparticles enter the bacterial cells and combine with cellular organelles, influencing respective cellular devices, modulating the cellular signal operation, and beginning cell destruction

The main reactive oxygen species (ROS) producing antimicrobial actions are active superoxide (O_2^-) and H_2O_2, built from the ferrite's nanoparticles. H_2O_2 generated from the surface of ferrites nanoparticles can penetrate the microbial cell wall and present cell loss (Fig. 6). Ashour and his group (Ashour et al. 2018b) synthesized different metal-substituted cobalt ferrite, and investigated their antimicrobial activity. Between the synthesized ferrite, zinc cobalt ferrite possessed high bactericidal potency upon *S. aureus* (16.0 mm) and *P. aeruginosa* (15.0 mm), in addition to high antifungal activity against *C. albicans* (15.0 mm). A laboratory experiment performed by (Žalnėravičius et al. 2016) showed that the size of ferrite is a critical factor for antimicrobial potency towards *S. cerevisiae* and some *Candida* species, especially *C. krusei, C. parapsilosis,* and *C. albicans*. The tiny and ultra-small parts of cobalt ferrite maintain decisive antimicrobial action upon all examined pathogenic microbes.

Perovskites are one of the exciting collections of substances that show high-temperature superconductivity, pyro-electricity, ferroelectricity, piezoelectricity, and exhibit catalytic and antimicrobial characteristics (Benlahrache et al. 2006). Lanthanum containing perovskite oxides was the most commonly considered and confirmed exceptional achievement in various biomedicine and catalysis (Singh et al. 2017). Lanthanum-doped $NaTaO_3$ and $MnTiO_3$ were investigated for photocatalytic treatments (Wang et al. 2015a). However, the purpose of La-perovskites in the area of bacterial treatment is inadequate. A few articles were prepared where some La-based perovskites oxides were applied as a microbial disinfectant (De et al. 2010; Yang et al. 2012; Zhang et al. 2014).

Investigations have been performed to confirm the antimicrobial potential of perovskite oxide, as shown in Table **1**. The antibacterial results collected by Singh et al. (Singh et al. 2017) noted that MIC results for the pathogenic bacteria *P. aeruginosa,* and *S. aureus* were from 50 µg/ml to 200 µg/ml, and the most negligible minimum inhibitory concentration state was achieved for $LaCo_{0.4}Fe_{0.6}O_3$ perovskite oxide, which confirms that $LaCo_{0.4}Fe_{0.6}O_3$ perovskite oxide owned unique antibacterial activity. So, the high antibacterial potential of lanthanum cobalt ferrate indicates the performance of an economical nanomaterial which could be a possible antibacterial factor in water remediation and other biomedical applications (Singh et al. 2017; Zhang et al. 2014). The bactericidal reaction mechanism of $LaCo_{0.4}Fe_{0.6}O_3$ perovskite against bacteria is due to more significant adsorption of the perovskite oxide because of their nature of the cationic charge, which improved communication with Gram-negative cells surfaces (the appearance of great lipopolysaccharide including a negative charge due to carboxylic moiety) and more limited width of the peptidoglycan sheet (Niazi and Gu 2009).

Heavy metal removal applications

Tatarchuk et al. prepared Magnesium-Zinc ferrites ($Mg_{1-x}Zn_xFe_2O_4$: x = 0–1) as magnetic adsorbents for the removal of both hexavalent chromium Cr (VI) and divalent nickel Ni (II) ions (Tatarchuk et al. 2021). Langmuir equation well fitted the adsorption of both ions. In addition, the adsorption processes of both ions had a chemical nature. Their results also showed that the prepared $Mg_{0.2}Zn_{0.8}Fe_2O_4$ sample exhibited the highest Cr (VI) adsorption efficiency of about (q_e = 30.49 mg/g). While a maximum Ni (II) removal percentage of 93.2% was achieved by $Mg_{0.4}Zn_{0.6}Fe_2O_4$ sample. Moreover, by increasing the zinc (Zn) content, the heavy metal removal percentage of the mixed ferrite samples increased.

Narayana et al. reported an optimized lead ions Pb (II) removal by a nanocomposite of inverse spinel nickel ferrite and reduced graphene oxide (Narayana et al. 2022). Their results showed that the prepared sample could obtain a

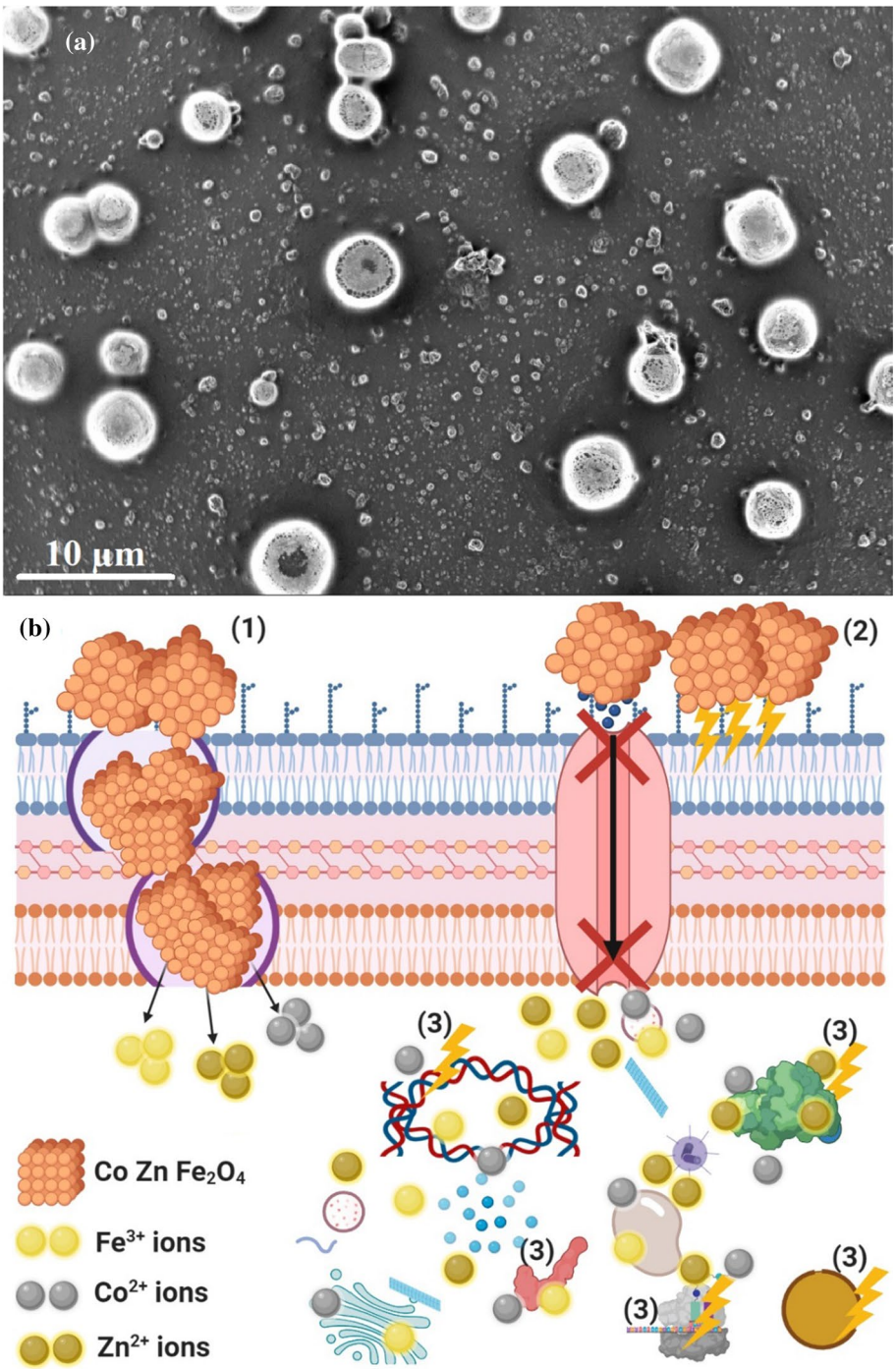

Fig. 6 **a** scanning electron microscope imaging of the treated *S. aureus* cells by $CoZnFe_2O_4$ where cells appear as possesses a-holes and pits on the outer surface, and **b** the corresponding schematic description about the main steps of antibacterial action of ferrite (Co-$ZnFe_2O_4$ nanoparticles as an example), where: (1) Cobalt zinc ferrite ($CoZnFe_2O_4$ nanoparticles) on the *S. aureus* outside and causing membrane destruction, followed by endocytosis and endosome formation and changed transport potential. (2) $CoZnFe_2O_4$ generate and enhance the reactive oxygen species pointing to *S. aureus* wall weakening. (3) $CoZnFe_2O_4$ enter the bacterial cells and combine with cellular organelles, influencing respective cellular devices, modulating the cellular signal operation, and beginning cell destruction. $CoZnFe_2O_4$ may assist as a carrier to efficiently release Co^{2+}, Zn^{2+}, and Fe^{3+} ions to the cytoplasm and layer, where proton motive power would lower the pH to be more invisible than 3.5 and promote the discharge of Co^{2+}, Zn^{2+}, and Fe^{3+} ions

maximum removal efficiency of about (99.8%). In addition, stability of 5 successive cycles was achieved.

The removal of different heavy metals such as Cr (VI), Cd (II), and Pb (II) from wastewater was also reported by Khoso et al. using magnetic Nickel-Ferrite Nanoparticles (NFNs) prepared by a co-precipitation method (Khoso et al. 2021). They also studied the effect of many parameters, including pH, dose, and contact time, on the adsorption efficiency. The best-found sample dosage was (30 mg) at lower pH values. Under optimal conditions, removal efficiencies of about 89%, 87%, and 79% were obtained for Cr (VI), Cd (II), and Pb (II), respectively. Moreover, adsorption kinetics fitted the pseudo-second-order model.

Mohammadi et al. prepared a nanocomposite of superparamagnetic $CoFe_2O_4$/polyaniline for the removal of both Cr (VI) ions and Acid Red 18 (AR 18) under external ultrasonic fields (Mohammadi et al. 2021). Both hydrothermal and in-situ polymerization routes prepared the presented

nanocomposite. A maximum monolayer adsorption efficiency of 103.11 mg g^{-1} was obtained by the prepared sample. The effect of pH on the adsorption efficiency was studied. It is worth mentioning that $CoFe_2O_4$/ polyaniline nanocomposite showed higher adsorption efficiency than bare $CoFe_2O_4$. In addition, the thermodynamic analysis revealed that the adsorption process was endothermic and spontaneous in nature.

Abdel Maksoud et al. have used adsorbent nanostructure based on carbon modified ZrO_2/Mn-Mg-Zn ferrite for cobalt and europium radionuclides from solutions (Abdel Maksoud et al. 2021e). Scanning electron microscopes image unveiled that the carbon modified ZrO_2/Mn-Mg-Zn ferrite composite owned a heterogeneous morphology (Fig. 7). The studied optical band gap values were found to be 1.45 for Mn-Mg-Zn ferrites, 2.38 eV for ZrO_2, and 1.54 eV for the composite. Many parameters have been studied as the effect of time, solution pH, and initial ion concentration. The kinetics models for the cobalt and europium radionuclides removal were examined. The obtained capacity for cobalt was 82.51 mg/g, and europium radionuclides were 136.98 mg/g.

Cao et al. prepared mesocrystalline anatase TiO_2-anchored $SrTiO_3$ nanodots with type-II heterojunction for the photocatalytic reduction of Cr (VI) ions under-stimulated solar light irradiation (Cao et al. 2021). The observed efficiency was ascribed to the favoured Cr (VI) adsorption, improved separation of the photogenerated charge carrier, and the well-preserved reduction efficiency because of the well-defined type-II heterojunction construction with strong interactions and tight interfacial contacts.

Additionally, Yang et al. prepared Cr-doped $SrTiO_3$ nanoplates using a facile one-pot solvothermal technique to remove Cr (VI) ions under visible light irradiation (Yang et al. 2019). Upon Cr^{3+} ions doping, they substituted the sites of Sr^{2+} ions in the crystal structure of $SrTiO_3$, which led to a reduction in the $SrTiO_3$ bandgap, making it active for visible light absorption. Their results revealed that the prepared sample with 0.9% Cr content showed the highest photocatalytic Cr (VI) reduction ability within 3.5 h. In addition, outstanding stability after six cycles was maintained.

Additionally, Yang et al. evaluated the performance of bimodal-pore microspheres of $SrTiO_3$ for Cr (VI) reduction under simulated sunlight (Yang et al. 2016). The microspheres were obtained by a sol–gel templating technique. The prepared sample possessed both outstanding performances under simulated sunlight, reaching an efficiency of nearly 100% after 2 h and good stability after six cycles. The recorded efficiency was attributed to the rapid mass transport, incident light's multi-reflections, and the efficient adsorption of reactants thanks to the largest interconnected structure.

Also, Abdel Maksoud has used nanostructured bismuth tungstate Bi_2WO_6 to remove radioactive caesium and europium radionuclides (Abdel Maksoud et al. 2021f). The effect of pH on the adsorption of caesium and europium radionuclides by using Bi_2WO_6 was studied. It is illustrated that the adsorption of europium is greater than the adsorption of caesium. Besides, the adsorption enhanced as the value of the pH rising.

Ramesh et al. used nanoporous Fe_2O_3 nanoparticles with high surface area, prepared by a hydrothermal method for the photocatalytic degradation of Cr (VI) under visible light (Mavinakere Ramesh and Shivanna 2018). Their results showed that, after 120 min of visible light irradiation, 82.11% of Cr (VI) solution was efficiently removed. The observed performance was ascribed to the efficient electron–hole separation. In addition, the prepared sample possessed a low bandgap and a hollow structure which is suitable for the enhanced photocatalytic performance.

While Yang et al. used the sol–gel method to prepare composites of Fe_3O_4-ZnAl-layered double hydroxide/

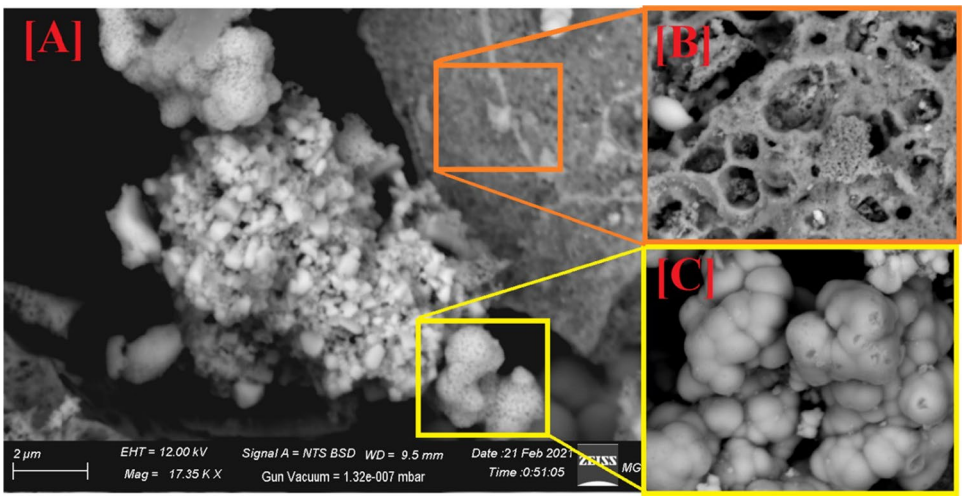

Fig. 7 Scanning electron microscopes images of **a** C modified ZrO_2/Mn-Mg-Zn ferrites composite **b** the spinel Mn-Mg-Zn ferrites, and **c** ZrO_2. Adapted from Ref. (Abdel Maksoud et al. 2021e)with copyright permission from Elsevier, 2022. The carbon modified ZrO_2/Mn-Mg-Zn ferrite composite owned a heterogeneous morphology

TiO_2 to remove Cr (VI) aqueous solutions (Yang et al. 2020), under ultraviolet irradiation, the prepared sample showed a good performance of 97% removal. Their results exhibited that adsorption kinetics, isotherm, and photocatalytic reaction followed the pseudo-second-order, Langmuir model, and the first-order equations, respectively. It is worth mentioning that the efficient separation of photo-generated electron–hole pairs was confirmed as depicted by the photocurrent and the electrochemical impedance analysis.

Conclusion

This review presented the adsorption procedure based on magnetic oxides to eliminate various contaminants (heavy metals, organic dyes, radionuclides, and pharmaceutical compounds) in wastewater. Furthermore, the synthesis methods and advanced properties of magnetic oxides materials have been reviewed. Moreover, the structural, optical, and magnetic properties of these materials have been analysed. The photocatalytic degradation performance of the magnetic oxide nanoparticles has been studied. The incorporation of the magnetic oxides materials with suitable adsorbents (tungsten oxide, titanium dioxide, reduced graphene oxide) lessened the rapid recombination of photogenerated (electron and holes) carriers and improved the photocatalytic degradation ability. Besides, the photodegradation of the pathogenic microbes via magnetic oxides have been presented, along with utilizing the magnetic oxides as candidate adsorbents for heavy metals and radionuclides removal has been examined. Finally, challenges were presented towards the efficient use of magnetic oxide nanoparticles as effective adsorbents for wastewater treatment.

Acknowledgements The authors would like to acknowledge the support given by the EPSRC project "Advancing Creative Circular Economies for Plastics via Technological-Social Transitions" (ACCEPT Transitions, EP/S025545/1). The authors wish to acknowledge the support of The Bryden Centre project (Project ID VA5048), which was awarded by The European Union's INTERREG VA Programme, managed by the Special EU Programmes Body (SEUPB), with match funding provided by the Department for the Economy in Northern Ireland and the Department of Business, Enterprise and Innovation in the Republic of Ireland.

References

Abbas N et al (2021) The photocatalytic performance and structural characteristics of nickel cobalt ferrite nanocomposites after doping with bismuth. J Colloid Interface Sci 594:902–913. https://doi.org/10.1016/j.jcis.2021.03.094

Abd Elkodous M et al (2019) Therapeutic and diagnostic potential of nanomaterials for enhanced biomedical applications. Colloids Surfaces B Biointerfaces. 180:411–428. https://doi.org/10.1016/j.colsurfb.2019.05.008

Abdel Maksoud MIA et al (2018) Synthesis and characterization of metals-substituted cobalt ferrite [Mx Co(1–x) Fe2O4; (M = Zn, Cu and Mn; x = 0 and 0.5)] nanoparticles as antimicrobial agents and sensors for Anagrelide determination in biological samples. Mater Sci Eng C. 92:644–656. https://doi.org/10.1016/j.msec.2018.07.007

Abdel Maksoud MIA et al (2020) Influence of Mg2+ substitution on structural, optical, magnetic, and antimicrobial properties of Mn–Zn ferrite nanoparticles. J Mater Sci Mater Electron 31:2598–2616. https://doi.org/10.1007/s10854-019-02799-4

Abdel Maksoud MIA et al (2020) Insight on water remediation application using magnetic nanomaterials and biosorbents. Coordinat Chem Rev 403:213096. https://doi.org/10.1016/j.ccr.2019.213096

Abdel Maksoud MIA et al (2021) Novel adsorbent based on carbon-modified zirconia/spinel ferrite nanostructures: Evaluation for the removal of cobalt and europium radionuclides from aqueous solutions. J Colloid Interface Sci. https://doi.org/10.1016/j.jcis.2021.08.166

Abdel Maksoud MIA et al (2021) Sorption characteristics of bismuth tungstate nanostructure for removal of some radionuclides from aqueous solutions. Separat Purificat Technol. https://doi.org/10.1016/j.seppur.2021.119478

Abdel Maksoud MIA et al (2021b) Advanced materials and technologies for supercapacitors used in energy conversion and storage: a review. Environ Chem Lett 19:375–439. https://doi.org/10.1007/s10311-020-01075-w

Abdel Maksoud MIA et al (2021c) MoS2-based nanocomposites: synthesis, structure, and applications in water remediation and energy storage: a review. Environ Chem Lett 19:3645–3681. https://doi.org/10.1007/s10311-021-01268-x

Abdel Maksoud MIA et al (2021d) Gamma irradiation-assisted synthesis of PANi/Ag/MoS2/LiCo0.5Fe2O4 nanocomposite: Efficiency evaluation of photocatalytic bisphenol A degradation and microbial decontamination from wastewater. Opt Mater. https://doi.org/10.1016/j.optmat.2021.111396

Abdel-Rafei MK et al (2021) Influence of Ce3+ substitution on antimicrobial and antibiofilm properties of ZnCexFe2−xO4 Nanoparticles (X = 0.0, 0.02, 0.04, 0.06, and 0.08) conjugated with ebselen and its role subsidised with γ-radiation in mitigating human tnbc and colorectal adenocarcinoma proliferation In Vitro. Int J Mol Sci. https://doi.org/10.3390/ijms221810171

Abdel-Rafei MK et al. (2021b) Influence of Ce3+ Substitution on Antimicrobial and Antibiofilm Properties of ZnCexFe2−xO4 Nanoparticles (X = 0.0, 0.02, 0.04, 0.06 and 0.08) Conjugated with Ebselen and Its Role Subsidised with γ-Radiation in Mitigating Human TNBC and Colorectal Adenocarcinoma Proliferation In Vitro. Int J Mol Sci. 22**,** 10171https://www.mdpi.com/1422-0067/22/18/10171

Abed, S. N., et al. Chapter 17 - Nanocarriers in Different Preclinical and Clinical Stages. In: R. K. Tekade, (Ed.), Basic Fundamentals of Drug Delivery. Academic Press, 2019, pp. 685–731.https://doi.org/10.1016/B978-0-12-817909-3.00017-0

Abirami R et al (2021) Preparation of pure PbTiO3 and (Ag–Fe) codoped PbTiO3 perovskite nanoparticles and their enhanced photocatalytic activity. Solid State Commun 327:114232

Abouelela MM et al (2021) A review on plasmonic nanoparticle-semiconductor photocatalysts for water splitting. J Cleaner Product 294:126200. https://doi.org/10.1016/j.jclepro.2021.126200

Aftab S, Nawaz T, Bilal Tahir M (2021) Recent development in shape memory based perovskite materials for energy conversion and storage applications. Int J Energy Res. https://doi.org/10.1002/er.7151

Ahmed A et al (2021) Facile synthesis of Zr4+ substituted Mn0.2Co0.8Fe2−xO4 nanoparticles and their composites with reduced graphene oxide for enhanced photocatalytic performance under visible light irradiation. Synthetic Metals. https://doi.org/10.1016/j.synthmet.2021.116766

Ahmed S et al (2021) Sol-gel synthesis of ferrites nanoparticles and investigation of their magnetic and photocatalytic activity for degradation of reactive blue 21 dye. J Mol Struct 1235:130262. https://doi.org/10.1016/j.molstruc.2021.130262

Ahmed S et al (2021) Sol-gel synthesis of ferrites nanoparticles and investigation of their magnetic and photocatalytic activity for degradation of reactive blue 21 dye. J Mol Struct 1235:130262

Ai L, Jiang J (2010) Influence of annealing temperature on the formation, microstructure and magnetic properties of spinel nanocrystalline cobalt ferrites. Current Appl Phys 10:284–288. https://doi.org/10.1016/j.cap.2009.06.007

Aisida SO et al (2019) Influence of PVA, PVP and PEG doping on the optical, structural, morphological and magnetic properties of zinc ferrite nanoparticles produced by thermal method. Physica B 571:130–136

Ajeesha T et al (2021) Nickel substituted MgFe2O4 nanoparticles via co-precipitation method for photocatalytic applications. Physica B 606:412660. https://doi.org/10.1016/j.physb.2020.412660

Ajeesha T et al (2021) Nickel substituted MgFe2O4 nanoparticles via co-precipitation method for photocatalytic applications. Physica B Condensed Matter. 606:412660

Ajiboye TO et al (2021) Photocatalytic removal of parabens and halogenated products in wastewater: a review. Environ Chem Lett 19:3789–3819. https://doi.org/10.1007/s10311-021-01263-2

Akinlolu K et al. (2019) Synthesis and characterization of A site doped lanthanum based perovskite catalyst for the oxidation of soot. IOP Conference Series: Materials Science and Engineering, Vol. 509. IOP Publishing, pp 012062

Alammar T et al (2017) Ionic-liquid-assisted microwave synthesis of solid solutions of Sr1−xBaxSnO3 perovskite for photocatalytic applications. Chemsuschem 10:3387

Almessiere MA et al (2019) Sonochemical synthesis and physical properties of Co0.3Ni0.5Mn0.2EuxFe2−xO4 nano-spinel ferrites. Ultrason Sonochem 58:104654. https://doi.org/10.1016/j.ultsonch.2019.104654

Almessiere MA et al (2020) Sonochemical synthesis of Dy3+ substituted Mn0.5Zn0.5Fe2−xO4 nanoparticles: structural, magnetic and optical characterizations. Ultrasonics Sonochemistry. 61:104836. https://doi.org/10.1016/j.ultsonch.2019.104836

Almessiere MA et al (2021) Review on functional bi-component nanocomposites based on hard/soft ferrites: structural, magnetic, electrical and microwave absorption properties. Nano-Struct Nano-Objects 26:100728. https://doi.org/10.1016/j.nanoso.2021.100728

Alp E et al (2021) Plasmon-enhanced photocatalytic and antibacterial activity of gold nanoparticles-decorated hematite nanostructures. J Alloys Compounds 852:157021. https://doi.org/10.1016/j.jallcom.2020.157021

Alsabah YA et al (2019) Structural and optical properties of A2YVO6 (A = Mg, Sr) double perovskite oxides. Results in Phys 15:102589. https://doi.org/10.1016/j.rinp.2019.102589

Alshahrani B et al (2021) Structural, optical, and magnetic properties of nanostructured Ag-substituted Co-Zn ferrites: insights on anticancer and antiproliferative activities. J Mater Sci: Mater Electron 32:12383–12401. https://doi.org/10.1007/s10854-021-05870-1

Altaf R et al (2021) Modified magnetite adsorbent (Zr–La@ Fe3O4) for nitrilotrismethylenephosphonate (NTMP) removal and recovery from wastewater. J Cleaner Product 278:123960

Alvarez PJ et al (2018) Emerging opportunities for nanotechnology to enhance water security. Nat Nanotechnol 13:634–641

Alzaid M et al (2020) Extraction of thickness, linear and nonlinear optical parameters of Ge20+ xSe80-x thin films at normal and slightly inclined light for optoelectronic devices. Opt Mater. 110:110539

Andersen HL et al (2018) Crystalline and magnetic structure–property relationship in spinel ferrite nanoparticles. Nanoscale 10:14902–14914. https://doi.org/10.1039/C8NR01534A

Ao R et al (2021) Effects of the preparation method on the simultaneous catalytic oxidation performances of LaCoO3 perovskites for NO and Hg0. Fuel 305:121617

Araujo RN et al (2021) α-Fe2O3 fibers: an efficient photocatalyst for dye degradation under visible light. J Alloys Compounds. 882:160683. https://doi.org/10.1016/j.jallcom.2021.160683

Asab G et al (2020) Synthesis of silica-coated Fe3O4 nanoparticles by microemulsion method: characterization and evaluation of antimicrobial activity. Int J Biomater. https://doi.org/10.1155/2020/4783612

Asab G et al. (2020a) Synthesis of silica-coated fe3o4 nanoparticles by microemulsion method: characterization and evaluation of antimicrobial activity. Int J Biomater. 2020

Asadi R et al (2020) Effective removal of Zn (II) ions from aqueous solution by the magnetic MnFe2O4 and CoFe2O4 spinel ferrite nanoparticles with focuses on synthesis, characterization, adsorption, and desorption. Adv Powder Technol 31:1480–1489

Ashour AH et al (2018) Antimicrobial activity of metal-substituted cobalt ferrite nanoparticles synthesized by sol–gel technique. Particuology. 40:141–151. https://doi.org/10.1016/j.partic.2017.12.001

Ashour A et al (2018) Antimicrobial activity of metal-substituted cobalt ferrite nanoparticles synthesized by sol–gel technique. Particuology 40:141–151

Aslam A et al (2021) Lanthanum doped Zn0.5Co0.5LaxFe2−xO4 spinel ferrites synthesized via co-precipitation route to evaluate structural, vibrational, electrical, optical, dielectric, and thermoelectric properties. J Phys ChemSolids. 154:110080. https://doi.org/10.1016/j.jpcs.2021.110080

Aslam A et al. (2021a) Lanthanum doped Zn0. 5Co0. 5LaxFe2− xO4 spinel ferrites synthesized via co-precipitation route to evaluate structural, vibrational, electrical, optical, dielectric, and thermoelectric properties. J Phys Chem Solids. 154**,** 110080

Attia MS et al (2021) Chitosan and EDTA conjugated graphene oxide antinematodes in Eggplant: toward improving plant immune response. Int J Biol Macromol 179:333–344

Badry MD et al. (2021) Hydrothermally assisted synthesis of magnetic iron oxide-chitosan nanocomposites: electrical and biological evaluation. challenge. 17**,** 20

Bai J et al (2017) Structural and magnetic properties of perovskite SrMnO3 thin films grown by molecular beam epitaxy. Thin Solid Films. 644:57–64. https://doi.org/10.1016/j.tsf.2017.08.052

Bantawal, H., et al. 2021. Vanadium doped CaTiO3 cuboids: Role of vanadium in improving the photocatalytic activity. Nanoscale Advances.

Basaleh A et al (2021) Visible light-driven photodegradation of ciprofloxacin over sol-gel prepared Bi2O3-modified La-doped NaTaO3 nanostructures. Ceram Int 47:19205–19212
Basaleh A et al. (2021a). La-doped NaTaO3 nanoparticles: sol-gel synthesis and synergistic effect of CdO decoration toward efficient visible-light degradation of ciprofloxacin in water. Ceramics Int
Baykal A et al (2013) Synthesis and characterization of high catalytic activity magnetic Fe3O4 supported Pd nanocatalyst. J Supercond Novel Magn 26:165–171. https://doi.org/10.1007/s10948-012-1702-2
Belaidi S et al. 2021. Synthesis of metal and non-metal doping hematite nanoparticles for adsorption and photocatalytic degradation of acid red 14 in aqueous solutions. Int J Environ Anall Chem. 1–14
Benlahrache MT et al (2006) Influence of polarization electric field on the dielectric properties of BaTiO3-based ceramics. Mater Sci Semiconductor Process 9:1115–1118. https://doi.org/10.1016/j.mssp.2006.10.051
Bhat, A. A., et al. 2021. Solvothermal synthesis of Fe doped MnSnO3: An approach of wide bandgap perovskite towards optical, luminescence, and electrochemical properties. International Journal of Energy Research.
Bhateria R, Singh R (2019) A review on nanotechnological application of magnetic iron oxides for heavy metal removal. J Water Process Eng 31:100845. https://doi.org/10.1016/j.jwpe.2019.100845
Bhuyan M et al (2021) Sol-gel synthesized double perovskite Gd2FeCrO6 nanoparticles: Structural, magnetic and optical properties. J Alloys Compounds. 878:160389
Bhuyan MDI et al (2021) Sol-gel synthesized double perovskite Gd2FeCrO6 nanoparticles: structural, magnetic and optical properties. J Alloys Compounds 878:160389. https://doi.org/10.1016/j.jallcom.2021.160389
Biasotto G et al (2011) Microwave-hydrothermal synthesis of perovskite bismuth ferrite nanoparticles. Mater Res Bull 46:2543–2547
Bibi I et al (2021) La1-xGdxCr1-yNiyO3 perovskite nanoparticles synthesis by micro-emulsion route: dielectric, magnetic and photocatalytic properties evaluation. Ceramics Int 47:5822–5831. https://doi.org/10.1016/j.ceramint.2020.11.033
Bloomfield SF et al (2016) Time to abandon the hygiene hypothesis: new perspectives on allergic disease, the human microbiome, infectious disease prevention and the role of targeted hygiene. Perspect Public Health 136:213–224
Borikar M et al. (2021) Characterization of nanostructured spinel NiCrxFe2-xO4 obtained by sol gel auto combustion method. Journal of Physics: Conference Series, Vol 1913. IOP Publishing, pp 012079
Bouziani, A., et al. 2020. Synthesis of α-Fe2O3/TiO2 heterogeneous composites by the sol-gel process and their photocatalytic activity. Journal of Photochemistry and Photobiology A: Chemistry. 400**,** 112718
Bradha M et al (2015) Synthesis of photocatalytic La(1–x)AxTiO3.5–δ (A=Ba, Sr, Ca) nano perovskites and their application for photocatalytic oxidation of congo red dye in aqueous solution. J Rare Earths 33:160–167. https://doi.org/10.1016/s1002-0721(14)60397-5
Bragg WH (1915) The Structure of Magnetite and the Spinels. Nature 95:561–561. https://doi.org/10.1038/095561a0
Buruga K et al (2019) A review on functional polymer-clay based nanocomposite membranes for treatment of water. J Hazard Mater 379:120584
Cai J et al. (2021) Enhanced photoelectrochemical water oxidation in hematite: accelerated charge separation with co doping. Appl Surface Sci. 150606
Can, M. M., et al. 2012. A comparative study of nanosized iron oxide particles; magnetite (Fe3O4), maghemite (γ-Fe2O3) and hematite (α-Fe2O3), using ferromagnetic resonance. Journal of Alloys and Compounds. 542**,** 241–247.https://doi.org/10.1016/j.jallcom.2012.07.091
Cao S et al (2021) Rational synthesis of SrTiO3 nanodots anchored mesocrystalline anatase TiO2 submicrospheres for photocatalytic reduction of CrVI. Separation Purificat Technol. 275:119096. https://doi.org/10.1016/j.seppur.2021.119096
Casbeer E et al (2012) Synthesis and photocatalytic activity of ferrites under visible light: a review. Sep Purif Technol 87:1–14
Chan HBS et al (2004) Carbon-encapsulated radioactive99mTc nanoparticles. Adv Mater 16:144–149. https://doi.org/10.1002/adma.200305407
Chatterjee S et al (2011) Effect of iron oxide and gold nanoparticles on bacterial growth leading towards biological application. J Nanobiotechnol 9:1–7
Chen Y et al (2016) Structure and growth control of organic-inorganic halide perovskites for optoelectronics: from polycrystalline films to single crystals. Adv Sci 3:1500392. https://doi.org/10.1002/advs.201500392
Chen W et al (2016) Polymerizable complex synthesis of SrTiO3:(Cr/Ta) photocatalysts to improve photocatalytic water splitting activity under visible light. Appl Catal B 192:145–151. https://doi.org/10.1016/j.apcatb.2016.03.057
Chen D et al (2017) Defective BiFeO3 with surface oxygen vacancies: facile synthesis and mechanism insight into photocatalytic performance. Sol Energy Mater Sol Cells 171:24–32. https://doi.org/10.1016/j.solmat.2017.06.021
Chen Y et al (2021) Preparation of carbon dots-hematite quantum dots-loaded hydroxypropyl cellulose-chitosan nanocomposites for drug delivery, sunlight catalytic and antimicrobial application. J Photochem Photobiol B Biol 219:112201
Chien S-WC et al. (2021) Investigating the effects of various synthesis routes on morphological, optical, photoelectrochemical and photocatalytic properties of single-phase perovskite BiFeO3. J Phys Chem Solids. 110342
Chinthala M et al (2021) Synthesis and applications of nano-MgO and composites for medicine, energy, and environmental remediation: a review. Environ Chem Lett. https://doi.org/10.1007/s10311-021-01299-4
Chique C et al (2020) Cryptosporidium spp. in groundwater supplies intended for human consumption–a descriptive review of global prevalence, risk factors and knowledge gaps. Water Res. 176:115726
Choong CE et al. (2021) Interfacial coupling perovskite CeFeO3 on layered graphitic carbon nitride as a multifunctional Z-scheme photocatalyst for boosting nitrogen fixation and organic pollutants demineralization. Chem Eng J. 131406
Cornell RM, Schwertmann U (2003) The iron oxides: structure, properties, reactions, occurrences and uses. John Wiley & Sons
Cui E et al (2020) Nanoscale SrFe0.5Ta0.5O3 double perovskite photocatalyst: Low-temperature solvothermal synthesis and photocatalytic NO oxidation performances. Appl Surface Sci 531:147324. https://doi.org/10.1016/j.apsusc.2020.147324
Dai Y et al (2020) Mini-review of perovskite oxides as oxygen electrocatalysts for rechargeable zinc–air batteries. Chemic Eng J 397:125516. https://doi.org/10.1016/j.cej.2020.125516
Dandie CE et al (2020) Disinfection options for irrigation water: reducing the risk of fresh produce contamination with human pathogens. Crit Rev Environ Sci Technol 50:2144–2174
Das N, Kandimalla S (2017) Application of perovskites towards remediation of environmental pollutants: an overview. Int J Environ Sci Technol 14:1559–1572
De D et al (2010) Antibacterial effect of lanthanum calcium manganate (La0. 67Ca0. 33MnO3) nanoparticles against Pseudomonas aeruginosa ATCC 27853. J Biomed Nanotechnol 6:138–144

de Souza ECC, Muccillo R (2010) Properties and applications of perovskite proton conductors. Mater Res 13:385–394. https://doi.org/10.1590/s1516-14392010000300018

de Mello LB et al (2019) Co-precipitation synthesis of (Zn-Mn)-co-doped magnetite nanoparticles and their application in magnetic hyperthermia. J Alloy Compd 779:698–705

Debnath S, Das R (2020) Study of the optical properties of Zn doped Mn spinel ferrite nanocrystals shows multiple emission peaks in the visible range–a promising soft ferrite nanomaterial for deep blue LED. J Mol Struct 1199:127044

Deepapriya S et al (2019) Estimating the ionicity of an inverse spinel ferrite and the cation distribution of La-doped NiFe 2 O 4 nanocrystals for gas sensing properties. Appl Phys A 125:1–13

DeLeo PC et al (2020) Assessment of ecological hazards and environmental fate of disinfectant quaternary ammonium compounds. Ecotoxicol Environ Safety. 206:111116

Demazeau G (2008) Solvothermal reactions: an original route for the synthesis of novel materials. J Mater Sci 43:2104–2114

Deng J et al (2021) S-doping α-Fe2O3 induced efficient electron-hole separation for enhanced persulfate activation toward carbamazepine oxidation: experimental and DFT study. Chem Eng J 420:129863

Dhiwahar AT et al (2021) Improved photocatalytic degradation of rhodamine B under visible light and magnetic properties using microwave combustion grown Ni doped copper ferrite spinel nanoparticles. Solid State Sci 113:106542

Díaz C et al. (2021) Preparation method effect of La0. 9K0. 1Co0. 9Ni0. 1O3 perovskite on catalytic soot oxidation. Fuel. 295**,** 120605

Dinari M, Dadkhah F (2020) Swift reduction of 4-nitrophenol by easy recoverable magnetite-Ag/layered double hydroxide/starch bionanocomposite. Carbohyd Polym 228:115392. https://doi.org/10.1016/j.carbpol.2019.115392

Ding F et al (2020) Structural, morphological and magnetic study of hydrothermal La3+ substitution in Mn–Zn nanoferrites. Appl Phys A 126:221. https://doi.org/10.1007/s00339-020-3406-y

Djellabi R et al (2022) A review of advances in multifunctional XTiO3 perovskite-type oxides as piezo-photocatalysts for environmental remediation and energy production. J Hazard Mater 421:126792. https://doi.org/10.1016/j.jhazmat.2021.126792

Doan VD et al (2020) Cu/Fe3O4@ carboxylate-rich carbon composite: one-pot synthesis, characterization, adsorption and photo-Fenton catalytic activities. Mater Res Bullet 129:110913

Dojcinovic MP, Vasiljevic ZZ, Pavlovic VP, Barisic D, Pajic D, Tadic NB, Nikolic MV (2021) Mixed Mg–Co spinel ferrites: structure, morphology, magnetic and photocatalytic properties. J Alloys Compounds 855:157429. https://doi.org/10.1016/j.jallcom.2020.157429

Domínguez-Arvizu J et al (2019) Study of NiFe2O4 nanoparticles optical properties by a six-flux radiation model towards the photocatalytic hydrogen production. Int J Hydrogen Energy 44:12455–12462

Dong YZ et al (2018) Fe 3 O 4/sepiolite magnetic composite particles and their magneto-responsive characteristics. Colloid Polym Sci 296:11–19

Eggleston CM (2008) Toward new uses for hematite. Science 320:184–185

El-Gendy NS, Nassar HN (2021) Biosynthesized magnetite nanoparticles as an environmental opulence and sustainable wastewater treatment. Sci Total Environ 774:145610. https://doi.org/10.1016/j.scitotenv.2021.145610

El-Khawaga AM et al (2020) Antimicrobial and photocatalytic degradation activities of chitosan-coated magnetite nanocomposite. J Cluster Sci. https://doi.org/10.1007/s10876-020-01869-6

El-Sayyad GS et al (2020) Merits of photocatalytic and antimicrobial applications of gamma-irradiated Co x Ni 1–x Fe 2 O 4/SiO 2/TiO 2; x= 0.9 nanocomposite for pyridine removal and pathogenic bacteria/fungi disinfection: implication for wastewater treatment. RSC Adv 10:5241–5259

Emídio ES et al (2020) Simultaneous degradation of the anticancer drugs 5-fluorouracil and cyclophosphamide using a heterogeneous photo-Fenton process based on copper-containing magnetites (Fe3-xCuxO4). Chemosphere 241:124990. https://doi.org/10.1016/j.chemosphere.2019.124990

Ermanda Y, Lubis S, Ramli M (2021) Preparation and characterization of activated carbon/hematite composite as efficient photocatalyst for naphthol blue black dye degradation. AIP Conference Proceedings. AIP Publishing LLC. https://doi.org/10.1063/5.0045372

Etacheri V et al (2012) Mg-doped ZnO nanoparticles for efficient sunlight-driven photocatalysis. ACS Appl Mater Interfaces 4:2717–2725. https://doi.org/10.1021/am300359h

Etacheri V et al (2013) A highly efficient TiO2–xCx nano-heterojunction photocatalyst for visible light induced antibacterial applications. ACS Appl Mater Interfaces 5:1663–1672. https://doi.org/10.1021/am302676a

Fadillah ND et al. (2021) Degradation of Titan Yellow Using ZnO/Ag Embedded with Fe3O4 Nanoparticles under Visible Light-Induced. Key Engineering Materials, 884. Trans Tech Publ, pp 54–59

Fan G et al (2012) Visible-light-induced photocatalyst based on cobalt-doped zinc ferrite nanocrystals. Ind Eng Chem Res 51:13639–13647. https://doi.org/10.1021/ie201933g

Fang Y et al (2019) First principle calculations of electronic, band structural, and optical properties of BixSr1-xTiO3 perovskite. J Phys Chem Solids 127:107–114

Farag RK et al (2019) Antimicrobial activity of hybrids terpolymers based on magnetite hydrogel nanocomposites. Materials 12:3604

Farghali, M. A., et al. 2021. A magnetic graphene nanocomposite for efficient removal of methylene blue from wastewater. Inorganic Chemistry Communications. 108823

Fayyaz, A., et al. 2021. Catalytic oxidation of naproxen in cobalt spinel ferrite decorated Ti3C2Tx MXene activated persulfate system: Mechanisms and pathways. Chemical Engineering Journal. 407**,** 127842.https://doi.org/10.1016/j.cej.2020.127842

Fazli A et al (2021) Cubic cobalt and zinc co-doped magnetite nanoparticles for persulfate and hydrogen peroxide activation towards the effective photodegradation of Sulfalene. Chem Eng J 404:126391. https://doi.org/10.1016/j.cej.2020.126391

Febrialita R et al (2021) Simbang darah (Iresine herbstii) extract mediated hydrothermal method in the synthesis of zinc ferrite spinel nanoparticles used for photocatalysis and antibacterial applications. J Environ Chemic Eng. 9:105140

Feng N et al (2017) K-Mn supported on three-dimensionally ordered macroporous La0. 8Ce0. 2FeO3 catalysts for the catalytic combustion of soot. Appl Surf Sci 399:114–122

Fodil H, Omari M (2016) Synthesis, structural and physicochemical characterization of BaFe1-xAlxO3−δ oxides. Chem Chemic Technol.https://doi.org/10.23939/chcht10.04.387

Fodil H, Omari M (2017) Synthesis, structural and physicochemical characterization of nanocrystalline La1−xNaxCrO3 powders by Sol-Gel method. J Inorg Organomet Polym Mater 27:1473–1481. https://doi.org/10.1007/s10904-017-0605-x

Gaidhane, M., et al. 2021. Nanocrystalline α-Fe2O3: A Superparamagnetic Material for w-LED Application and Waste Water Treatment

Gandon A et al (2021) Synthesis of single-phase and controlled monodisperse magnetite Fe3O4 nanoparticles. The Canadian Journal of Chemical Engineering 99:479–488

Gao J-M et al (2021) High-efficiency leaching of valuable metals from saprolite laterite ore using pickling waste liquor for synthesis of spinel-type ferrites MFe2O4 with excellent magnetic properties.

J Mater Res Technol 10:988–1001. https://doi.org/10.1016/j.jmrt.2020.12.063
García JG et al (2021) Novel photoactive magnetic semiconductor nanocomposites with potential magneto-optical properties. Appl Nanosci. https://doi.org/10.1007/s13204-021-01980-8
Geetha K et al (2021) Enhanced magnetic and photocatalytic characteristics of cerium substituted spinel MgFe2O4 ferrite nanoparticles. Physica B 615:413083. https://doi.org/10.1016/j.physb.2021.413083
George M et al (2021) Evaluation of Cu–MgFe2O4 spinel nanoparticles for photocatalytic and antimicrobial activates. J Phys Chem Solids 153:110010. https://doi.org/10.1016/j.jpcs.2021.110010
Ghasemi R et al (2020) Effect of Cu substitution on the magnetic and magnetic induction heating response of CdFe2O4 spinel ferrite. J Magnet Magnetic Mater 499:166201
Gonçalves RGL et al (2019) Performance of magnetite/layered double hydroxide composite for dye removal via adsorption, Fenton and photo-Fenton processes. Appl Clay Sci 179:105152. https://doi.org/10.1016/j.clay.2019.105152
Gonçalves NPF et al (2020) Humic acid coated magnetic particles as highly efficient heterogeneous photo-Fenton materials for wastewater treatments. Chem Eng J 390:124619. https://doi.org/10.1016/j.cej.2020.124619
Grabowska, E., 2016. Selected perovskite oxides: Characterization, preparation and photocatalytic properties—A review. Applied Catalysis B: Environmental. 186**,** 97–126.https://doi.org/10.1016/j.apcatb.2015.12.035
Gul S et al (2020) Al-substituted zinc spinel ferrite nanoparticles: preparation and evaluation of structural, electrical, magnetic and photocatalytic properties. Ceram Int 46:14195–14205. https://doi.org/10.1016/j.ceramint.2020.02.228
Guo, T., et al. 2021a. Efficient persulfate activation by hematite nanocrystals for degradation of organic pollutants under visible light irradiation: Facet-dependent catalytic performance and degradation mechanism. Applied Catalysis B: Environmental. 286**,** 119883
Guo, T., et al. 2021b. Enhanced degradation of tetracycline in water over Cu-doped hematite nanoplates by peroxymonosulfate activation under visible light irradiation. Journal of Hazardous Materials. 416**,** 125838
Gupta SM, Tripathi M (2011) A review of TiO2 nanoparticles. Chin Sci Bull 56:1639–1657. https://doi.org/10.1007/s11434-011-4476-1
Gusain R et al (2019) Adsorptive removal and photocatalytic degradation of organic pollutants using metal oxides and their composites: a comprehensive review. Adv Colloid Interface Sci 272:102009. https://doi.org/10.1016/j.cis.2019.102009
Habibi, M. K., et al. 2021. Synthesis of ZnFe2O4: 1wt% Ce3+/Carbon fibers composite and investigation of its adsorption characteristic to remove Congo red dye from aqueous solutions. Journal of Alloys and Compounds. 161901
Haghniaz R et al (2021) Anti-bacterial and wound healing-promoting effects of zinc ferrite nanoparticles. J Nanobiotechnol 19:38. https://doi.org/10.1186/s12951-021-00776-w
Hakeem A et al (2021) Magnetic, dielectric and structural properties of spinel ferrites synthesized by sol-gel method. J Market Res 11:158–169
Hammad M et al (2021) Large-scale synthesis of iron oxide/graphene hybrid materials as highly efficient photo-Fenton catalyst for water remediation. Environ Technol Innov. 21:101239. https://doi.org/10.1016/j.eti.2020.101239
Han P et al (2021) Perovskite CaZrO 3 for efficient ozonation treatment of organic pollutants in wastewater. Catal Sci Technol 11:3697–3705
Hassan H et al (2020) Assessment of zinc ferrite nanocrystals for removal of 134 Cs and 152+ 154 Eu radionuclides from nitric acid solution. J Mater Sci: Mater Electron 31:1616–1633
He X et al (2021) Heterojunction photocatalysts for degradation of the tetracycline antibiotic: a review. Environ Chem Lett. https://doi.org/10.1007/s10311-021-01295-8
Heidari P, Masoudpanah SM (2021) Structural, magnetic and optical properties and photocatalytic activity of magnesium-calcium ferrite powders. J Phys Chem Solids 148:109681. https://doi.org/10.1016/j.jpcs.2020.109681
Hezam, F., et al. 2021. Synthesis and magnetic properties of Ni0.5MgxZn0. 5-xFe2O4 (0.0≤ x≤ 0.5) nanocrystalline spinel ferrites. Mater Chem Phys. 257**,** 123770
Hodges BC et al (2018) Challenges and prospects of advanced oxidation water treatment processes using catalytic nanomaterials. Nat Nanotechnol 13:642–650
Hoque SM et al (2016) Synthesis and characterization of ZnFe2O4 nanoparticles and its biomedical applications. Mater Lett 162:60–63
Hu G et al (2000) Structural tuning of the magnetic behavior in spinel-structure ferrite thin films. Phys Rev B 62:R779–R782. https://doi.org/10.1103/PhysRevB.62.R779
Hu Y et al (2005) The effects of annealing temperature on the sensing properties of low temperature nano-sized SrTiO3 oxygen gas sensor. Sens Actuators B Chem 108:244–249. https://doi.org/10.1016/j.snb.2004.10.053
Hu Y et al (2020) Layered perovskite oxides and their derivative nanosheets adopting different modification strategies towards better photocatalytic performance of water splitting. Renew Sustain Energy Rev 119:109527
Hu P et al (2021) Assessment of magnetic techniques for understanding complex mixtures of magnetite and hematite: the Inuyama red chert. J Geophys Res Solid Earth. 126:e2020JB019518
Huang S-H, Chen D-H (2009) Rapid removal of heavy metal cations and anions from aqueous solutions by an amino-functionalized magnetic nano-adsorbent. J Hazard Mater 163:174–179. https://doi.org/10.1016/j.jhazmat.2008.06.075
Huang X et al (2018) Synthesis and applications of nanoporous perovskite metal oxides. Chem Sci 9:3623–3637. https://doi.org/10.1039/C7SC03920D
Huo YS et al (2014) A polyacrylamide gel route to different-sized CaTiO3 nanoparticles and their photocatalytic activity for dye degradation. J Sol-Gel Sci Technol 71:254–259. https://doi.org/10.1007/s10971-014-3366-9
Hussain K et al (2021) Evaluation of structural, optical, dielectric, electrical, and magnetic properties of Ce3+ doped Cu0. 5Cd0. 25Co0. 25Fe2-xO4 spinel nano-ferrites. Ceram Int 47:3401–3410
Hussain K et al (2021) Evaluation of structural, optical, dielectric, electrical, and magnetic properties of Ce3+ doped Cu0.5Cd0.25Co0.25Fe2-xO4 spinel nano-ferrites. Ceramics Int 47:3401–3410. https://doi.org/10.1016/j.ceramint.2020.09.185
Hyder F, Manjura Hoque S (2017) Brain tumor diagnostics and therapeutics with superparamagnetic ferrite nanoparticles. Contrast Media Mol Imag. 2017
Hyeon T et al (2002) Synthesis of highly crystalline and monodisperse cobalt ferrite nanocrystals. J Phys Chem B 106:6831–6833. https://doi.org/10.1021/jp026042m
Jadhav SA et al (2021) Visible light photocatalytic activity of magnetically diluted Ni–Zn spinel ferrite for active degradation of rhodamine B. Ceram Int 47:13980–13993
Jadhav, V. V., et al. Chapter 3 - Properties of ferrites. In: R. S. Mane, V. V. Jadhav, Eds.), Spinel Ferrite Nanostructures for Energy Storage Devices. Elsevier, 2020, pp. 35–50.https://doi.org/10.1016/B978-0-12-819237-5.00003-1

Jamil TS et al (2018) Visible light activity of BaFe1-xCuxO3-δ as photocatalyst for atrazine degradation. Ecotoxicol Environ Saf 163:620–628. https://doi.org/10.1016/j.ecoenv.2018.07.106

Jamzad M, Bidkorpeh MK (2020) Green synthesis of iron oxide nanoparticles by the aqueous extract of Laurus nobilis L. leaves and evaluation of the antimicrobial activity. J Nanostruct Chem 10:193–201

Jamzad M, Kamari Bidkorpeh M (2020) Green synthesis of iron oxide nanoparticles by the aqueous extract of Laurus nobilis L. leaves and evaluation of the antimicrobial activity. J Nanostruct Chem 10:193–201. https://doi.org/10.1007/s40097-020-00341-1

Janaki S et al (2018) A Novel approach for synthesis of LaFeO3/bentonite Nanocomposite for degradation of methylene blue with enhanced photocatalytic activity. Mater Res Express. 6:035013

Jang JS et al (2011) Photocatalytic hydrogen production in water-methanol mixture over iron-doped CaTiO3. Bull Korean Chem Soc 32:95–99. https://doi.org/10.5012/bkcs.2011.32.1.95

Jia Y et al (2019) Au nanoparticles enhanced Z-scheme Au-CoFe2O4/MoS2 visible light photocatalyst with magnetic retrievability. Appl Surface Sci. 463:854–862. https://doi.org/10.1016/j.apsusc.2018.09.008

Jing J et al. (2021) Highly efficient removal of bisphenol A by a novel Co-doped LaFeO3 perovskite/PMS system in salinity water. Sci Total Environ. 149490

Jorgetto A, d. O., et al (2018) Magnetically-extractable hybrid of magnetite, mesoporous silica and titania for the photo-degradation of organic compounds in water. Appl Surf Sci 457:121–133. https://doi.org/10.1016/j.apsusc.2018.06.218

Jun B-M et al (2020) Accelerated photocatalytic degradation of organic pollutants over carbonate-rich lanthanum-substituted zinc spinel ferrite assembled reduced graphene oxide by ultraviolet (UV)-activated persulfate. Chem Eng J 393:124733. https://doi.org/10.1016/j.cej.2020.124733

Kalita E, Baruah J (2020) Environmental remediation. Colloidal Metal Oxide Nanoparticles. Elsevier, pp 525–576

Kamaraj M et al (2019) Biofabrication of iron oxide nanoparticles as a potential photocatalyst for dye degradation with antimicrobial activity. Int J Environ Sci Technol 16:8305–8314. https://doi.org/10.1007/s13762-019-02402-7

Kappadan S et al (2016) Tetragonal BaTiO3 nanoparticles: an efficient photocatalyst for the degradation of organic pollutants. Mater Sci Semicond Process 51:42–47. https://doi.org/10.1016/j.mssp.2016.04.019

Karthik V et al (2021) Graphene-based materials for environmental applications: a review. Environ Chem Lett 19:3631–3644. https://doi.org/10.1007/s10311-021-01262-3

Kaykan L et al. (2021) Influence of the preparation method and aluminum ion substitution on the structure and electrical properties of lithium–iron ferrites. Appl Nanosci. 1–9

Kefeni KK et al. (2017a) Ferrite nanoparticles: synthesis, characterisation and applications in electronic device. Mater Sci Eng, B 215:37–55

Kefeni KK et al. (2017b) Application of spinel ferrite nanoparticles in water and wastewater treatment: a review. Sep Purif Technol 188:399–422

Kefeni, K. K., Mamba, B. B., 2020. Photocatalytic application of spinel ferrite nanoparticles and nanocomposites in wastewater treatment: Review. Sustainable Materials and Technologies. 23**,** e00140.https://doi.org/10.1016/j.susmat.2019.e00140

Kefeni KK et al. (2020) Spinel ferrite nanoparticles and nanocomposites for biomedical applications and their toxicity. Mater Sci Eng C. 107, 110314

Keijser B et al (2008) Pyrosequencing analysis of the oral microflora of healthy adults. J Dent Res 87:1016–1020

Kendall RJ et al (2016) Wildlife toxicology: emerging contaminant and biodiversity issues. CRC Press

Khalil WF et al (2020) Graphene oxide-based nanocomposites (GO-chitosan and GO-EDTA) for outstanding antimicrobial potential against some Candida species and pathogenic bacteria. Int J Biol Macromol 164:1370–1383

Khan I, Qurashi A (2018) sonochemical-assisted in situ electrochemical synthesis of Ag/α-Fe2O3/TiO2 nanoarrays to harness energy from photoelectrochemical water splitting. ACS Sustain Chem Eng 6:11235–11245. https://doi.org/10.1021/acssuschemeng.7b02848

Khishigdemberel I et al (2020) Structural, infrared and magnetic properties of MgAlxFe2-xO4 compounds: effect of the preparation methods and Al substitution. Solid State Sci 109:106400

Khoso WA et al (2021) Synthesis, characterization and heavy metal removal efficiency of nickel ferrite nanoparticles (NFN's). Sci Rep 11:3790. https://doi.org/10.1038/s41598-021-83363-1

Kim H-J et al (2011) Template-free solvothermal synthesis of hollow hematite spheres and their applications in gas sensors and Li-ion batteries. J Mater Chem 21:6549–6555

Kim C et al (2018) Engineered superparamagnetic nanomaterials for arsenic (V) and chromium (VI) sorption and separation: quantifying the role of organic surface coatings. Environ Sci Nano 5:556–563

Kirankumar, V. S., Sumathi, S., 2020a. A review on photodegradation of organic pollutants using spinel oxide. Materials Today Chemistry. 18**,** 100355.https://doi.org/10.1016/j.mtchem.2020.100355

Kirankumar V, Sumathi S (2020) A review on photodegradation of organic pollutants using spinel oxide. Mater Today Chem 18:100355

Kongsat P et al (2021) Synthesis of structure-controlled hematite nanoparticles by a surfactant-assisted hydrothermal method and property analysis. J Phys Chem Solids. 148:109685

Kostyukhin EM et al (2021) Hydrothermal microwave-assisted synthesis of LaFeO3 catalyst for N2O decomposition. J Am Ceram Soc 104:492–503

Kumar A et al (2021) High interfacial charge carrier separation in Fe3O4 modified SrTiO3/Bi4O5I2 robust magnetic nano-heterojunction for rapid photodegradation of diclofenac under simulated solar-light. J Clean Prod 315:128137. https://doi.org/10.1016/j.jclepro.2021.128137

Kurian, J., et al. 2021. High magnetic fluid hyperthermia efficiency in copper ferrite nanoparticles prepared by solvothermal and hydrothermal methods. Journal of Magnetism and Magnetic Materials. 538**,** 168233

Kushwaha HS, Vaish R (2016) Enhanced visible light photocatalytic activity of curcumin-sensitized perovskite Bi0. 5Na0. 5TiO3 for rhodamine 6G degradation. Int J Appl Ceram Technol 13:333–339

Kusigerski V et al (2019) Magnetic properties and heating efficacy of magnesium doped magnetite nanoparticles obtained by co-precipitation method. J Magnetism Magnet Mater. 475**,** 470–478.https://doi.org/10.1016/j.jmmm.2018.11.127

Kwak BS, Kang M (2015) Photocatalytic reduction of CO2 with H2O using perovskite CaxTiyO3. Appl Surf Sci 337:138–144. https://doi.org/10.1016/j.apsusc.2015.02.078

Lakhanpal S et al (2021) Magnetite coated sand adsorbent for Cr (VI) removal from synthetic and pharmaceutical wastewater: adsorption isotherms and kinetics. Arab J Geosci 14:1–15

Lassoued A (2021) Synthesis and characterization of Zn-doped α-Fe2O3 nanoparticles with enhanced photocatalytic activities. J Mol Struct 1239:130489. https://doi.org/10.1016/j.molstruc.2021.130489

Lassoued A, Li JF (2020) Magnetic and photocatalytic properties of Ni–Co ferrites. Solid State Sci 104:106199. https://doi.org/10.1016/j.solidstatesciences.2020.106199

Lee S, Park J-W (2020) Hematite/graphitic carbon nitride nanofilm for fenton and photocatalytic oxidation of methylene blue. Sustainability 12:2866

Leonel AG et al (2021) Advanced functional nanostructures based on magnetic iron oxide nanomaterials for water remediation: a review. Water Res 190:116693. https://doi.org/10.1016/j.watres.2020.116693

LI Q et al (2005) Study on cytotoxicity and oxidative effects of different sizes of hematite (Fe_2O_3) nanoparticles on CHL cell in vitro [J]. China J Modern Med 15:1921–1926

Li G et al (2020) Highly enhanced degradation of organic pollutants in hematite/sulfite/photo system. Chem Eng J 386:124007

Lim PF et al. (2019) Perovskite Oxide–Based Photocatalysts for Excellent Visible Light–Driven Photocatalysis and Energy Conversion. Plant Nanobionics. Springer, pp 35–54

Liu J et al (2019) The significant effect of photo-catalyzed redox reactions on the immobilization of chromium by hematite. Chem Geol 524:228–236. https://doi.org/10.1016/j.chemgeo.2019.06.005

Liu L et al (2020a) Cooperation of oxygen vacancies and 2D ultrathin structure promoting CO2 photoreduction performance of Bi4Ti3O12. Sci Bull 65:934–943

Liu X et al (2020b) Significantly enhanced piezo-photocatalytic capability in BaTiO3 nanowires for degrading organic dye. J Materiom 6:256–262

Liu J et al (2021) Enhanced photocatalytic water splitting with surface defective SrTiO3 nanocrystals. Front Energy. https://doi.org/10.1007/s11708-021-0735-2

Lu F, Astruc D (2020) Nanocatalysts and other nanomaterials for water remediation from organic pollutants. Coordinat Chem Rev 408:213180

Luo J, Maggard PA (2006) Hydrothermal synthesis and photocatalytic activities of SrTiO3-Coated Fe2O3 and BiFeO3. Adv Mater 18:514–517. https://doi.org/10.1002/adma.200500109

Ma Z et al (2021) Tackling challenges in perovskite-type metal oxide photocatalysts. Energy Technol 9:2001019. https://doi.org/10.1002/ente.202001019

Madhukara Naik M et al (2019) Green synthesis of zinc doped cobalt ferrite nanoparticles: Structural, optical, photocatalytic and antibacterial studies. Nano-Struct Nano-Objects. 19:100322. https://doi.org/10.1016/j.nanoso.2019.100322

Magdalane CM et al (2021) Synthesis and characterization of TiO2 doped cobalt ferrite nanoparticles via microwave method: investigation of photocatalytic performance of congo red degradation dye. Surfaces Interfaces. 101296

Mahani AA et al (2018) Sol-gel derived flexible silica aerogel as selective adsorbent for water decontamination from crude oil. Mar Pollut Bull 129:438–447

Mahasti NNN et al (2020) Recovery of magnetite from fluidized-bed homogeneous crystallization of iron-containing solution as photocatalyst for Fenton-like degradation of RB5 azo dye under UVA irradiation. Sep Purif Technol 247:116975. https://doi.org/10.1016/j.seppur.2020.116975

Majid F et al (2021) Synthesis and characterization of NiFe2O4 ferrite: Sol–gel and hydrothermal synthesis routes effect on magnetic, structural and dielectric characteristics. Mater Chem Phys. 258:123888

Makofane A et al (2021) Photocatalytic degradation of methylene blue and sulfisoxazole from water using biosynthesized zinc ferrite nanoparticles. Ceramics Int

Maksoud MA et al (2018) Synthesis and characterization of metals-substituted cobalt ferrite [Mx Co (1–x) Fe2O4;(M= Zn, Cu and Mn; x= 0 and 0.5)] nanoparticles as antimicrobial agents and sensors for Anagrelide determination in biological samples. Mater Sci Eng C 92:644–656

Maksoud MA et al (2019) Antibacterial, antibiofilm, and photocatalytic activities of metals-substituted spinel cobalt ferrite nanoparticles. Microb Pathog 127:144–158

Maksoud MA et al (2020) Nanostructured Mg substituted Mn-Zn ferrites: a magnetic recyclable catalyst for outstanding photocatalytic and antimicrobial potentials. J Hazard Mater. 399:123000

Maksoud MA et al (2020a) Influence of Mg 2+ substitution on structural, optical, magnetic, and antimicrobial properties of Mn–Zn ferrite nanoparticles. J Mater Sci Mater Electron 31:2598–2616

Maksoud MA et al (2020b) Unveiling the effect of Zn 2+ substitution in enrichment of structural, magnetic, and dielectric properties of cobalt ferrite. J Inorg Organomet Polym Mater 30:3709–3721

Manikandan A et al (2015) Magnetically Recyclable Spinel $Mn_xZn1–x$ Fe2O4 ($0.0 \leq x \leq 0.5$) Nano-Photocatalysts. Adv Sci Eng Med 7:33–46. https://doi.org/10.1166/asem.2015.1654

Manjunatha CR, Nagabhushana BM, Raghu MS, Pratibha S, Dhananjaya N, Narayana A (2019) Perovskite lanthanum aluminate nanoparticles applications in antimicrobial activity, adsorptive removal of direct blue 53 dye and fluoride. Mater Sci Eng C 101:674–685. https://doi.org/10.1016/j.msec.2019.04.013

Manohar A et al (2021) Mixed Zn–Ni spinel ferrites: Structure, magnetic hyperthermia and photocatalytic properties. Ceram Int 47:7052–7061

Mansour H et al (2020) Novel α-Fe 2 O 3/TiO 2 nanocomposites with enhanced photocatalytic activity. Appl Phys A 126:1–10

Marcinowski P et al (2020) Magnetite and hematite in advanced oxidation processes application for cosmetic wastewater treatment. Processes 8:1343

Maria Holban A et al (2014) Novel drug delivery magnetite nanosystems used in antimicrobial therapy. Curr Org Chem 18:185–191

Martinez-Julian F et al (2014) Probing lithiation kinetics of carbon-coated ZnFe2O4 nanoparticle battery anodes. J Phys Chem c 118:6069–6076

Maruthupandy M, Riquelme D, Rajivgandhi G, Muneeswaran T, Cho WS, Anand M, Manoharan N, Quero F (2021) Dual-role of graphene/bacterial cellulose/magnetite nanocomposites as highly effective antibacterial agent and visible-light-driven photocatalyst. J Environ Chemic Eng 9(5):106014. https://doi.org/10.1016/j.jece.2021.106014

Mascolo MC et al (2013) Room temperature co-precipitation synthesis of magnetite nanoparticles in a large pH window with different bases. Materials 6:5549–5567

Masudi A et al (2020) Magnetite-based catalysts for wastewater treatment. Environ Sci Pollut Res 27:4664–4682

Mathew DS, Juang R-S (2007) An overview of the structure and magnetism of spinel ferrite nanoparticles and their synthesis in microemulsions. Chemic Eng J 129:51–65. https://doi.org/10.1016/j.cej.2006.11.001

Mavinakere Ramesh A, Shivanna S (2018) Visible light assisted photocatalytic degradation of chromium (VI) by using nanoporous Fe2O3. J Mater. 2018

McKee AM, Cruz MA (2021) Microbial and viral indicators of pathogens and human health risks from recreational exposure to waters impaired by fecal contamination. J Sustain Water Built Environ 7:03121001

Medinger J et al (2021) Solvothermal synthesis combined with design of experiments—optimization approach for magnetite nanocrystal clusters. Nanomaterials 11:360

Meena S et al (2021) Enhanced sunlight driven photocatalytic activity and electrochemical sensing properties of Ce-doped MnFe2O4 nano magnetic ferrites. Ceram Int 47:14760–14774

Meisen U, Kathrein H (2000) Influence of particle size, shape and particle size distribution on properties of magnetites for the

production of toners. J Imag Sci Technol. 44**,** 508–513https://www.scopus.com/inward/record.uri?eid=2-s2.0-0034315059&partnerID=40&md5=c54c2dad7ac88faabd496516b2b6ef6a
Meng Y et al (2014) Synthesis of barium ferrite ultrafine powders by a sol–gel combustion method using glycine gels. J Alloy Compd 583:220–225
Meng C et al (2021) Hydrothermal preparation of novel rGO-KTaO3 nanocubes with enhanced visible light photocatalytic activity. Spectrochimica Acta Part A: Mol Biomol Spectroscopy. 250:119352
Mezni A et al (2021). Ternay Au@ TiO 2/α-Fe 2 O 3 Nanocomposite with Nanoring Structure: Synthesis, Characterization and Photocatalytic Activity. J Inorgan Organometall Polymers Mater. 1–8
Mishra A, Prasad R (2014) Preparation and application of perovskite catalysts for diesel soot emissions control: an overview. Catalysis Rev 56:57–81
Mmelesi OK et al. (2020) Cobalt ferrite nanoparticles and nanocomposites: photocatalytic, antimicrobial activity and toxicity in water treatment. Mater Sci Semiconductor Process. 105523
Mohammadi H et al (2021) Removal of hexavalent chromium ions and acid red 18 by superparamagnetic CoFe2O4/polyaniline nanocomposites under external ultrasonic fields. Microporous Mesoporous Mater 324:111275. https://doi.org/10.1016/j.micromeso.2021.111275
Mohammed HB et al. (2021) Eugenol-functionalized magnetite nanoparticles modulate virulence and persistence in pseudomonas aeruginosa clinical strains. Molecules. 26**,** 2189. https://www.mdpi.com/1420-3049/26/8/2189
Mohan H et al (2021) Highly efficient visible light driven photocatalytic activity of zinc/ferrite: carbamazepine degradation, mechanism and toxicity assessment. J Hazard Mater 416:126209. https://doi.org/10.1016/j.jhazmat.2021.126209
Namikuchi EA et al. (2021) PEG size effect and its interaction with Fe3O4 nanoparticles synthesized by solvothermal method: morphology and effect of pH on the stability. Nano Express
Narayana PL et al (2022) Predictive capability evaluation and optimization of Pb(II) removal by reduced graphene oxide-based inverse spinel nickel ferrite nanocomposite. Environ Res. 204:112029. https://doi.org/10.1016/j.envres.2021.112029
Nasab AS et al (2021) Synthesis of praseodymium titanate nanoparticles supported on core–shell silica coated magnetite via mild condition and their photocatalytic capability evaluation. J Mater Sci Mater Electron 32:13527–13538. https://doi.org/10.1007/s10854-021-05929-z
Ng Q et al (2015) Magnetic nanoparticles augmented composite membranes in removal of organic foulant through magnetic actuation. J Membr Sci 493:134–146
Nguyen V-H et al (2020) Perovskite oxide-based photocatalysts for solar-driven hydrogen production: Progress and perspectives. Solar Energy. 211, 584–599.https://doi.org/10.1016/j.solener.2020.09.078
Nguyen TA et al. (2021) Influence of the synthetic conditions on the crystal structure, magnetic and optical properties of holmium orthoferrite nanoparticles. J Mater Sci Mater Electron. 1–10
Nhlapo TA et al (2018) Magnetic properties of Mn0. 1Mg0. 2TM0. 7Fe2O4 (TM= Zn Co, or Ni) prepared by hydrothermal processes: The effects of crystal size and chemical composition. J Magn Magn Mater 448:123–129
Nhlapo T et al (2021) Temperature-dependent magnetic behavior of Mn-Mg spinel ferrites with substituted Co, Ni & Zn, synthesized by hydrothermal method. J Mol Struct 1245:131042
Niazi JH, Gu MB (2009) Toxicity of metallic nanoparticles in microorganisms-a review. Atmospheric and Biological Environmental Monitoring. 193–206
Nigam A, Pawar S (2020) Structural, magnetic, and antimicrobial properties of zinc doped magnesium ferrite for drug delivery applications. Ceram Int 46:4058–4064
Nilius B et al (2007) Transient receptor potential cation channels in disease. Physiol Rev 87:165–217
Nizamuddin S et al (2019) Iron oxide nanomaterials for the removal of heavy metals and dyes from wastewater. Nanoscale Mater Water Purif. 447–472
Nkurikiyimfura I et al (2020) Temperature-dependent magnetic properties of magnetite nanoparticles synthesized via coprecipitation method. J Alloys Compounds. 846:156344
Noh J et al (2014) A density functional theory investigation of the electronic structure and spin moments of magnetite. Sci Technol Adv Mater 15:044202. https://doi.org/10.1088/1468-6996/15/4/044202
Okejiri F et al (2020) Room-temperature synthesis of high-entropy perovskite oxide nanoparticle catalysts through ultrasonication-based method. ChemSusChem 13:111–115. https://doi.org/10.1002/cssc.201902705
de Oliveira Guidolin T et al (2021) Photocatalytic pathway on the degradation of methylene blue from aqueous solutions using magnetite nanoparticles. J Cleaner Product. 128556
Osman AI et al (2019) Production and characterisation of activated carbon and carbon nanotubes from potato peel waste and their application in heavy metal removal. Environ Sci Pollut Res 26:37228–37241
Osman AI et al (2019) Bioethanol and biodiesel: Bibliometric mapping, policies and future needs. Ren Sustain Energy Rev 152:111677. https://doi.org/10.1016/j.rser.2021.111677
Özkan DÇ et al (2021) Synthesis and characterizations of LaMnO 3 perovskite powders using sol–gel method. J Mater Sci: Mater Electron. 1–19
Pei J et al (2019) Hierarchical CaTiO3 nanowire-network architectures for H2 evolution under visible-light irradiation. J Alloy Compd 806:889–896. https://doi.org/10.1016/j.jallcom.2019.07.294
Pereira C et al (2012) Superparamagnetic MFe2O4 (M= Fe Co, Mn) nanoparticles: tuning the particle size and magnetic properties through a novel one-step coprecipitation route. Chem Mater 24:1496–1504
Pham TN et al (2020) Spinel ferrite (AFe2O4)-based heterostructured designs for lithium-ion battery, environmental monitoring, and biomedical applications. RSC Adv 10:31622–31661. https://doi.org/10.1039/D0RA05133K
Phumying S et al (2021) A simple synthesis and the magnetic properties of egg white solution-assisted hydrothermally prepared magnetite (Fe3O4) nanoparticles. Japanese J Appl Phys. 60**,** SCCF04
Platnich CM et al (2021) Simple solvothermal approach to highly nanostructured hematite thin films. Can J Chem 99:355–361
Polo-Garzon F, Wu Z (2018) Acid–base catalysis over perovskites: a review. J Mater Chem a 6:2877–2894
Popkov VI, Albadi Y (2021) The effect of co-precipitation temperature on the crystallite size and aggregation/agglomeration of GdFeO_3 nanoparticles. Наносистемы: физика, химия, математика. 12**,** 224–231
Popov N et al (2021) Influence of Cr doping on the structural, magnetic, optical and photocatalytic properties of α-Fe2O3 nanorods. J Phys Chem Solids 148:109699. https://doi.org/10.1016/j.jpcs.2020.109699
Pullar RC (2012) Hexagonal ferrites: a review of the synthesis, properties and applications of hexaferrite ceramics. Progress in Mater Sci 57:1191–1334. https://doi.org/10.1016/j.pmatsci.2012.04.001
Qin H et al (2021) Spinel ferrites (MFe2O4): Synthesis, improvement and catalytic application in environment and energy field. Adv Colloid Interface Sci. 102486

Querido MM et al (2019) Self-disinfecting surfaces and infection control. Colloids Surf B 178:8–21
Radoń A et al (2019) Catalytic activity of non-spherical shaped magnetite nanoparticles in degradation of Sudan I, Rhodamine B and Methylene Blue dyes. Appl Surf Sci 487:1018–1025. https://doi.org/10.1016/j.apsusc.2019.05.091
Rahimi M et al (2013) The effect of zinc doping on the structural and magnetic properties of Ni 1–x Zn x Fe 2 O 4. J Mater Sci 48:2969–2976
Rahman ZU et al (2021) A facile approach to fabricate magnetic and mesoporous Fe 3 O 4@ Au@ mTiO 2 composites. J Mater Sci: Mater Electron 32:8837–8847
Rakibuddin M, Kim H (2020) Sol-gel derived Fe3O4 quantum dot decorated silica composites for effective removal of arsenic (III) from water. Mater Chem Phys. 240:122245
Ramana EV et al (2014) Ferroelectric and magnetic properties of magnetoelectric (Na0.5Bi0.5)TiO3–BiFeO3 synthesized by acetic acid assisted sol–gel method. Journal of the European Ceramic Society. 34, 4201–4211.https://doi.org/10.1016/j.jeurceramsoc.2014.06.027
Raming TP et al (2002) The synthesis and magnetic properties of nanosized hematite (α-Fe2O3) particles. J Colloid Interface Sci. 249:346–350. https://doi.org/10.1006/jcis.2001.8194
Ramu AG et al (2021) A facile synthesis of metal ferrites and their catalytic removal of toxic nitro-organic pollutants. Environ Pollut 270:116063
Ranganathan R, Ray A (2002) Ferrites—what is new? Pramana 58:995–1002. https://doi.org/10.1007/s12043-002-0206-1
Reddy DHK, Yun Y-S (2016) Spinel ferrite magnetic adsorbents: Alternative future materials for water purification? Coordination Chemistry Reviews. 315, 90–111.https://doi.org/10.1016/j.ccr.2016.01.012
Rehman A et al (2020) Nanocrystalline hematite α-Fe2O3 synthesis with different precursors and their composites with graphene oxide. Ceram Int 46:8227–8237
Remya KP et al (2020) Tailoring the morphology and size of perovskite BiFeO3 nanostructures for enhanced magnetic and electrical properties. Mater Design 192:108694. https://doi.org/10.1016/j.matdes.2020.108694
Rheima AM et al. (2021) Synthesis and structural characterization of ZnTiO3 nanoparticles via modification sol-gel prosses for assessment of their antimicrobial activity. Int J Pharm Res. 13
Rioult M et al (2016) Oxygen vacancies engineering of iron oxides films for solar water splitting. J Physic Chem c 120:7482–7490. https://doi.org/10.1021/acs.jpcc.6b00552
Rojas-Mantilla HD et al (2021) Nontronite mineral clay NAu-2 as support for hematite applied as catalyst for heterogeneous photo-Fenton processes. Chemosphere 277:130258. https://doi.org/10.1016/j.chemosphere.2021.130258
Rosa EV et al (2021) Carbon nitride nanosheets magnetically decorated with Fe3O4 nanoparticles by homogeneous precipitation: adsorption-photocatalytic performance and acute toxicity assessment. Environ Nanotechnol, Monitor Manag. 100549
Rouhani Z et al (2019) Response surface optimization of hydrothermal synthesis of Bismuth ferrite nanoparticles under supercritical water conditions: Application for photocatalytic degradation of Tetracycline. Environ Nanotechnol, Monitor Manag 11:100198
Sagala L et al. (2021) Synthesis and characterization of nanoparticles Zn0. 7Ni0. 15Cu0. 15Fe2O4 using the co-precipitation method. Journal of Physics: Conference Series, Vol. 1882. IOP Publishing, pp 012012
Sahni M et al (2021) Effect of Yb/Co co-dopants on surface chemical bonding states of BiFeO3 nanoparticles with promising photocatalytic performance in dye degradation. J Phys Chem Solids 152:109926. https://doi.org/10.1016/j.jpcs.2020.109926
Sani S et al (2021). One-step statistical design of experiment for the screening and optimization of magnetite nanoparticles yields from solvothermal synthesis. Microporous and Mesoporous Materials. 312, 110775
Santosa SJ et al (2021) Composite of magnetite and Zn/Al layered double hydroxide as a magnetically separable adsorbent for effective removal of humic acid. Colloids Surfaces A Physicochem Eng Aspects 614:126159
Sardana N et al (2018) Synthesis and characterization of dendrimer modified magnetite nanoparticles and their antimicrobial activity for toxicity analysis. J Integrat Sci Technol 6:1–5
Schuele WJ, Deetscreek VD (1961) Preparation, growth, and study of ultrafine ferrite particles. J Appl Phys. https://doi.org/10.1063/1.2000416
Serdiuk V et al (2021) Synthesis and properties of magnetite nanoparticles with peroxide-containing polymer shell and nanocomposites based on them. J Appl Polym Sci 138:50928
Shabbir A et al (2019) Zirconium substituted spinel nano-ferrite Mg0.2Co0.8Fe2O4 particles and their hybrids with reduced graphene oxide for photocatalytic and other potential applications. Ceramics Int 45:16121–16129. https://doi.org/10.1016/j.ceramint.2019.05.130
Sharma RP et al (2019) Sol–gel auto-combustion mediated cobalt ferrite nanoparticles: a potential material for antimicrobial applications. Int Nano Lett 9:141–147. https://doi.org/10.1007/s40089-019-0268-4
Shaterian M et al (2021) Controllable synthesis of ZnFe 2 O 4 submicroparticles by poly (diallyldimethylammonium chloride)-assisted solvothermal method. J Polym Res 28:1–12
Sherstyuk DP et al (2021) Effect of Co content on magnetic features and SPIN states IN Ni–Zn spinel ferrites. Ceramics Int 47:12163–12169. https://doi.org/10.1016/j.ceramint.2021.01.063
Shi R et al (2017) Recent progress in photocatalytic CO2 reduction over perovskite oxides. Solar RRL. 1:1700126. https://doi.org/10.1002/solr.201700126
de Silva FG et al (2019) Structural and magnetic properties of spinel ferrite nanoparticles. J Nanosci Nanotechnol 19:4888–4902. https://doi.org/10.1166/jnn.2019.16877
Sim Y et al (2019) Oxidative coupling of methane over LaAlO3 perovskite catalysts prepared by a co-precipitation method: effect of co-precipitation pH value. J Energy Chem 35:1–8
Singh S et al (2015) Separation of hematite from banded hematite jasper (BHJ) by magnetic coating. J Central South Univ 22:437–444
Singh C et al (2017) Doped LaCoO3 perovskite with Fe: a catalyst with potential antibacterial activity. Vacuum 146:468–473. https://doi.org/10.1016/j.vacuum.2017.06.039
Singh J et al (2019) Dynamic CO2 adsorption on activated carbon adsorbents synthesized from polyacrylonitrile (PAN): Kinetic and isotherm studies. Microporous Mesoporous Mater 280:357–366. https://doi.org/10.1016/j.micromeso.2019.02.031
Singh P et al (2019) Systematic review on applicability of magnetic iron oxides–integrated photocatalysts for degradation of organic pollutants in water. Mater Today Chem 14:100186. https://doi.org/10.1016/j.mtchem.2019.08.005
Skliri E et al (2018) Assembly and photochemical properties of mesoporous networks of spinel ferrite nanoparticles for environmental photocatalytic remediation. Appl Cataly B Environ 227:330–339. https://doi.org/10.1016/j.apcatb.2018.01.045
Slimani Y et al (2019) Calcination effect on the magneto-optical properties of vanadium substituted NiFe2O4 nanoferrites. J Mater Sci: Mater Electron 30:9143–9154. https://doi.org/10.1007/s10854-019-01243-x
Solano E et al (2012) Facile and efficient one-pot solvothermal and microwave-assisted synthesis of stable colloidal solutions of

MFe2O4 spinel magnetic nanoparticles. J Nanopart Res 14:1034. https://doi.org/10.1007/s11051-012-1034-y
Sugimoto M (1999) The past, present, and future of ferrites. J Am Ceramic Soc 82:269–280. https://doi.org/10.1111/j.1551-2916.1999.tb20058.x
Sun S et al (2004) Monodisperse MFe2O4 (M = Fe Co, Mn) nanoparticles. J Am Chem Soc 126:273–279. https://doi.org/10.1021/ja0380852
Sun J et al (2021) Solvothermal synthesis and photocatalytic activities of cubic potassium tantalite and cuprum doped potassium tantalite. Spectrochimica Acta Part A: Mol Biomol Spectroscopy. 246, 118995
Šutka A, Gross KA (2016) Spinel ferrite oxide semiconductor gas sensors. Sens Actuators, B Chem 222:95–105
Taffa DH et al (2016) Photoelectrochemical and theoretical investigations of spinel type ferrites (M x Fe 3–x O 4) for water splitting: a mini-review. J Photon Energy. 7:012009
Tanbir K et al (2020) Gd-doped soft Mn–Zn nanoferrites: synthesis, microstructural, magnetic and dielectric characterizations. J Mater Sci: Mater Electron 31:3529–3538. https://doi.org/10.1007/s10854-020-02901-1
Tatarchuk T et al (2017) Structural, Optical, and Magnetic Properties of Zn-Doped CoFe2O4 Nanoparticles. Nanoscale Res Lett 12:141. https://doi.org/10.1186/s11671-017-1899-x
Tatarchuk T et al (2021) Magnesium-zinc ferrites as magnetic adsorbents for Cr(VI) and Ni(II) ions removal: cation distribution and antistructure modeling. Chemosphere. 270:129414. https://doi.org/10.1016/j.chemosphere.2020.129414
Tatarchuk, T., et al. Spinel ferrite nanoparticles: synthesis, crystal structure, properties, and perspective applications. International Conference on Nanotechnology and Nanomaterials. Springer, 2016, pp. 305–325
Teja AS, Koh P-Y (2009) Synthesis, properties, and applications of magnetic iron oxide nanoparticles. Progress Crystal Growth Characterizat Mater 55:22–45. https://doi.org/10.1016/j.pcrysgrow.2008.08.003
Teraoka Y et al (2006) Fe-based perovskite-type oxides as excellent oxygen-permeable and reduction-tolerant materials. Solid State Ionics 177:2245–2248. https://doi.org/10.1016/j.ssi.2006.05.037
Thesing A et al (2020) Peering into the Formation of Template-Free Hierarchical Flowerlike Nanostructures of SrTiO3. ACS Omega 5:33007–33016
Townsend TK et al (2012) Overall photocatalytic water splitting with NiOx–SrTiO3–a revised mechanism. Energy Environ Sci 5:9543. https://doi.org/10.1039/c2ee22665k
Tran CV et al (2021) New TiO2-doped Cu–Mg spinel-ferrite-based photocatalyst for degrading highly toxic rhodamine B dye in wastewater. J Hazard Mater 420:126636. https://doi.org/10.1016/j.jhazmat.2021.126636
Tu TH et al (2019) Synthesis and application of graphene oxide aerogel as an adsorbent for removal of dyes from water. Mater Lett. 238:134–137. https://doi.org/10.1016/j.matlet.2018.11.164
Ullah Z et al (2013) Influence of Pb doping on structural, electrical and magnetic properties of Sr-hexaferrites. J Alloys Compounds 555:263–267. https://doi.org/10.1016/j.jallcom.2012.12.061
Vadiyar MM et al (2016) Low cost flexible 3-D aligned and cross-linked efficient ZnFe 2 O 4 nano-flakes electrode on stainless steel mesh for asymmetric supercapacitors. J Mater Chem a 4:3504–3512
Vadiyar MM et al (2017) Anchoring ultrafine ZnFe2O4/C nanoparticles on 3D ZnFe2O4 nanoflakes for boosting cycle stability and energy density of flexible asymmetric supercapacitor. ACS Appl Mater Interfaces 9:26016–26028
Valente F et al (2017) Nanoparticle drug delivery systems for inner ear therapy: an overview. Journal of Drug Delivery Science and Technology 39:28–35
Van Nguyen C et al (2021) One-step heating hydrothermal of iridium-doped cubic perovskite strontium titanate towards hydrogen evolution. Mater Lett 282:128686
Vasil'ev, B. V., et al. 2021. Synthesis and magnetic properties of cobalt ferrite nanoparticles formed under hydro and solvothermal conditions. Наносистемы: физика, химия, математика. 12**,** 492–504
Verma R et al (2020) Ni addition induced modification of structural, magnetic properties and bandgap of Ni-Zn nano ferrites. Mater Today: Proc 32:329–333
Verma R et al. (2021) Impact of Cd content on properties of Ni1-xCdxFe2O4 nanoferrites prepared without post-preparation thermal treatment. Mater Today: Proc
Verwey EJW, Heilmann EL (1947) Physical Properties and Cation Arrangement of Oxides with Spinel Structures I. Cation Arrangement in Spinels. J Chem Phys 15:174–180. https://doi.org/10.1063/1.1746464
Wagner M et al (2002) Disinfection of wastewater by hydrogen peroxide or peracetic acid: development of procedures for measurement of residual disinfectant and application to a physicochemically treated municipal effluent. Water Environ Res 74:33–50
Wang M, Yin Y (2016) Magnetically responsive nanostructures with tunable optical properties. J Am Chem Soc 138:6315–6323
Wang W et al (2015a) Research progress of perovskite materials in photocatalysis- and photovoltaics-related energy conversion and environmental treatment. Chem Soc Rev 44:5371–5408. https://doi.org/10.1039/C5CS00113G
Wang B et al (2015b) SrTiO3 single crystals enclosed with high-indexed 023 facets and 001 facets for photocatalytic hydrogen and oxygen evolution. Appl Catal B 166–167:320–326. https://doi.org/10.1016/j.apcatb.2014.11.032
Wang G et al (2018) Synthesis and characterization of polymer-coated manganese ferrite nanoparticles as controlled drug delivery. Appl Surf Sci 428:258–263
Wang H et al (2021) Synthesis and application of perovskite-based photocatalysts in environmental remediation: a review. J Mol Liquids 334:116029. https://doi.org/10.1016/j.molliq.2021.116029
Wu Y, He T (2018) Ag loading induced visible light photocatalytic activity for pervoskite SrTiO3 nanofibers. Spectrochim Acta Part A Mol Biomol Spectrosc 199:283–289. https://doi.org/10.1016/j.saa.2018.03.078
Wu K et al (2019) Zinc ferrite based gas sensors: a review. Ceram Int 45:11143–11157
Xiao H et al (2020) Ruddlesden-Popper Perovskite Oxides for Photocatalysis-Based Water Splitting and Wastewater Treatment. Energy Fuels 34:9208–9221. https://doi.org/10.1021/acs.energyfuels.0c02301
Xie X et al. (2021a) Spinel structured MFe2O4 (M= Fe, Co, Ni, Mn, Zn) and their composites for microwave absorption: A review. Chem Eng J. 131160
Xie L et al. (2021b) Enhanced redox activity and oxygen vacancies of perovskite triggered by copper incorporation for the improvement of electro-Fenton activity. Chem Eng J. 131352
Xu F et al (2012) Magnetite nanocrystal clusters with ultra-high sensitivity in magnetic resonance imaging. ChemPhysChem 13:336–341
Yang H et al (2012) Antibacterial analyse of perovskite. J Shanghai Jiaotong Univ (science) 17:337–340
Yang D et al (2016) Fabrication of bimodal-pore SrTiO3 microspheres with excellent photocatalytic performance for Cr(VI) reduction under simulated sunlight. J Hazard Mater. 312:45–54. https://doi.org/10.1016/j.jhazmat.2016.03.032
Yang Z et al (2018) High-performance single-crystalline perovskite thin-film photodetector. Adv Mater 30:1704333. https://doi.org/10.1002/adma.201704333

Yang D et al (2019) Removing Cr (VI) in water via visible-light photocatalytic reduction over Cr-doped SrTiO3 nanoplates. Chemosphere. 215:586–595. https://doi.org/10.1016/j.chemosphere.2018.10.068

Yang Y et al (2020) Adsorption and photocatalytic reduction of aqueous Cr(VI) by Fe3O4-ZnAl-layered double hydroxide/TiO2 composites. J Colloid Interface Sci 562:493–501. https://doi.org/10.1016/j.jcis.2019.11.088

Yazdani F, Seddigh M (2016) Magnetite nanoparticles synthesized by co-precipitation method: the effects of various iron anions on specifications. Mater Chem Phys 184:318–323

Yin W-J et al (2019) Oxide perovskites, double perovskites and derivatives for electrocatalysis, photocatalysis, and photovoltaics. Energy Environ Sci 12:442–462. https://doi.org/10.1039/C8EE01574K

Yu L, Sun A (2021) Influence of different complexing agents on structural, morphological, and magnetic properties of Mg–Co ferrites synthesized by sol–gel auto-combustion method. J Mater Sci: Mater Electron 32:10549–10563

Yu Q et al (2016) Preparation and photocatalytic activity of triangular pyramid NaNbO 3. Appl Catal B 199:166–169. https://doi.org/10.1016/j.apcatb.2016.06.028

Yu H et al (2018) Synthesis and characterization of KTa0. 63Nb0. 37O3 and Cu doped KTa0. 63Nb0. 37O3 nanocrystallines. Mater Lett 216:77–80

Žalnėravičius R et al (2016) Size-dependent antimicrobial properties of the cobalt ferrite nanoparticles. J Nanopart Res 18:300. https://doi.org/10.1007/s11051-016-3612-x

Zanchettin G et al (2021) High performance magnetically recoverable Fe3O4 nanocatalysts: fast microwave synthesis and photo-fenton catalysis under visible-light. Chem Eng Process–Process Intensificat 166:108438. https://doi.org/10.1016/j.cep.2021.108438

Zhai Z et al (2021) 2D/2D black-BiOCl/ Fe2O3 heterojunction photo-Fenton catalytic system for enhanced visible-light tetracycline degradation. Colloids Surf A 626:126953. https://doi.org/10.1016/j.colsurfa.2021.126953

Zhang L et al (2014) Antibacterial activities of mechanochemically synthesized perovskite strontium titanate ferrite metal oxide. Colloids Surf, A 456:169–175

Zhang J et al (2017) Molecular dynamics simulation of the interfacial thermal resistance between phosphorene and silicon substrate. Int J Heat Mass Transfer 104:871–877. https://doi.org/10.1016/j.ijheatmasstransfer.2016.08.021

Zhang Y et al (2017) Sulfurized hematite for photo-Fenton catalysis. Progress Nat Sci Mater Int 27:443–451. https://doi.org/10.1016/j.pnsc.2017.08.006

Zhang R et al (2020) Enhanced piezo-photocatalytic performance by piezoelectric and visible light photoexcitation coupling through piezoelectric Na 0.5 Bi 0.5 TiO 3 micron crystals. RSC Adv 10:7443–7451

Zhang Z et al (2021) Efficient removal of methylene blue using the mesoporous activated carbon obtained from mangosteen peel wastes: kinetic, equilibrium, and thermodynamic studies. Microporous Mesoporous Mater. 315:110904

Zhang L et al (2021) Creation of oxygen vacancies to activate Fe2O3 photoanode by simple solvothermal method for highly efficient photoelectrochemical water oxidation. Int J Hydrogen Energy 46:12897–12905

Zhou X et al (2019) Construction of LaNiO3 nanoparticles modified g-C3N4 nanosheets for enhancing visible light photocatalytic activity towards tetracycline degradation. Sep Purif Technol 211:179–188. https://doi.org/10.1016/j.seppur.2018.09.075

Zhu X et al (2021) A comparative study of spinel ZnFe2O4 ferrites obtained via a hydrothermal and a ceramic route: structural and magnetic properties. Ceram Int 47:15173–15179

Zysler RD et al (2001) Investigation of magnetic properties of interacting Fe2O3 nanoparticles. J Magnet Magnet Mater 224:5–11. https://doi.org/10.1016/S0304-8853(00)01328-7